DOE/NASA/0238-1
NASA CR-174753

Electrocatalysis of Fuel Cell Reactions: Investigation of Alternate Electrolytes

Der-Tau Chin, K-L. Hsueh,
and H. H. Chang
Clarkson College of Technology
Potsdam, New York 13676

January 1984

Prepared for
NATIONAL AERONAUTICS AND SPACE ADMINISTRATION
Lewis Research Center
Cleveland, Ohio 44135
Under Grant NAG 3-238

for
U.S. DEPARTMENT OF ENERGY
Morgantown Energy Technology Center
Morgantown, West Virginia 26505
Under Interagency Agreement DE-AI21-80ET17088

SUMMARY

This work is concerned with a study of oxygen reduction and transport properties of the electrolyte in the phosphoric acid fuel cell. The areas covered in the work were: (i) development of a theortical expression for the rotating ring-disk electrode technique; (ii) determination of the intermediate reaction rate constants for oxygen reduction on platinum in phosphoric acid electrolyte; (iii) determination of oxygen reduction mechanism in trifluoromethanesulfonic acid (TFMSA) which has been considered as an alternate electrolyte for the acid fuel cells; and (iv) the measurement of transport properties of the phosphoric acid electrolyte at high concentrations and temperatures.

(1) Theoretical Analysis of the Rotating Ring-Disk Electrode Method

The previous theoretical treatments of the rotating ring-disk electrode method to distinguish between the mechanisms of electroreduction of O_2 to H_2O with and without the formation of H_2O_2 as an intermediate, were examined. A new expression was derived for $I_{dl}/(I_{dl}-I_d)$ as a function of $\omega^{-1/2}$ (where I_{dl} is the disk limiting current, I_d is the disc current and ω is the rotational speed of electrode) for five possible reaction models. This, along with the corresponding expressions for I_d/I_r vs. $\omega^{-1/2}$ (I_r is the ring current), enables the calculations of the individual rate constants for the intermediate steps of O_2 reduction. The experimental data of I_d and I_r were obtained for O_2 reduction on platinum in 0.55 M H_2SO_4 at 25°C. By use of these experimental results in the present theoretical treatment, it is shown that: (1) the most applicable model over the entire potential region was the one suggested by Damjanovic, Genshaw and Bockris: (2) the models involving the adsorption/desorption of H_2O_2 were applicable only over a narrow region of

potential: and (3) the models involving the chemical decomposition of H_2O_2 were inconsistent with the dependence of $I_{d1}/(I_{d1}-I_d)$ vs. $\omega^{-1/2}$.

(2) Oxygen Reduction in Phosphoric Acid

The oxygen reduction reaction was investigated at platinum electrodes in phosphoric acid in the concentration range 0.7M (6.6%) to 17.5M (95%) at 25°C using the rotating ring-disc electrode technique. The mechanism of the oxygen electrode reaction was discussed in terms of the direct four-electron transfer reduction to water and the formation of hydrogen peroxide as an intermediate in a parallel two-electron transfer reaction. The rate constants of the intermediate reaction steps were calculated from the ring-disc data for various potentials and electrolyte concentrations. The characteristics of the reaction were found to be markedly dependent on the concentration of phosphoric acid.

(3) Oxygen Reduction in TFMSA

Trifluoromethane sulfonic acid (TFMSA) has been considered as an alternate electrolyte for fuel cell applications. The kinetics of oxygen reduction at Pt was studied using a rotating ring-disc electrode technique in TFMSA (0.05, 0.1, 1.0, and 6.0M) and in 1.0M TFMSA with phosphoric acid additive (0.003 and 0.1M). The amount of hydrogen peroxide intermediate produced in TFMSA on oxide-covered Pt surface (electrode potential scanned from 1.0 to 0.3 V vs. RHE) was found to be higher than that on oxide-free surface (electrode potential scanned from 0.3 to 1.0 V vs. RHE). A half reaction order with respect to oxygen was observed for the oxygen reduction in TFMSA solutions. The reaction order increased to one with the addition of phosphoric acid to 1.0 M TFMSA. A possible mechanism of oxygen reduction was proposed to explain the half reaction order with respect to oxygen.

(4) Transport Properties of Phosphoric Acid Electrolyte

The transport properties of phosphoric acid are important to the fuel cell performances. In this work, the kinematic viscosity and specific conductivity of the electrolyte, have been measured over a range of phosphoric acid concentrations from 0.5 to 19 M (6 - 100%) and temperatures from 25 to 200°C. The specific conductivity was measured with a Beckman conductivity bridge and a conductivity cell. The kinematic viscosity was measured with Cannon-Fenske viscometers. The results indicate that the conductivity in concentrated phosphoric acid follows a non-Stokian transport mechanism.

ACKNOWLEDGEMENT

(1) This project was supported by a NASA Grant NAG 3-238. The grant originally covered the period, January 1 - December 31, 1982. The project was extended to December 31, 1983 with a no-cost extension.

(2) This work was carried out in collaboration with Dr. S. Srinivasan, the principle investigator on the DOE sponsored program ''Electrocatalysis of Fuel Cell Reactions'' at Los Alamos National Laboratory, Los Alamos, NM, 87544. The authors gratefully acknowledge his help and contributions to the project.

(3) The contribution of K-L. Hsueh was in partial fulfillment of the requirement of his Ph.D. degree in Chemical Engineering from Clarkson College of Technology. His experimental work, a part of theortical analysis and part of dissertation writing were carried out at Los Alamos National Laboratory while he was a graduate research associate during the period May 1981 - August 1982. He received a Ph.D. degree from Clarkson College in 1983. A copy of his dissertation abstract is attached in the appendix.

(4) The contribution of H.H. Chang is in partial fulfillment of a M.S. degree in Chemical Engineering from Clarkson College of Technology. A part of his experimental work was carried out at Los Alamos while he was a guest research assistant during the period June - August, 1982. He was supported by a Clarkson teaching assistantship during the period of January - August, 1983. He will complete his M.S. degree in May, 1984.

TABLE OF CONTENTS

I. INTRODUCTION

The energy crisis of 1973 stimulated the renaissance of fuel cells (1). Fuel cells are superior to other electricity generators in several respects (2); such as: high efficiency, pollution free and silent operation. In fuel cells, the fuels are converted to hydrogen-rich gases and then fed into the fuel cell. The direct current generated from the cell is converted to alternating current by the power conditioner. The heat released from the fuel cell is utilized for the endothermic reaction in the fuel processor.

The essential criteria for fuel cells are dependent on the types of applications. The requirements for civilian terrestrial use are high efficiency, high power density, low capital cost and long life. The phosphoric acid fuel cell (3) appears to be the best candidate when natural gas and naphtha are used as fuels. This fuel cell is operated at 200^{o}C and there is a need to transfer waste heat from the fuel cells to the fuel processor. Molten carbonate (1,4) and solid electrolyte (1,5) fuel cells appear to be promising when coupled with a coal gasifier operating at temperatures of 1000 ~ 1500^{o}C.

The major cause of the efficiency loss in the fuel cell is due to the slow reaction rate of oxygen reduction at the cathode (8). The overpotential of the hydrogen electrode is less than 20 mV at 200 mA/cm^{2}; however, the overpotential of the oxygen electrode is 400 mV at the same current density. The oxygen electrode reaction is the major cause of efficiency loss in phosphoric acid fuel cells. It has been shown that the overpotential loss for the oxygen reduction reaction can be reduced with additives, such as, trifluoromethane sulfonic acid (TFMSA) into phosphoric acid electrolyte. The exchanging current density in aqueous TFMSA is one hundred times higher than

that in 85% H_3PO_4. The mechanism of oxygen reduction in H_3PO_4 and TFMSA is not known. The objective of this work are:

i) Study of electrode kinetics of oxygen reduction in fuel cell electrolytes- The reduction of oxygen involves two parallel reaction paths. One reaction path is the direct reduction of oxygen to water. The second path is the reduction of oxygen to hydrogen peroxide, followed by the reduction of hydrogen peroxide to water. An evaluation of the rate constants of individual reaction path of oxygen reduction is essential for the understanding of oxygen reduction kinetics. A method to calculate these rate constants from the rotating ring-disk experiment has been developed in this work. The kinetics of oxygen reduction was studied by using the rotating ring-disk electrode technique in phosphoric acid and trifluoromethanesulfonic acid (TFMSA). The results are summarized in this report.

ii) Investigation of transport properties of phosphoric acid electrolyte- The physical properties of electrolyte are important to the fuel cell performance (3). The conductivity of the electrolyte can affect the cell IR loss. The maximum operating temperature is limited by the boiling point of the electrolyte. Besides, the rate of oxygen reduction is proportional to the solubility and diffusivity of dissolved oxygen in the electrolyte (12). The information of transport properties in phosphoric acid over a wide concentration range would clearify the change in solvent structure (from water to phosphoric acid) when the electrolyte changes from aqueous solution to concentrated phosphoric acid medium. For these purposes, the conductivity and viscosity of phosphoric acid were measured over a range of concentrations from 0.7 to 17.5M (6.6 - 100%) and the temperature from 25 to 200°C.

II. ELECTRODE KINETICS OF OXYGEN REDUCTION

The aims of this work is to investigate the effects of the electrolyte on the kinetics of oxygen reduction at platinum. For this purpose, the rotating ring-disk electrode technique was used. All the kinetics studies were carried out on the platinum electrode because platinum is the best catalyst for the fuel cell reaction. Since the phosphoric acid is presently used in the fuel cell and trifluoromethanesulfonic acid (TFMSA) shows promise for fuel cell applications (13), the investigation was carried out in these two acids.

There are four sections in this chapter. In section 2.1, the experimental procedures and preparation of electrode, electrolytes, and glassware are described. In section 2.2, a set of new equations for the calculation of rate constants of the intermediate reaction steps from the rotating ring-disk electrode is developed. In section 2.3, the results for the reduction of oxygen in phosphoric acid over the concentration range of 0.7 - 17.5M are analyzed by the method presented in section 2.2. The results of oxygen reduction in aqueous TFMSA (0.05 ~ 6.0M) and in a mixed acid which containing 1.0M TFMSA and 0.003 ~ 0.1M phosphoric acid are presented in section 2.4.

2.1 EXPERIMENTAL

Experimental set-up

A glass cell with one compartment for the test and auxiliary electrodes and another for the reference electrode was used in the electrode kinetics experiments. A platinum ring-disk electrode (Pine Instrument) with a collection efficiency of 17.6% served as the working electrode. The electrode potentials were measured against a dynamic hydrogen electrode (DHE) and were converted to a reversible hydrogen electrode (RHE) scale. A large platinum gauze was used as the counter electrode. The potentials of the disk and ring electrodes were controlled by a potentiostat (Pine Instrument RDE 3) and the rotational speed of the electrode was controlled by an analytical rotator

(Pine Instrument ASR 2). The currents at the disk and ring electrodes were recorded on a dual pen X-Y-Y' recorder (Soltec 6431).

Preparation of electrolytes, gases, and glassware

The cell, the electrodes and the glassware were cleaned with chromic acid (0.1 mol. $K_2Cr_2O_7$ dissolved into 1 ℓ H_2SO_4) followed by soaking in a 1.1 H_2SO_4/HNO_3 solution for 8 hr. and then in double distilled water for another 8 hr. The 0.55M sulfuric acid was prepared by diluting concentrated sulfuric acid (ultra pure, Alfa, Ventron Div.) with double distilled water. Phosphoric acid (85%, electronic grade, J.T. Baker) was treated with 10% hydrogen perioxide (90%, stabilizer free, FMC) and heated to 50-70^{o}C for 1 hr. The solution was concentrated to 85% by evaporation at 160^{o}C in a Teflon vessel. The solution was diluted with double distilled water to the desired concentrations. Trifluoromethanesulfonic acid (3M Co.), was distilled twice under vacuum (B.P. $<$ 40^{o}C). The distillate was added to double distilled water to form trifluoromethanesulfonic acid (TFMSA) monohydrate which was then vacuum-distilled (B.P. $<$ 80^{o}C). Before use, the monohydrate was diluted with double distilled water to the desired concentration.

Experimental procedure

Before the electrode kinetics experiments, the solution was deaerated with purified nitrogen gas and a cyclic voltammogram on the platinum disk electrode was examined to insure the purity of solutions. Then the purified oxygen was bubbled through the electrolyte for 1 hr. During the rotating ring-disk electrode experiments, the potential of the disk electrode was scanned from 1.0 to 0.3 V vs. DHE at a scan rate of 5 mV/S, while the potential of the ring electrode was maintained at 1.1 V vs. DHE (this is a limiting current potential for the oxidation of hydrogen peroxide to oxygen). Experiments were carried out for a range of rotational speed from 400 to 4900 rpm at 20-25^{o}C.

2.2 THEORETICAL ANALYSIS OF THE ROTATING RING-DISK ELECTRODE METHOD

The rotating ring-disk electrode technique has been extensively used for the investigation of the mechanism of the oxygen reduction in which hydrogen peroxide is formed as an intermediate (14-19). In this method, the reduction of oxygen takes place on a central disk electrode and the generated hydrogen peroxide is detected at a concentric ring electrode with a larger radius. The purpose of this work is to modify previous theoretical treatments (15,16,19) and to determine the rate constants of the intermediate steps for the reaction models shown in Fig. 1. The rotating ring-disk electrode experimental data obtained for oxygen reduction at platinum in 0.55M sulfuric acid are used to illustrate the procedure of the present theoretical analysis.

Modification of theoretical treatments for the calculation of rate constants

Based on the material balances, the mathematical expression which would permit the calculations of the rate constants of the intermediate steps for the oxygen reduction reaction can be derived for each of the models presented in Fig. 1. For the sake of brevity, only the equations for Model 1 are presented here. The details of the analysis are given in Reference 6 and 9.

From the material balance of oxygen and hydrogen peroxide species in Model 1 (Fig. 2.1), the relations among the ring current, I_r and the expressions for ring (I_r) and the disk current, I_d, the limiting current at the disk, I_{dl}, and the rotating speed of electrode, ω can be expressed as:

$$\frac{I_d}{I_r} = \frac{1}{N}\left[1+2\,\frac{k_1}{k_2}\right] + \left[\frac{2(k_1/k_2+1)}{N\ Z_2}k_3\right]\omega^{-1/2} \qquad (1)$$

$$\frac{I_{dl}}{I_{dl}-I_d} = 1 + \frac{k_1+k_2}{Z_1}\,\omega^{-1/2} \qquad (2)$$

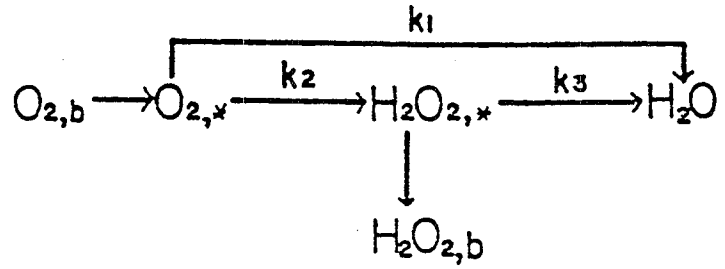

Model 1

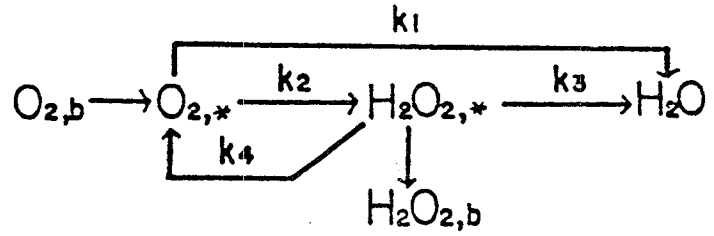

Model 2

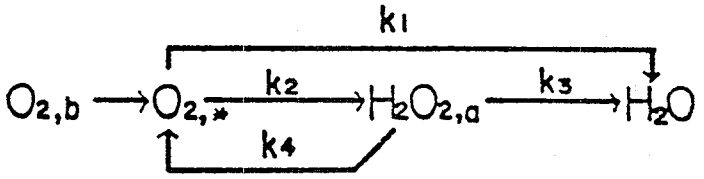

Model 3

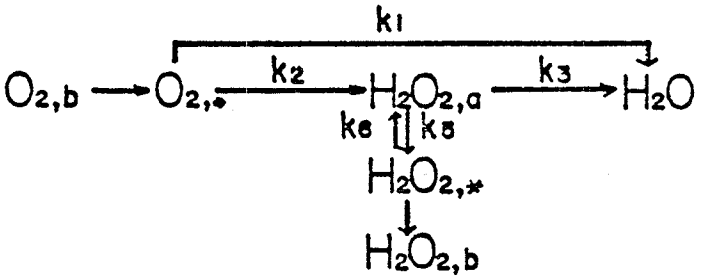

Model 4

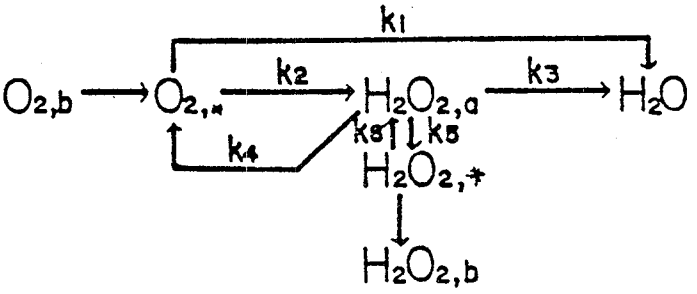

Model 5

Fig. 1 Reaction schemes for the electroreduction of O_2 considered in the present work.

Accordingly, the rate constants k_1, k_2, and k_3 may be determined from the intercepts and slopes of the plot of I_d/I_r vs. $\omega^{-1/2}$ and from the slopes of the plot of $I_{d1}/(I_{d1}-I_d)$ vs. $\omega^{-1/2}$ at different disk potential.

Evaluation of the rate constants

Two important expressions for the calculation of the rate constants are: (i) $I_{d1}/(I_{d1}-I_d)$ as a function of $\omega^{-1/2}$; and (ii) I_d/I_r as a function of $\omega^{-1/2}$. Figure 2 shows that the plot of $I_{d1}/(I_{d1}-I_d)$ vs. $\omega^{-1/2}$ at different electrode potentials exhibits a linear behavior with an intercept equal to 1. The plots of I_d/I_r vs. $\omega^{-1/2}$ at various electrode potentials are given in Fig. 3 (from 0.75 to 0.55 V vs. RHE) and in Fig. 4 (from 0.55 to 0.35 V vs. RHE). Using Model 1, it is possible to calculate the rate constants over the entire potential range (from 0.8 to 0.4 V vs. RHE); the rate constants in H_2SO_4 as a function of electrode potential are presented in Fig. 5. The ratio of k_1 to k_2 is about 5 ~ 12 and is potential-dependent. Since k_1 is larger than k_2, oxygen is mainly reduced to water via the direct four-electron transfer reaction path and only small amount of oxygen is reduced to water via the series reaction path which involves hydrogen peroxide as an intermediate. The rate constant k_3 is greater than k_2. This indicates that hydrogen peroxide is reduced to water at a relatively rapid rate. Therefore, only a little amount of hydrogen peroxide diffuses into the bulk electrolyte as evidenced by the small ring currents. The faradaic efficiency for oxygen reduction is about 97%.

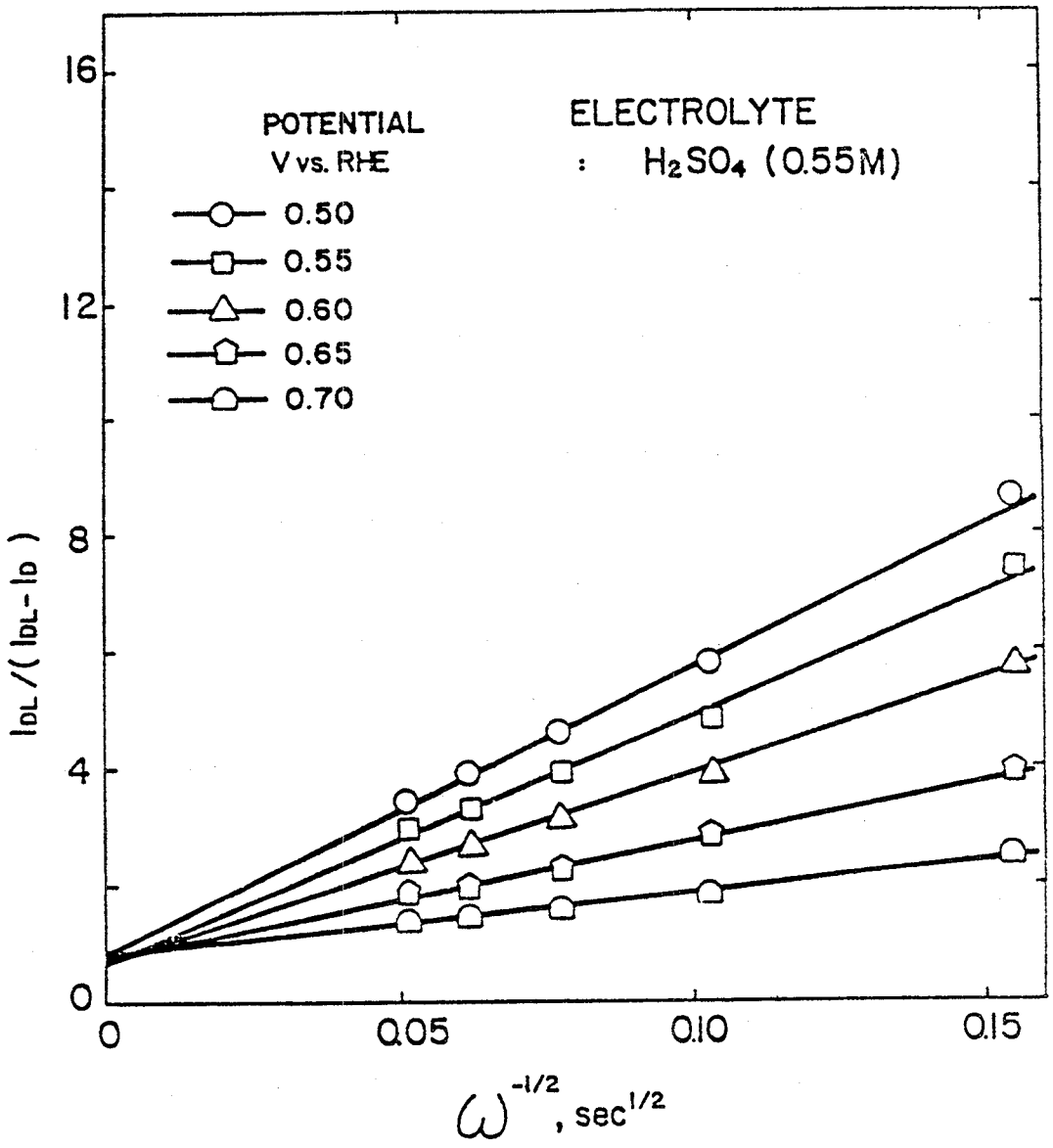

Fig. 2. $I_{d1}/(I_{d1} - I_d)$ as a function of $\omega^{-1/2}$ at various disc potentials.

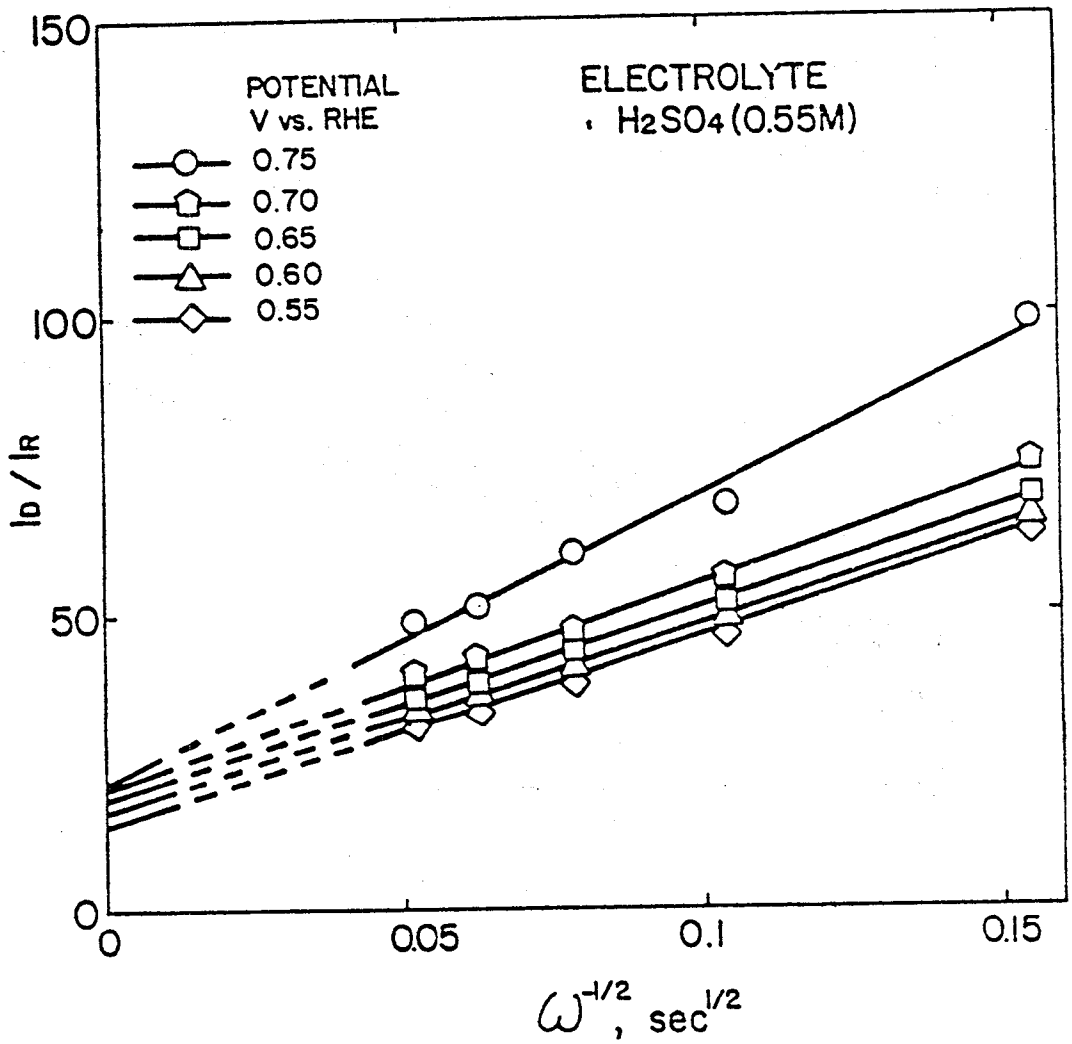

Fig. 3 I_d/I_r vs. $\omega^{-1/2}$ in the potential region 0.75 ~ 0.55, V vs. RHE

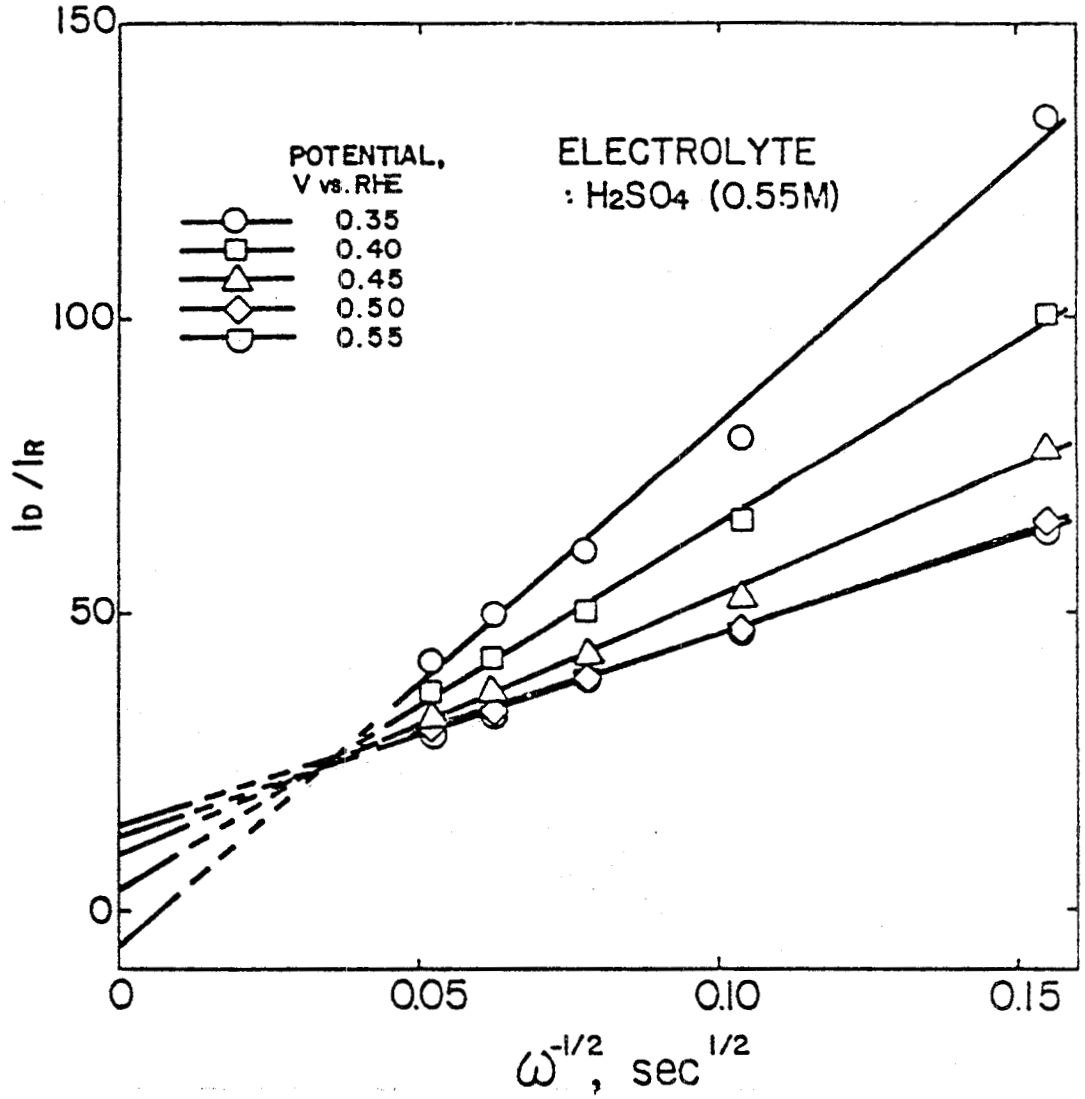

Fig. 4 I_d/I_r vs. $\omega^{-1/2}$ in the potential region 0.55 ~ 0.35, V vs. RHE

ENTER:D 84N20013

DISPLAY 84N20013/2

84N20013*# ISSUE 10 PAGE 1529 CATEGORY 44 RPT#: NASA-CR-173261 NAS 1.26:173261 83/00/00 63 PAGES UNCLASSIFIED DOCUMENT

UTTL: Electrocatalysis of fuel cell reactions: Investigation of alternate electrolytes TLSP: Final Report, 1 Jan. 1982 - 31 Dec. 1983

AUTH: A/CHIN, D. T.; B/HSUEH, K. L.; C/CHANG, H. H.

CORP: Clarkson Coll. of Technology, Potsdam, N.Y. CSS: (Dept. of Chemical Engineering.) AVAIL.NTIS SAP: HC A04/MF A01

MAJS: /*ELECTROCATALYSTS/*ELECTROLYTES/*FUEL CELLS

MINS: / ELECTRODES/ OXYGEN/ PHOSPHORIC ACID/ PLATINUM/ REDUCTION (CHEMISTRY)/ TRANSPORT PROPERTIES

ABA: Author

ABS: Oxygen reduction and transport properties of the electrolyte in the phosphoric acid fuel cell are studied. A theoretical expression for the rotating ring-disk electrode technique; the intermediate reaction rate constants for oxygen reduction on platinum in phosphoric acid electrolyte; oxygen reduction mechanism in trifluoromethanesulfonic acid (TFMSA), considered as an alternate electrolyte for the acid fuel cells; and transport properties of the phosphoric acid electrolyte at high concentrations and temperatures are covered.

ENTER:

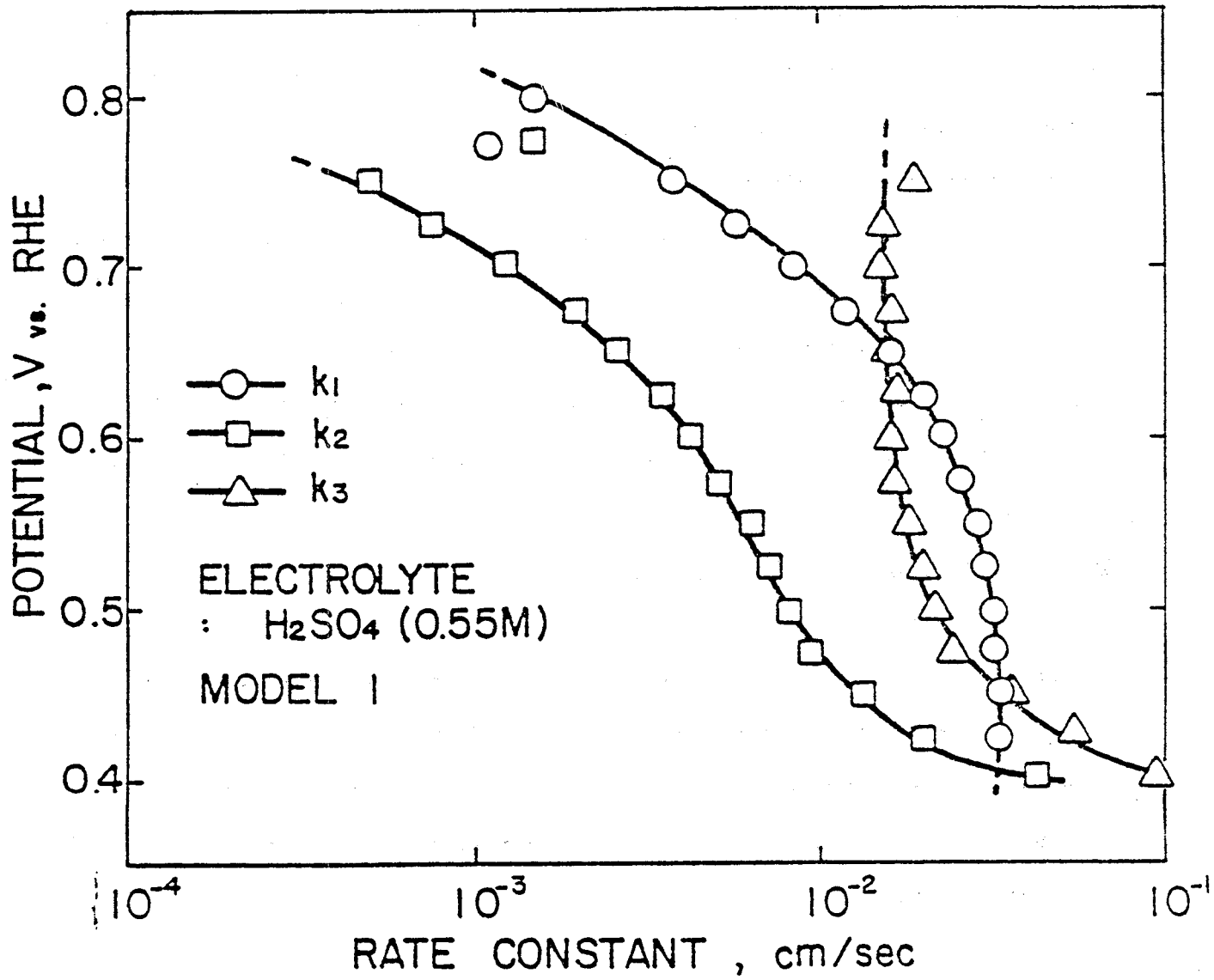

Fig. 5 Rate constants of intermediate steps for O_2 reduction on Pt in 1N H_2SO_4. These constants were calculated based on Model 1.

2.3 KINETICS OF OXYGEN REDUCTION AT PLATINUM IN PHOSPHORIC ACID

Concentrated phosphoric acid is presently used as the electrolyte in advanced fuel cells. The factor limiting the efficiency of this fuel cell is the overpotential for oxygen reduction reaction. The structure and physical properties of concentrated phosphoric acid are not well understood, but these certainly play a role in the kinetics of the oxygen reduction reaction. The double layer of mercury/concentrated phosphoric acid interface is thicker than in aqueous media (20). It is resonable to assume that there is a transition of the interfacial and bulk properties when the electrolyte concentration increases from a water-based to a phosphoric acid-based solvent structure. For this reason, the present study was undertaken to elucidate the effect of the concentration of phosphoric acid solutions (from 0.7 to 17.5M) on the kinetics of oxygen reduction at platinum electrodes.

Mass Transfer-Corrected Tafel Behavior

A rotating ring-disk electrode was used to measure the polarization curves of oxygen reduction at platinum, and to quantitatively determine the amount of the hydrogen perioxide intermediate formed during the reduction process. The mass transfer corrected Tafel behavior for oxygen reduction on platinum for different phosphoric acid concentrations is shown in Fig. 6. The plots correspond to the equation

$$E = \frac{2.3RT}{\alpha F} \log I_o - \frac{2.3RT}{\alpha F} \log \frac{I_{dl} I_d}{I_{dl} - I_d} \qquad (3)$$

The Tafel plots presented in Fig. 6 are independent of rotation speed. In the region from 0.6 to 0.8 V vs. RHE, the Tafel slopes are about 120 mV. This result is similar to that (12,21,22) in other acid media. This indicates that the overall reduction of oxygen is controlled by the first charge transfer step under the Langmuir adsorption condition.

Mechanistic Aspects of Electroreduction of Oxygen

Based on Model 1 and the procedure illustrated in the method the preceding theoretical analysis section, the values of k_1, k_2, and k_3 for oxygen reduction in phosphoric acid have been calculated. The rate constants (k_1, k_2, and k_3) are presented as a function of electrode potential for various phosphoric acid concentrations in Fig. 7-10. In all cases, the ratio k_1/k_2 is greater than 10, implying that most of oxygen reduces to water directly through the four electron transfer reaction.

From Fig. 7 to 9, it is apparent that for phosphoric acid concentrations up to 8M, k_2 has the same potential-dependence as k_1. This means that the rate determining step is probably the same for the both reaction paths. At higher concentrations, k_2 becomes independent of potential; this indicates that the rate of the reaction is controlled by a chemical step prior to the electron transfer step.

The behavior of k_3 is similar to that of k_2; it decreases with increasing phosphoric acid concentration. The significant decrease in k_2 and k_3 with increasing phosphoric acid concentration leads to an increase in the faradaic efficiency for the reduction of oxygen to water. This is important because at the high phosphoric acid concentrations used in the fuel cells, the amount of hydrogen peroxide formed during the operation is negligible.

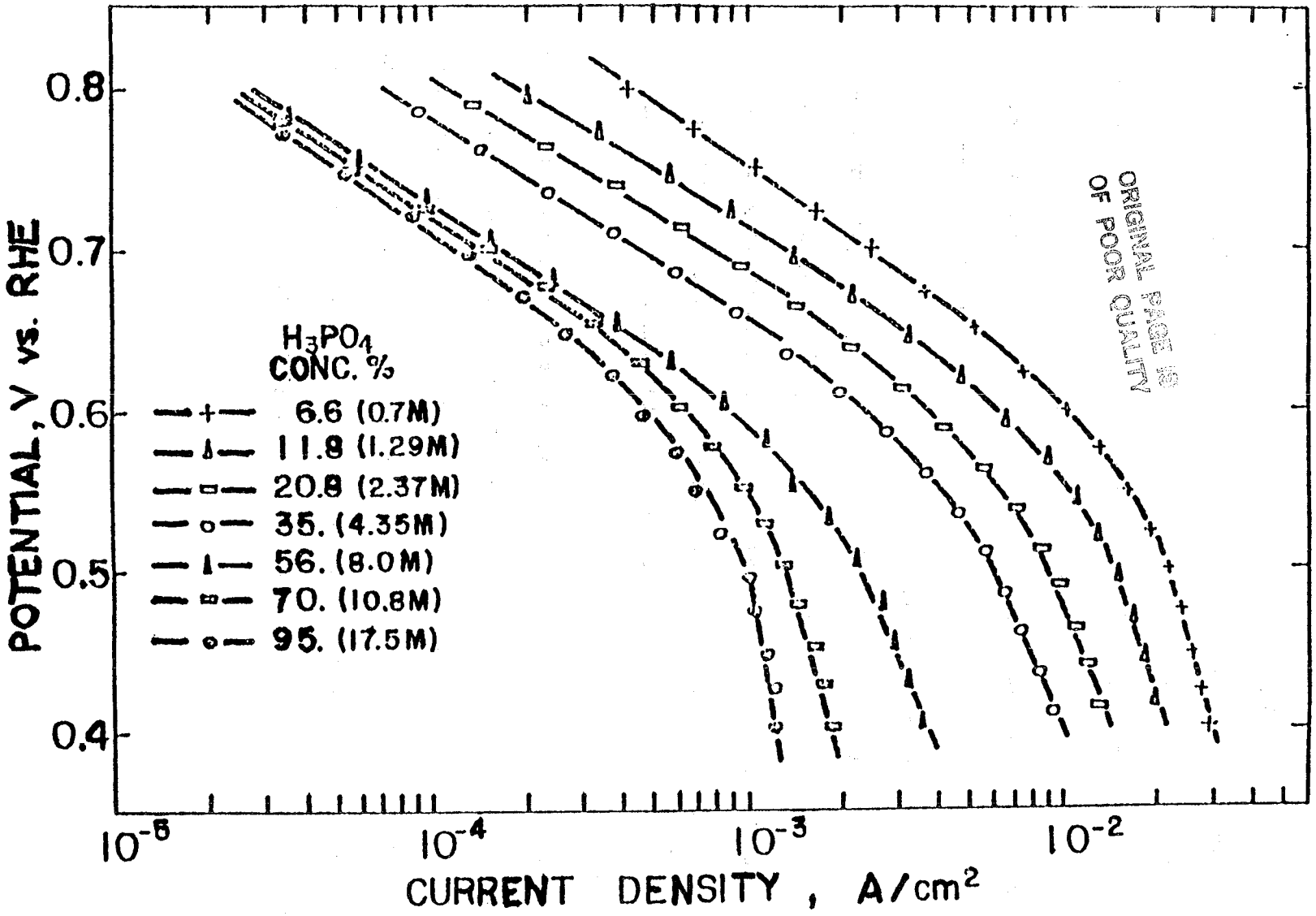

Fig. 6 Mass-transfer-corrected Tafel behavior for oxygen reduction on Pt in H_3PO_4 over the concentration range 6.6 to 95 w/o at 25°C. Tafel behavior is independent of electrode rotating speed in the 400- to 3600-rpm region.

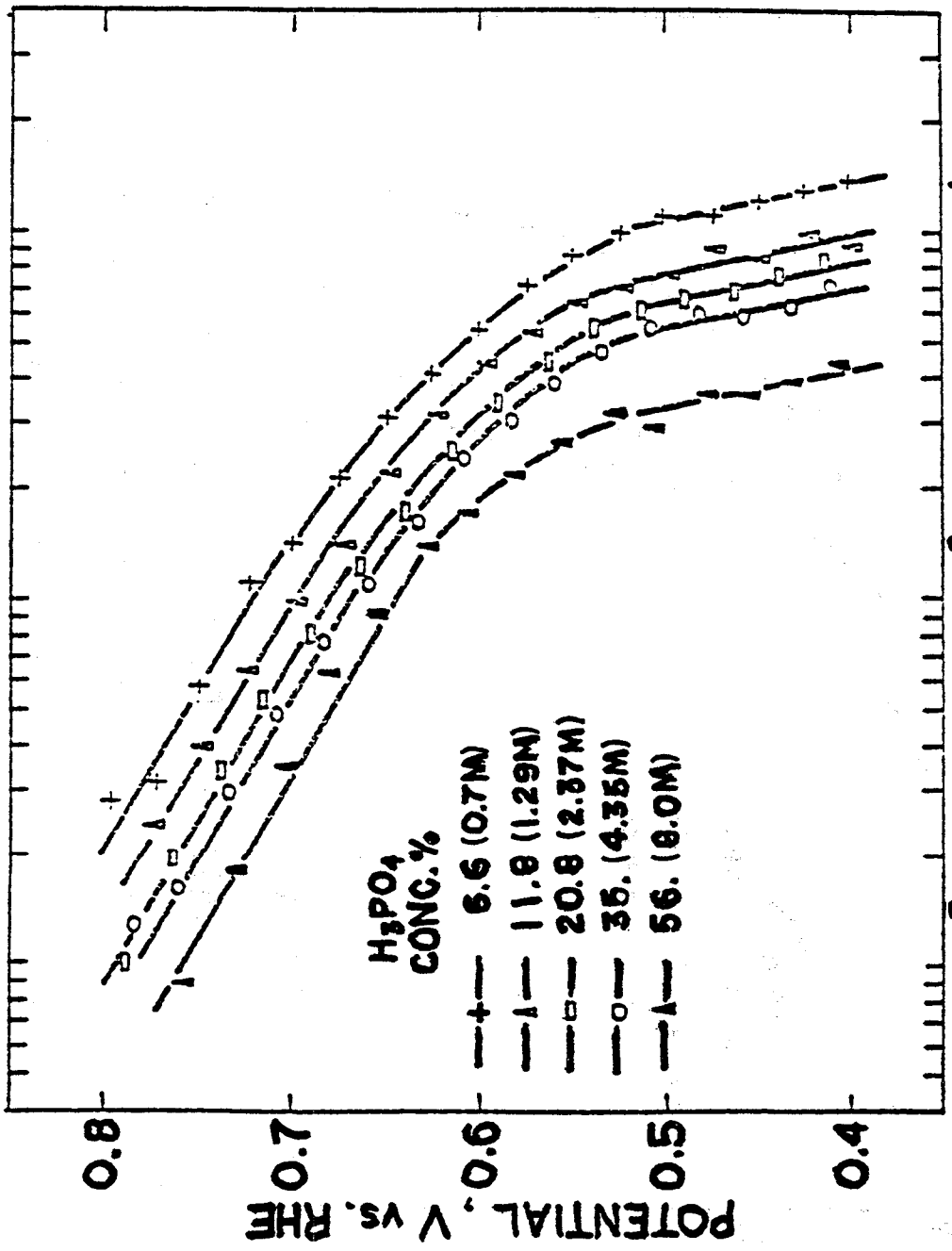

Fig. 7 Potential dependence of rate constant k_1 for oxygen reduction at Pt in H_3PO_4 in the concentration range 6.6 to 56 w/o at 25°C.

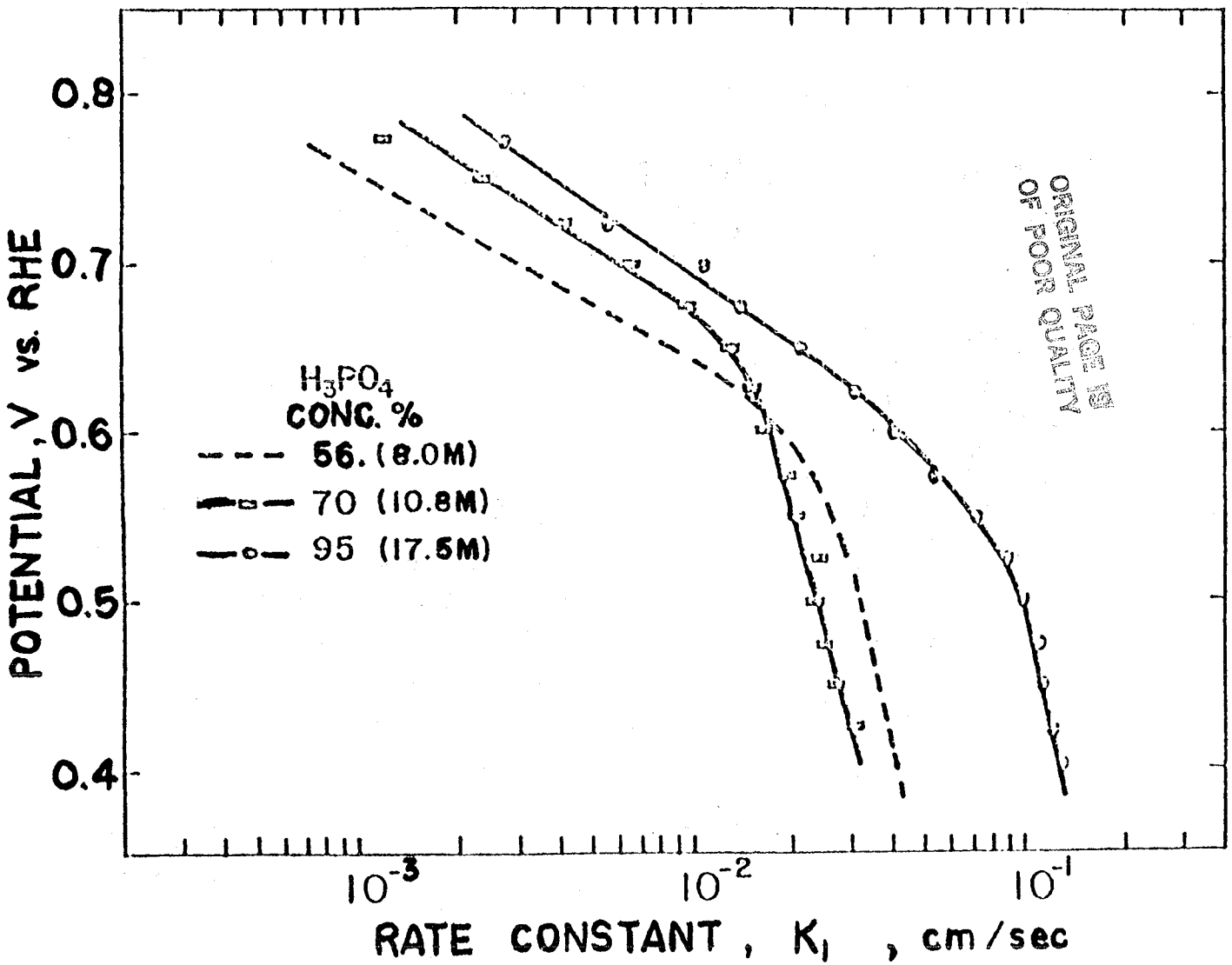

Fig. 8 Potential dependence of rate constant k_1 for oxygen reduction at Pt in H_3PO_4 in the concentration range 56 to 95 w/o at 25°C.

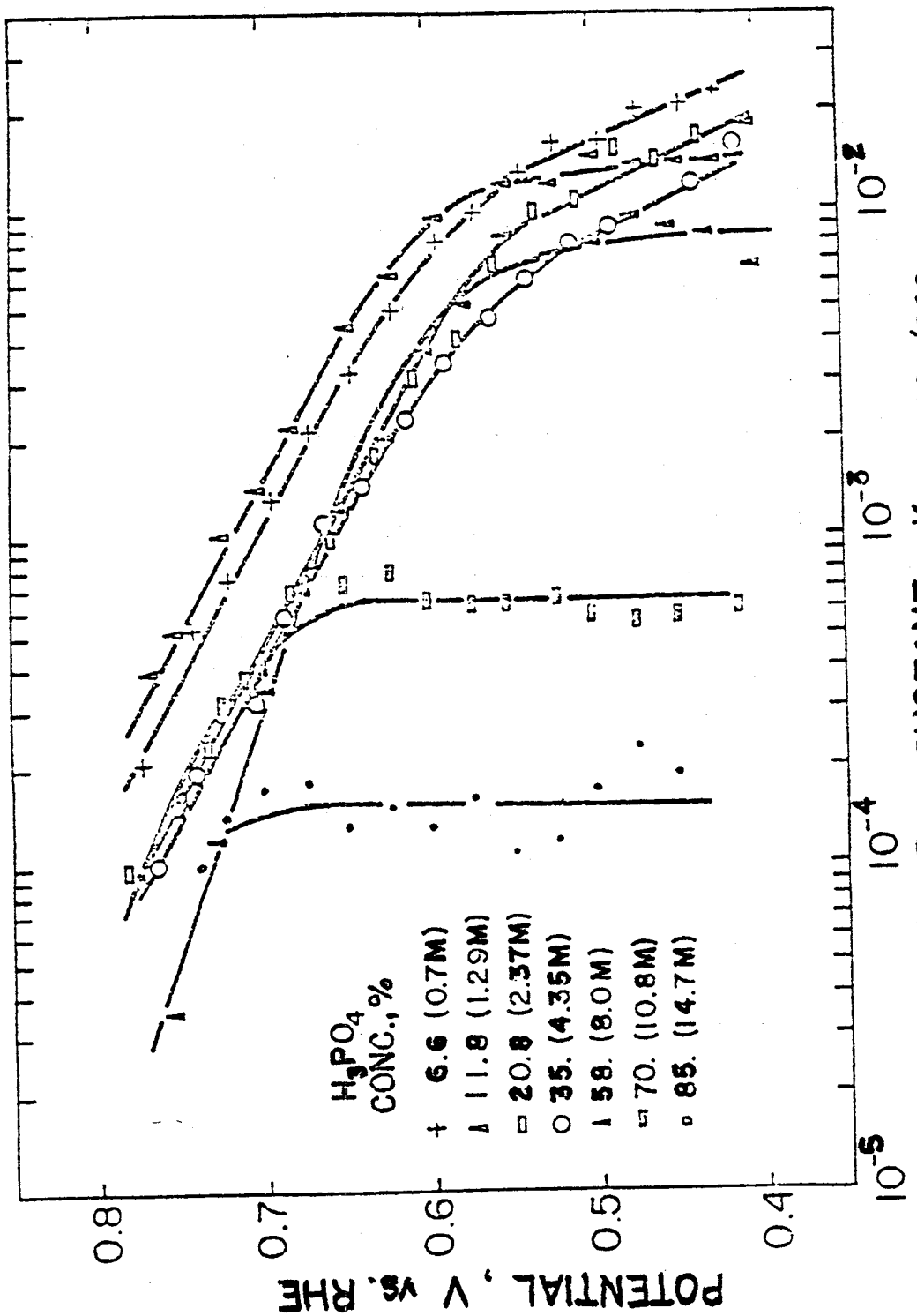

Fig. 9 Potential dependence of rate constant k_2 for oxygen reduction at Pt in H_3PO_4 in the concentration range 6.6 to 85 w/o at 25°C.

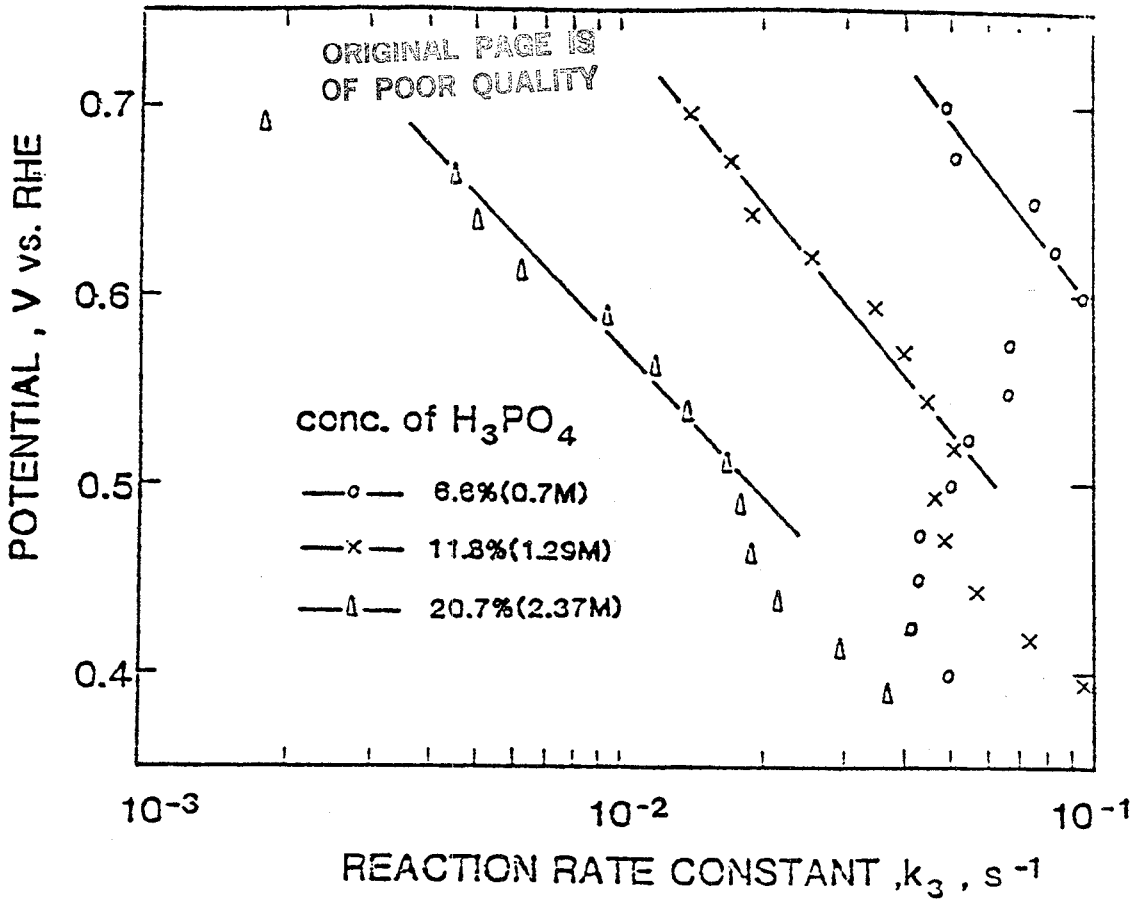

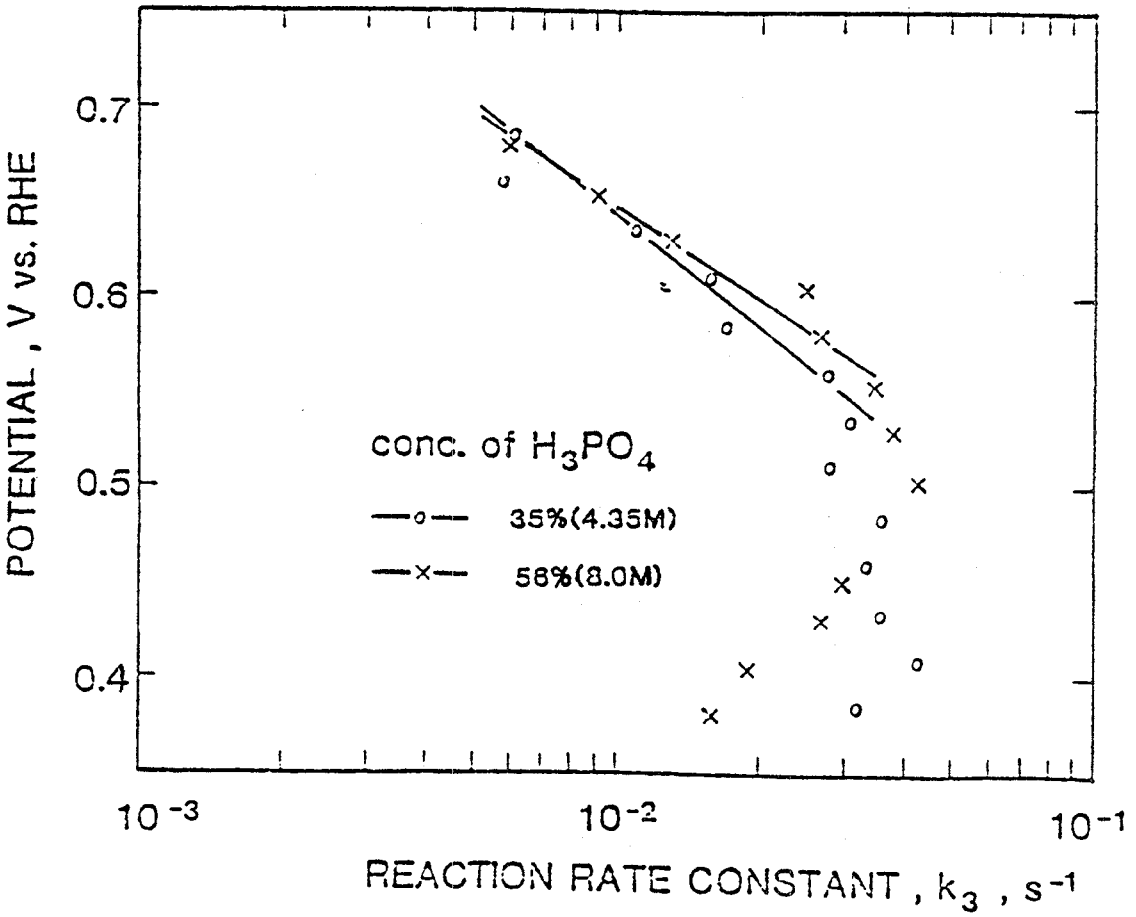

Fig. 10 Potential dependence of rate constant k_3 for oxygen reduction of Pt in H_3PO_4 in the concentration range 6.6 to 56 w/o at 25°C.

Conclusions

From the results of the rotating ring-disk experiment, the following conclusions may be reached for the oxygen reduction on pt in concentrated phosphoric acid solution: (i) In the potential range 0.8 to 0.6V, the slope of the mass transfer-corrected Tafel plots is equal to 120 mV/decade and is independent of concentration; (ii) The rate constants for k_1 and k_2 have the same potential dependence with the ratio of k_1/k_2 greater than 10.

2.4 ELECTRODE KINETICS OF OXYGEN REDUCTION ON PLATINUM IN TRIFLUOROMETHANESULFONIC ACID (TFMSA)

Trifluoromethanesulfonic acid (TFMSA, CF_3SO_3H) and its homologues of higher molecular weight are considered alternatives to phosphoric acid as acid electrolytes for fuel cell. The reaction rate of oxygen reduction at platinum in TFMSA is about two order of magnitude higher than that in phosphoric acid (23). Although there have been some investigations of oxygen reduction on platinum in aqueous TFMSA and in TFMSA monohydrate on smooth and porous electrode (23), its kinetics in this electrolyte is not yet fully understood. The purpose of this study is to investigate the kinetics of oxygen reduction at smooth platinum in aqueous TFMSA (0.05 ~ 6.0M) and in a mixed acid containing 1.0M TFMSA and 0.003 ~ 0.1M phosphoric acid.

Effects of Surface Oxide at Platinum on the Kinetics of Oxygen Reduction in TFMSA

During the rotating ring-disk experiment, when the electrode potential is scanned from 1.0 to 0.3 V vs. RHE, the surface of the platinum electrode is first covered with a layer of oxide and then gradually reduced to bare platinum at the end of the scan. Conversely when the electrode potential is scanned from 0.3 to 1.0 V vs. RHE, the electrode starts with an oxide-free surface and then the oxide is gradually formed at the potentials above 0.8 V vs. RHE.

The influence of the surface oxide on the kinetics of oxygen reduction at platinum in 0.05M TFMSA is shown in Fig. 11 (at ω = 900 rpm). The disk current (I_d) for oxygen reduction on the oxide-free surface (potential scanned from 0.3 to 1.0 V vs. RHE) was higher than that on the oxide-covered surface (potential scanned from 1.0 to 0.3 V vs. RHE). The maximum amount of hydrogen peroxide detected on the ring electrode (I_r) for the oxide-covered disk electrode was 400% higher than that for the oxide-free disk electrode.

Reaction Order with Respect to Oxygen for the Oxygen Reduction Reaction at Platinum in TFMSA

An attempt was made to determine the rate constants for oxygen reduction at platinum in TFMSA with the procedure of the theoretical analysis described in Section 2.2. Negative intercepts were observed for both the $I_{d1}/(I_{d1}-I_d)$ vs. $\omega^{-1/2}$ and I_d/I_r vs. $\omega^{-1/2}$ plots in all the TFMSA solutions (0.05 ~ 6.0M) as well as in 1.0M TFMSA solution with phosphoric acid additives (0.003 ~ 6.0M). One possible explanation is that the reaction order with respect to oxygen in the TFMSA medium is not unity. According to the following equation (24):

$$\log I_d = \log I_k + m \log (1 - I_d/I_{d1}) \qquad (4)$$

a plot of log I_d vs. log $(1 - I_d/I_{d1})$ should be linear with a slope equal to the reaction order of oxygen, m. A typical plot of log I_d vs. log $(1 - I_d/I_{d1})$ in 0.05M TFMSA is presented in Fig. 12. The slopes of the straight lines reveal a fractional reaction order. In the concentrations of TFMSA investigated, the reaction order of oxygen were between 0.4 and 0.5. In the mixtures of 1.0M TFMSA and 0.003 - 0.1M phosphoric acid, the reaction order of oxygen increased from 0.5 as the concentration of phosphoric acid increased.

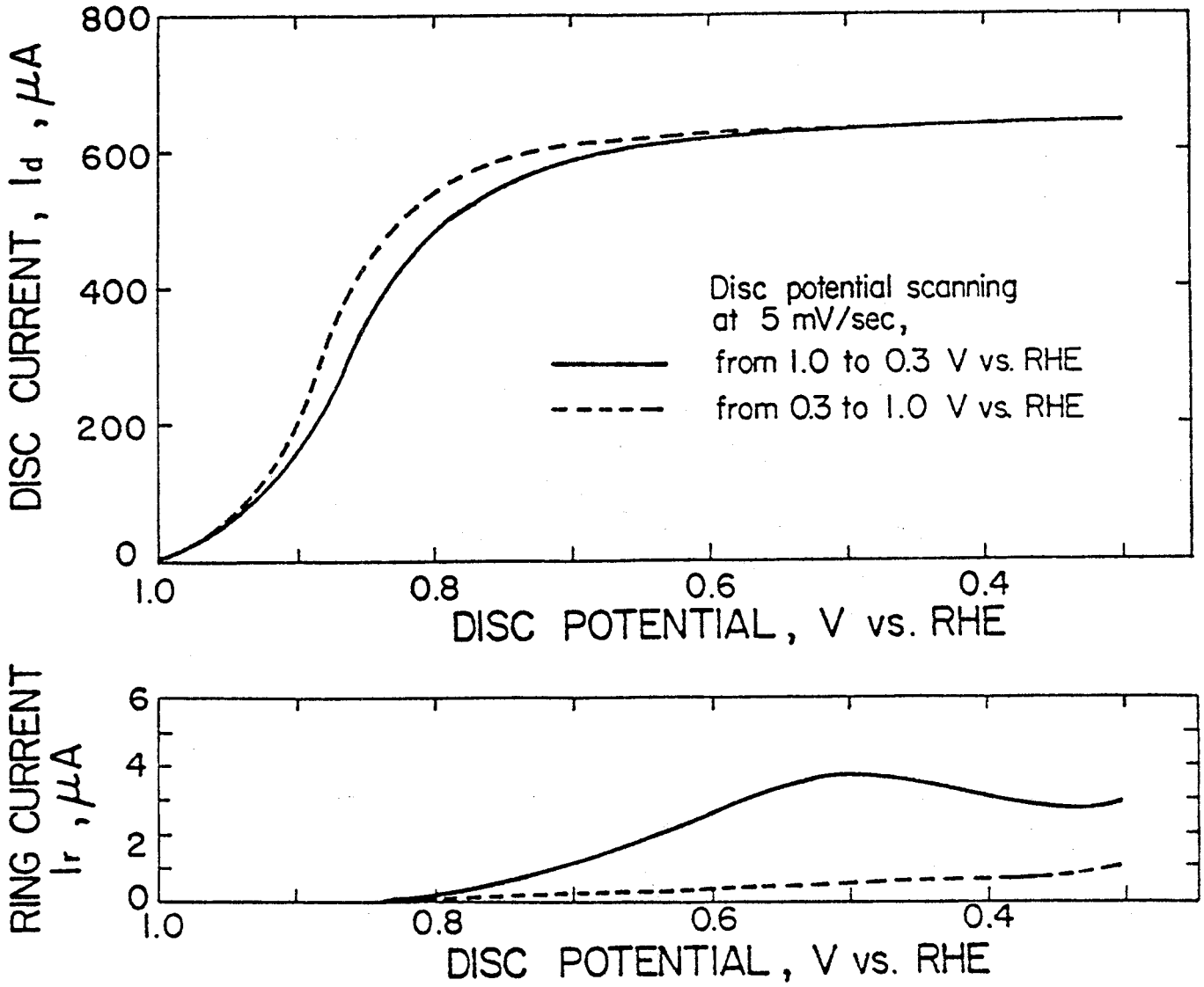

Fig. 11 The rotating ring-disc electrode data at ω = 900 rpm for oxygen reduction at Pt in 0.05 M TFMSA.

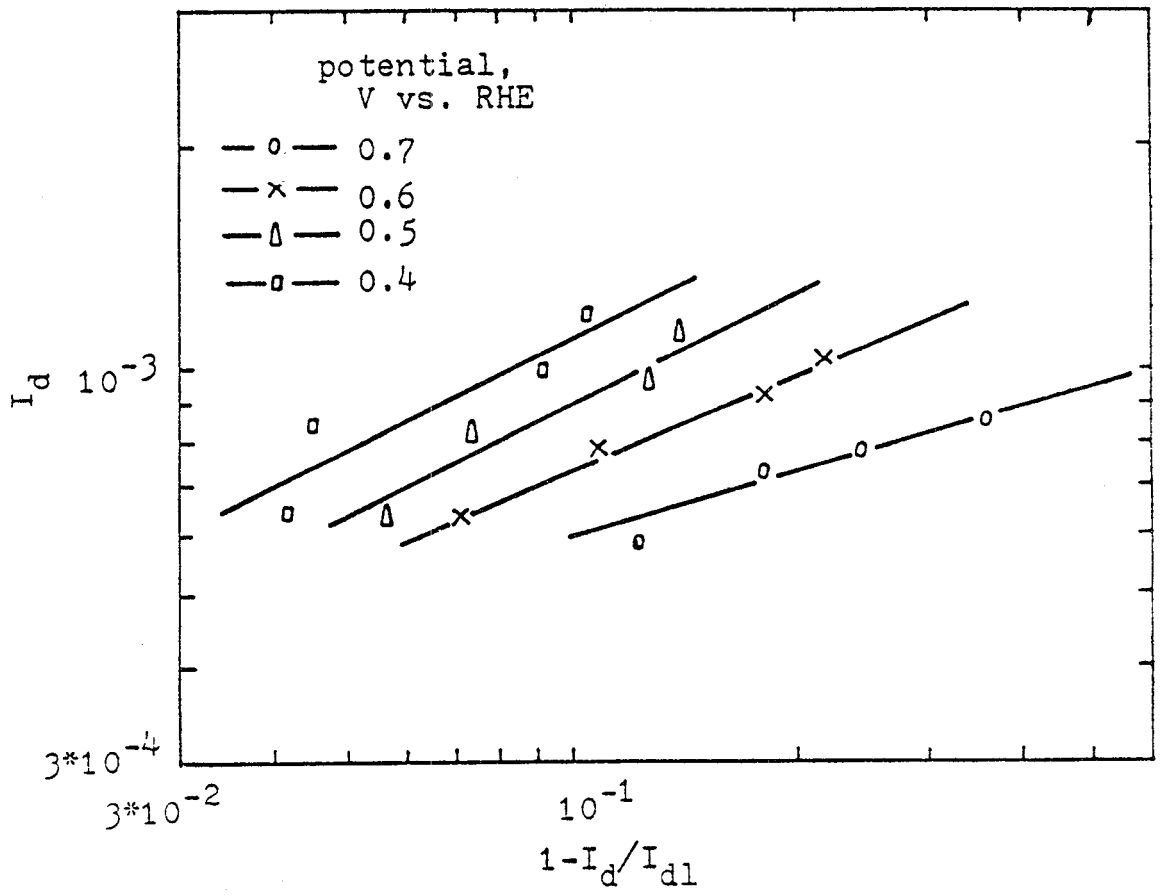

Fig. 12 Plot of log I_d vs. log(1 - I_d/I_{dl}). Data were obtained from the rotating ring-disk electrode experiments for oxygen reduction at Pt in 0.05 M TFMSA.

Mechanism of Oxygen Reduction at Platinum in TFMSA

For the reaction order of oxygen not equal to one, the mass transfer corrected Tafel equation is:

$$E = \frac{2.3RT}{\alpha F} \log I_o - \frac{2.3RT}{\alpha F} \log I_d \left(\frac{I_{d1}}{I_{d1} - I_d}\right)^m \qquad (5)$$

The plot of E vs. log $I_d[I_{d1}/(I_{d1}-I_d)]^m$ should be independent of ω, if m is chosen properly. The plots with m=0.5 for oxygen reduction at platinum in TFMSA and in 1M TFMSA containing three concentrations of phosphoric acid are shown in Fig. 13 and 14, respectively. These plots are independent of ω. At a given potential, the reduction current decreased as the concentration of TFMSA of of phosphoric acid increased. The decrease in the oxygen reduction current in concentrated TFMSA is probably due to a lower oxygen solubility and/or higher anion adsorption. The decrease in the oxygen reduction current with the addition of phosphoric acid is due to the electrochemical active sites being blocked by the adsorption of phosphate ions.

Based on the proposed mechanism (21,25), the reaction order of one-half with respect to oxygen can be explained by considering a fast dissociation step (large k_1 and k_2 in Fig. 15) and that step 3 is rate determining (small k_3). By assuming that the adsorption of oxygen is under Langmuir condition, the disk current can be expressed by :

$$I_d = K[H^+][O_2]^{1/2} \exp\left[-\frac{\alpha F}{RT} E\right] \qquad (6)$$

In the above equation I_d is proportional to $[O_2]^{1/2}$.

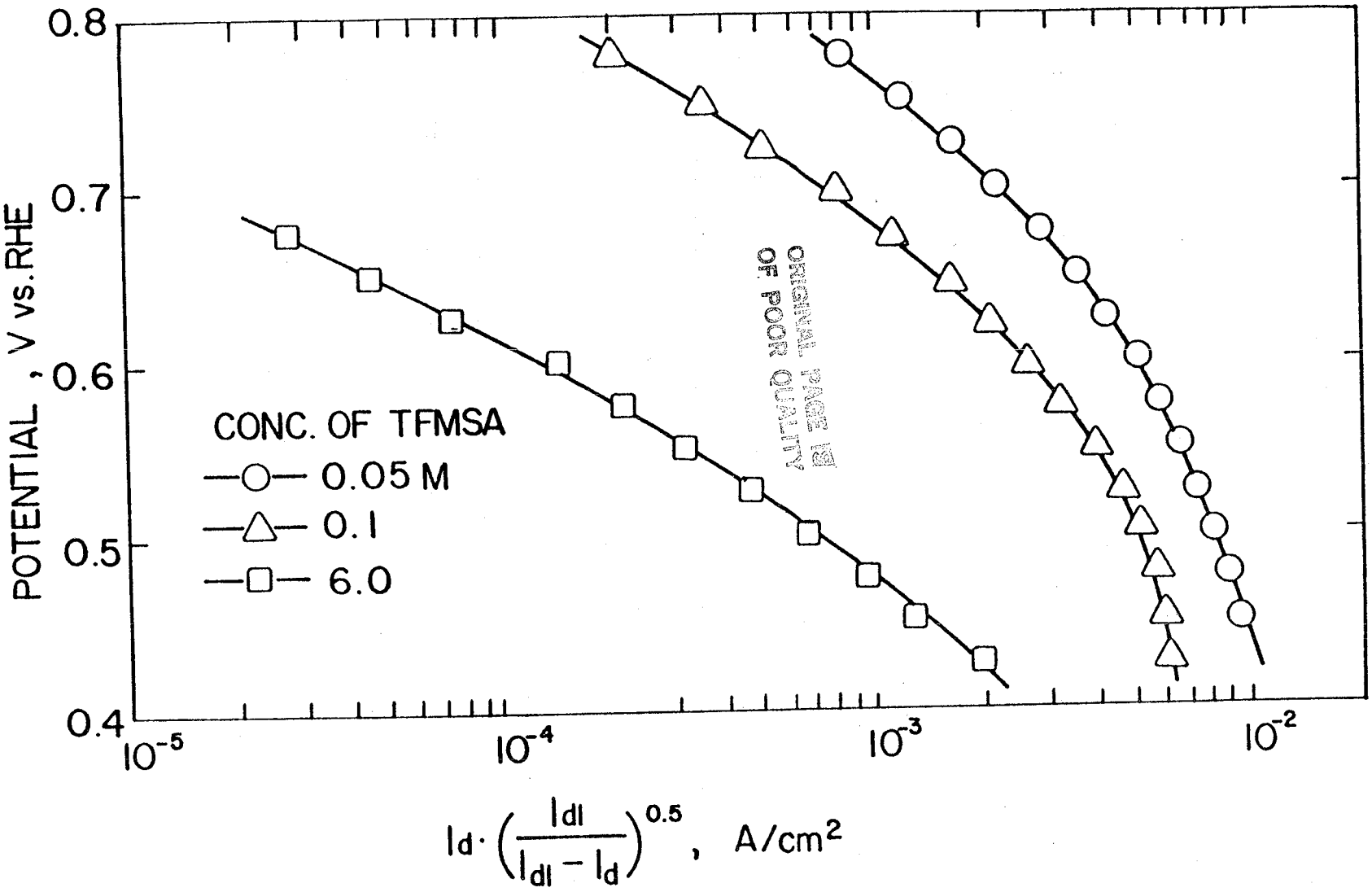

Fig. 13 The plot of potential against log $I_d[I_{d1}/(I_{d1} - I_d)]^{1/2}$ for oxygen reduction at Pt in different concentrations of TFMSA. This plot is independent of ω over the range of (400–3600 rpm).

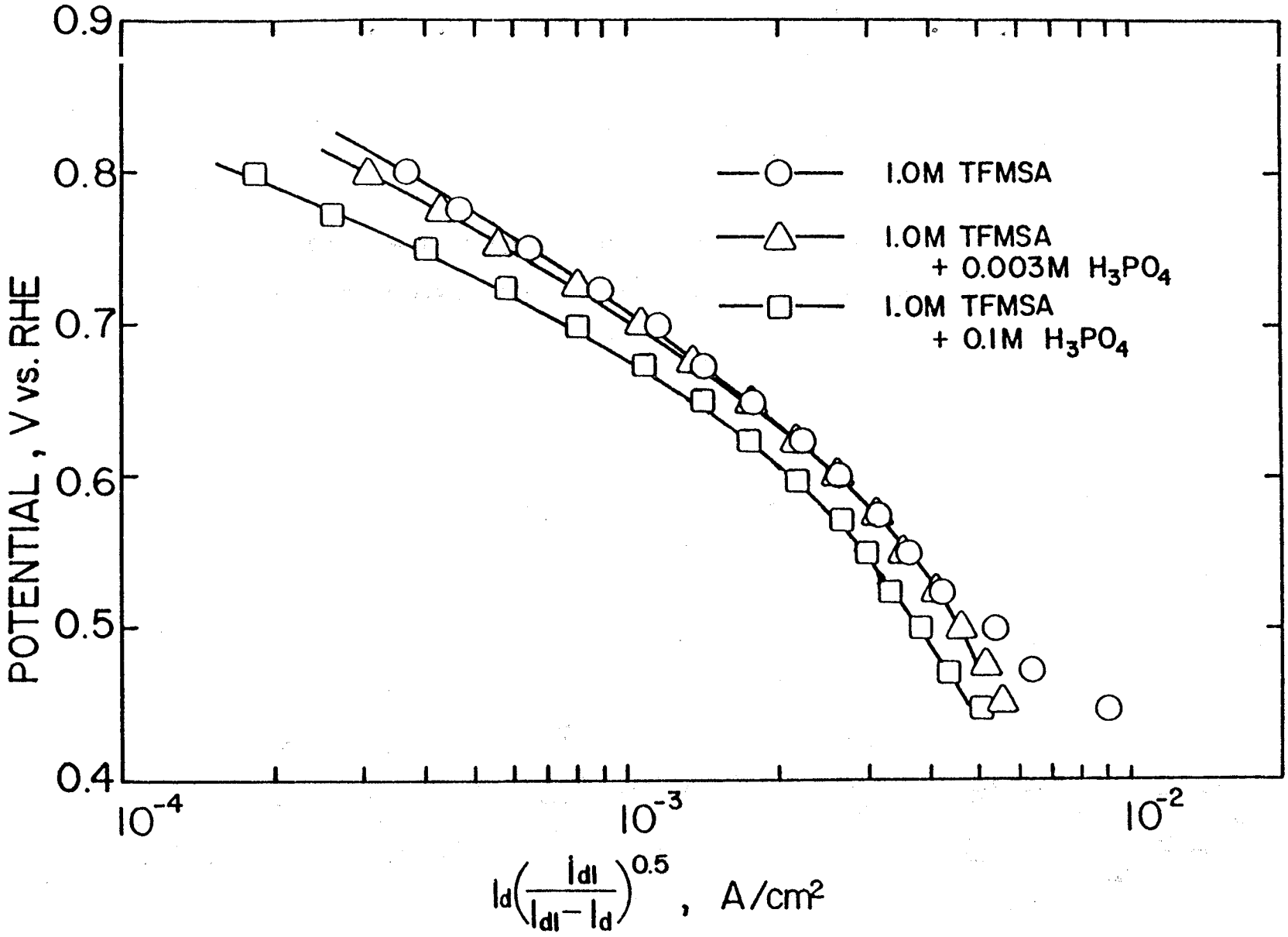

Fig. 14 The plot of potential against log $I_d[I_{d1}/(I_{d1}-I_{d1})]^{1/2}$ for oxygen reduction at Pt in 1.0 M TFMSA with the additives of H_3PO_4. This plot is independent of ω over the range of (400-3600 rpm).

Possible Mechanism of Oxygen Reduction at Pt in TFMSA :

Under Langmuir adsorption condition , $\theta \neq \theta$ (E)

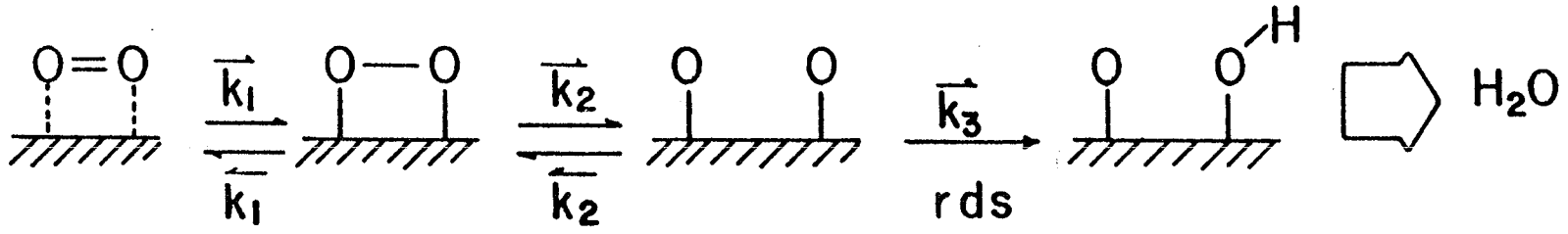

Fig. 15 Possible Mechanism of Oxygen Reduction at Pt in TFMSA:

Under Langmuir adsorption condition, $\theta \neq \theta$ (E)

Conclusions

From the rotating ring-disk electrode experimental data of oxygen reduction at platinum in TFMSA, it can be concluded that (i) a lower oxygen reduction current and a larger amount of hydrogen peroxide were observed for the oxide-covered platinum surface as compared to the oxide-free surface; (ii) a half reaction order with respect to the oxygen concentration was obtained; (iii) on the basis of the present experimental results, a reaction mechanism involving the fast dissociative adsorption of oxygen followed by the slow first charge transfer step was proposed for oxygen reduction at platinum in TFMSA.

III. TRANSPORT PROPERTIES OF PHOSPHORIC ACID ELECTROLYTE

3.1 LITERATURE REVIEW

The transport properties of the phosphoric acid electrolyte are needed to study the electrode kinetics of oxygen reduction reaction and to optimize the fuel cell performance. Among these, the electric conductivity, viscosity, diffusivity and solubility of oxygen in the electrolyte are the most important properties.

Electric Conductivity

Several sets of conductivity data for phosphoric acid at various concentrations and temperatures are available in the literature. Some of the early data are presented in the Monsanto Technical Bulletin (26), which also includes unpublished data of Helmer et al. (27). Increased attention has been shown recently in obtaining conductivity at high concentrations and temperatures. (28-34); such an emphasis has left a gap in the literature on the data of conductivity and other properties. Table 1 summarize the available data of electric conductivity (35). It is evident that over the concentrations range of 0-85% phosphoric acid, there are no data available for temperatures greater than 25°C. Also, for the concentrations range of 85 - 100% H_3PO_4, no data are available for temperatures greater than 150°C. A more complete set of data is needed.

It is suggested that for dilute phosphoric acid concentrations, the major contribution to conductivity must come from the Stokesian ion transport, whereas in more concentrated solutions the major contribution to conductance comes from proton switch (chain type) mechanism. The existence of proton switch mechanism in water is well established. There are evidences which support the existence of proton switch mechanism in H_3PO_4.

Greenwood and Thompson (32) considered the self dissociation of anhydrous phosphoric acid according to the equilibria:

$$2\ H_3PO_4 \rightleftarrows H_4PO_4^+ + H_2PO_4^- \quad \text{[fast]} \tag{7}$$

$$2\ H_3PO_4 \rightleftarrows H_3O^+ + H_3P_2O_7^- \quad \text{[slow]} \tag{8}$$

The first equilibrium is labelled fast because the conductivity of freshly melted phosphoric acid is high ($7.68 \times 10^{-2}\ \Omega^{-1}\ cm^{-1}$). Since the ionic dissociation is very small (as low as 4.5% for the hemi-hydrate), and the viscosity is high for H_3PO_4, the observed high conductivity can not be explained in terms of Stokesian diffusion. This means that other type of transport mechanism must have a significant contribution to the conductivity. Gileadi (36) has represented the switch mechanism for $H_2PO_4^-$ migration as shown in Fig. 16, where phosphoric acid molecules and phosphate anions are associated by hydrogen bonds. Under an electric field, the proton tends to migrate. According to Gileadi, the switching of protons can be accomplished by either rotating or the rearrangement of the internal bonds as shown in the figure. The latter being more favorable considering the large energy that would be required to reorient the associated phosphoric acid molecules. The same view point of a hydrogen bonded network has also been proposed by Akiyama et al. (34). To support their hypothesis, these authors calculated the molar conductance of concentrated phosphoric acid assuming both water and phosphoric acid contribute to conduction. The calculated molar conductance was constant between 60 and 76% P_2O_5 content. Further evidence for proton migration comes from the work of Greenwood and Thompson (32). They hypothesize that if a certain H-bonding structure is responsible for proton migration, then the conductivity would decrease if the probability of H-bond formation is reduced. To prove this, these authors prepared the co-ordinated complex of H_3PO_4 and BF_3.

Table 1. Specific Conductivity of Phosphoric Acid as a Function of Concentration and Temperature. Compiled from References 37, 7, 8, 9.

unit: $ohm^{-1} \cdot cm^{-1}$

0°-45.0°C

Temp °C	0°	18°	25°	29.3	30°	35	40°	45.0
wt% H_3PO_4								
1			0.0102					
2			.0175					
3			.0226					
4			.0281					
5	0.0409		.0334					
10	.0615	0.0566	.0617					
15	.0772	.0850	.0918					
20	.0934	.1129	.1236					
25	.1096	.1402	.1553					
30	.1259	.1654	.1836					
35	.1415	.1858	.2068					
40	.1472	.2010	.2236					
45	.1488	.2087	.2336					
50	.1427	.2073	.2324					
55	.1317	.1978	.2263					
60	.1195	.1833	.2117					
65	.1052	.1650	.1905					
70	.0844	.1436	.1656					
75	.0608	.1209	.1373					
80	.0460	.0979	.1118					
85	.0348	.0780	.0907					
85.10	.							
85.79	.		.0888		0.102		0.134	
88.47	.		.0801		.0928		.122	
88.68								
89.10								
90	.0245		.0673	0.0850				
90.45								
90.54			.0734		.0858		.114	
91.42								
92.75								
93.73			.0641		.0756		.102	
95	.0184		.0612	.0696				
96.97								
97.07			.0535		.0639		.0870	
97.96								
98.93								
99.57								
99.75			.0447		.0534		.0740	
99.72								
100			.04675		.05589	.06598	.07680	.08836
101.63			.0355		.0432		.0606	
104.43			.0210		.0262		.0389	
106.77			.0115		.0148		.0234	
110.49			.00336		.00471		.00865	
112.58			.00175		.00256		.00495	
115.66			.000860		.00125		.00245	
118.16			.000183		.000282		.000597	

Table 1. SPECIFIC CONDUCTIVITY (continued)

unit: $ohm^{-1}\ cm^{-1}$

	50.0°-170.42°								
Temp °C	50°	55°	60.0	65.0	130.00	140.12	150.25	160.92	170.42
wt% H_3PO_4									
1									
2									
3									
4									
5									
10									
15									
20									
25									
30									
35									
40									
45									
50									
55									
60									
65									
70									
75									
80									
85									
85.10					0.4904	0.5299	0.5685		
85.79	0.167		0.202						
88.47	.154		.189						
88.68									
89.10					.4747	.5169	.5589	0.6033	
90									
90.45					.4702	.5133	.5568	.6020	0.6411
90.54	.146		.180						
91.42					.4665	.5098	.5536	.5996	.6397
92.75					.4606	.5055	.5495	.5960	.6384
93.73	.131		.165						
95									
96.97					.4369	.4816	.5280	.5763	.6184
97.07	.115		.145						
97.96					.4274	.4717	.5178	.5664	.6082
98.93					.4137	.4578	.5029	.5516	.5936
99.57					.4019	.4461	.4904	.5386	.5819
99.75	.0975		.124						
99.72					.3986	.4421	.4872	.5347	.5774
100	.1013	0.1138	.1270	0.1406					
101.63	.0814		.106						
104.43	.0550		.0744						
106.77	.0346		.0490						
110.49	.0141		.0220						
112.58	.00855		.0137						
115.66	.00429		.00699						
118.16	.00108		.00183						

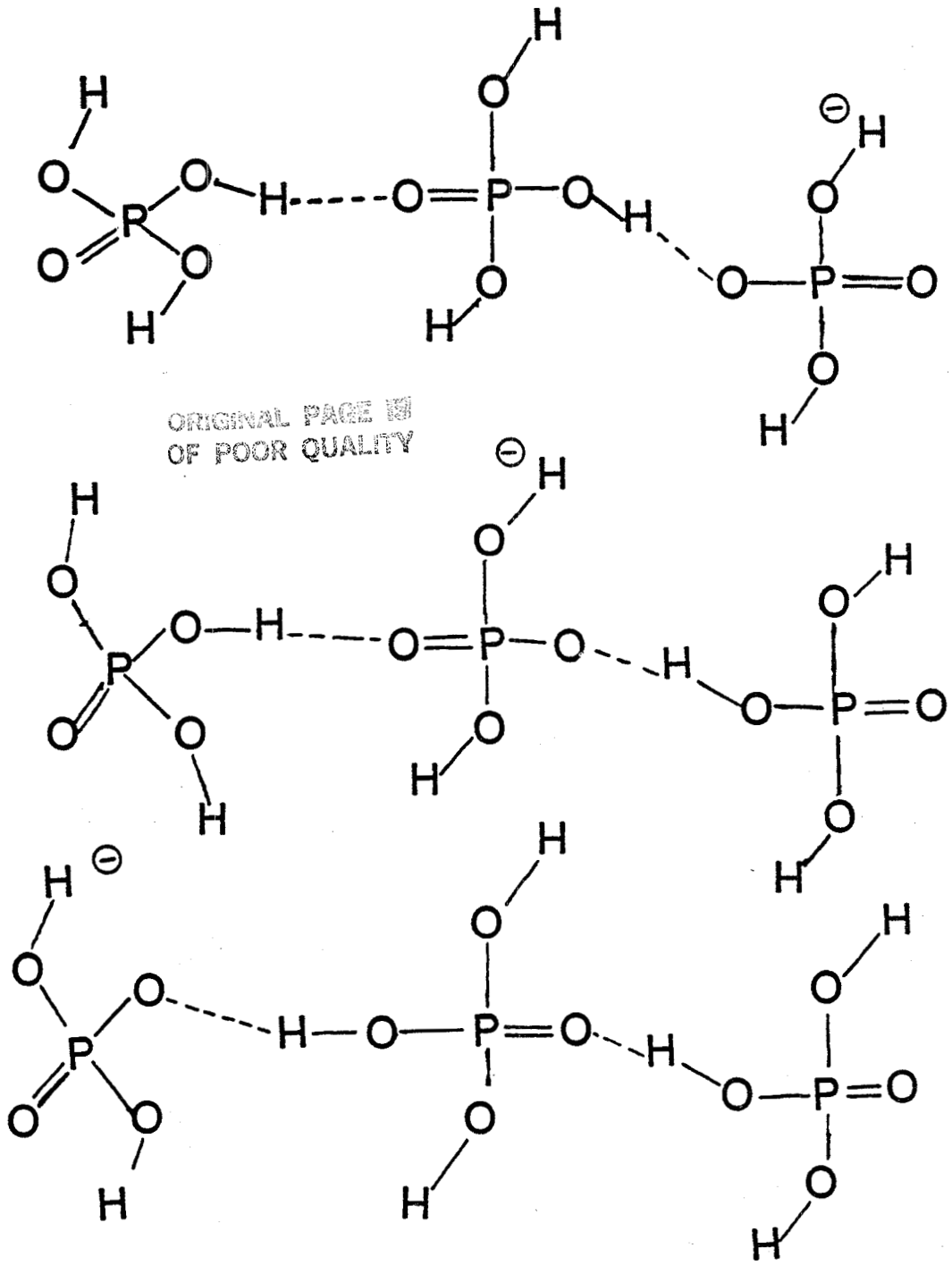

Fig. 16 A schematic diagram of the hopping mechanism in H_3PO_4

The viscosity and electric conductivity of these complexes were markedly different from those of H_3PO_4. These results could be explained only by the presence of a hydrogen bonding network in H_3PO_4. Munson (38) studies the effect of various ionic solutes on the conduction of H_3PO_4 and came to the same conclusions as those of Greenwood and Thompson.

Kinetic Viscosity

The existing literature data on the kinematic viscosity of phosphoric acid are summarized in Table 3-2. The accuracy of the data is estimated to be ± 15%. Saji (40) reported viscosity data for concentrated phosphoric acids which deviated from that reported in Table 2; the difference occurs red because the acid was dehydrated by heating and contains higher proportions of Poly-acids. The effect of various impurities like Al, Fe, k, Ca, Mg on the viscosity of phosphoric acid has been discussed by Cate and Deming (41), and by Dahlgren (42). The cations increase the viscosity, while anions have negligible effect. The effects are negligible at the concentration below 0.1% by weight of the impurity; the magnitude of the effect is also dependent on the concentration of the phosphoric acid.

As seen in Table 2, there are some gaps in the kinematic viscosity data. For 0-85% H_3PO_4, no data are available for temperature greater than 180°C. The kinematic viscosity data have been correlated by Kondrachenko et al. (43-44) with a polynomial equation for the concentration range 90-103% H_3PO_4 at temperature from 20 to 90°C.

Table 2 KINEMATIC VISCOSITY OF PHOSPHORIC ACID SOLUTIONS

% H_3PO_4	Temperature, °C																	
	20	25	30	40	50	60	70	80	90	100	110	120	130	140	150	160	170	180
0	1.0	0.90	0.80	0.66	0.56	0.48	0.42	0.37	0.33	0.30								
5	1.1	0.99	0.89	0.74	0.63	0.54	0.47	0.42	0.37	0.33								
10	1.2	1.1	0.99	0.83	0.71	0.64	0.54	0.47	0.42	0.38								
15	1.4	1.2	1.1	0.94	0.81	0.69	0.61	0.56	0.47	0.43								
20	1.6	1.4	1.3	1.1	0.92	0.78	0.69	0.60	0.54	0.48								
25	1.8	1.6	1.5	1.2	1.0	0.89	0.79	0.69	0.61	0.55								
30	2.2	1.9	1.7	1.4	1.2	1.0	0.90	0.79	0.70	0.62								
35	2.6	2.2	2.0	1.6	1.3	1.1	1.0	0.90	0.79	0.71								
40	3.0	2.6	2.3	1.9	1.5	1.3	1.2	1.0	0.90	0.81								
45	3.6	3.1	2.7	2.2	1.8	1.5	1.3	1.2	1.0	0.92								
50	4.3	3.7	3.3	2.6	2.1	1.8	1.6	1.4	1.2	1.1								
55	5.3	4.5	4.0	3.2	2.5	2.1	1.9	1.6	1.4	1.2	1.1							
60	6.6	5.6	5.0	3.9	3.1	2.5	2.2	1.9	1.7	1.4	1.3							
65	8.4	6.8	6.2	4.9	3.8	3.1	2.6	2.3	2.0	1.7	1.5	1.4						
70	11	9.2	7.8	6.1	4.7	3.9	3.2	2.7	2.4	2.0	1.8	1.6						
75	15	12	10	7.8	5.9	4.8	3.9	3.3	2.8	2.4	2.1	1.9	1.7					
80	20	17	14	10	7.6	6.2	4.9	4.1	3.4	3.0	2.6	2.3	2.0	1.8				
85	28	23	19	14	10	8.1	6.3	5.1	4.2	3.8	3.2	2.8	2.4	2.2	1.9			
90	41	34	27	19	14	11	8.3	6.5	5.4	4.8	4.1	3.5	3.0	2.8	2.4			
95	68	55	42	30	20	15	12	8.7	7.3	6.2	5.2	4.4	3.8	3.3	3.0	2.6	2.3	2.1
100	140	100	81	53	36	25	19	14	11	9.2	7.2	6.2	5.2	4.5	4.1	3.5	3.2	2.9
105	600	440	330	173	110	70	50	33	25	19	15	12	9.6	8.0	7.1	6.0	5.2	4.5
110		2200	1600	810	410	270	170	100	67	50	38	29	22	18	15	13	10	8.8
115						1500	1000	600	380	250	190	120	95	68	54	41	34	28
118								2000	1200	830	550	400	320	210	170	130	107	87

Diffusivity and Solubility of Oxygen in Phosphoric Acid Electrolyte

Oxygen solubility in concentrated phosphoric acid solution was first determined by Gubbins and Walker (45) using a gas chromatrographic method. Yatskovskii and Fedotov (46) measured the solubility and diffusivity of oxygen at 25°, 45° and 60°C as a function of the phosphoric acid concentration (up to 85% by weight) using an electrochemical method; in this method, a platinum wire was sealed into a capillary and oxygen diffused to the electrode through the open end of the capillary. Klinedinst et al. (47) extended the measurement from 85% to 96% acid concentrations. The authors used a diffusion current-time curve to a platinum wire electrode to determine the oxygen solubility and diffusivity.

There was reasonable agreement between the results of Gubbins et al. and those of Yatskovskii et al.; in both these investigations the solubility decreased with concentrations of the acid. The results of Klinedinst et al. were consistent with those of Gubbins and Walker at a given concentration and temperature, but the concentration dependence was exactly opposite to that observed by Gubbins. The activation energy for oxygen diffusivity reported by Klinedinst was also different from the value calculated by Yatskovskii et al. Unfortunately, a critical comparison of these results is not possible since Klinedinst did not carry out measurement for the concentrations lower than 85% at 25°C.

3-2 EXPERIMENTAL

In the present work, the electric conductivity and kinematic viscosity of phosphoric acid electrolyte have been measured over a range of concentrations from 7% to 100%, and the temperatures from 25° to 200°C.

Electric Conductivity

Electrical conductivity data were measured with an A.C. conductivity bridge and conductivity cell (Beckman). The cell constant of the conductivity cell was calibrated with standard 0.01 N kCl solution.

The specific conductivity of phosphoric acid was measured over a concentration range of 0-100% and a temperature range of 25-200°C. The electrolytes were made from stock 85% phosphoric acid (Fisher). For concentrations 0-85% acid, the different solutions were diluted from 85% H_3PO_4 with distilled water. For concentrations greater than 85%, the solutions were made by concentrating purified acid inside a vacuum oven. The solution was poured into a three arm round-bottom flask, and immersed in an oil bath. A reflux column was used to condense any vapor at high temperatures (greater than 100°C.) A thermometer was used to monitor the temperature of the solution for each concentration, the specific conductivity data for different temperatures were taken at a 10°C temperature increment.

Kinematic Viscosity

Kinematic viscosity data were measured with a Canon-Fenske viscometer made by Industrial Glass Co. The time constants of the vocometers were calibrated against water and glycerol solutions at different temperatures. The range of concentrations measured for kinematic viscosity was the same as that of specific conductivity. The temperature range was slightly different; it was from 25 to 180°C. The measurement was carried out in a constant temperature air oven.

3.3 RESULTS

Electric Conductivity

The specific conductivity of phosphoric acid solution has been measured over a concentration range of 6-100% (by weight) and a temperature range of 25-200°C. The data are presented in graphical form in Figs. 17-22.

Figure 17 is a plot of specific conductivity as a function of concentrations at 25, 100 and 170°C. For each temperature, the curve exhibits a maximum at a certain concentration; this maximum shifts toward higher concentration with increasing temperature. Figures 18-22 are the

semi-logarithmic plots of specific conductivity versus reciprocal of absolute temperature at different concentrations. Figure 18 is for concentration range of 0.05 to 2.37 M phosphoric acid. It is seen that conductivity increases with temperature and that straight lines can be drawn for the conductivity at the low concentrations. At higher concentrations, the Arrhenius type correlation does not hold. This can be seen in Figs. 19-22; for there concentrations, a second order polynomial fit of ln k vs. 1/T should give a better description of the experimental data.

Kinematic Viscosity

The kinematic viscosity of phosphoric acid was measured for the concentration range of 6-100% and the temperature range of 25-180^{o}C. The data are presented graphically in Figs. 23-27.

Figure 23 is a plot of kinematic viscosity as a function of concentrations at 25, 100, and 170^{o}C. The kinetic viscosity increases exponentially as the concentration increases. However, the increases becomes less drastic at high temperatures. The kinetic viscosity decreases with increasing temperature. Figures 24-27 are the semi-logarithmic plots of kinematic viscosity versus reciprocal temperatures at different concentrations. The kinematic data seem to obey the Arrhenius law at the concentration and temperature range investigated.

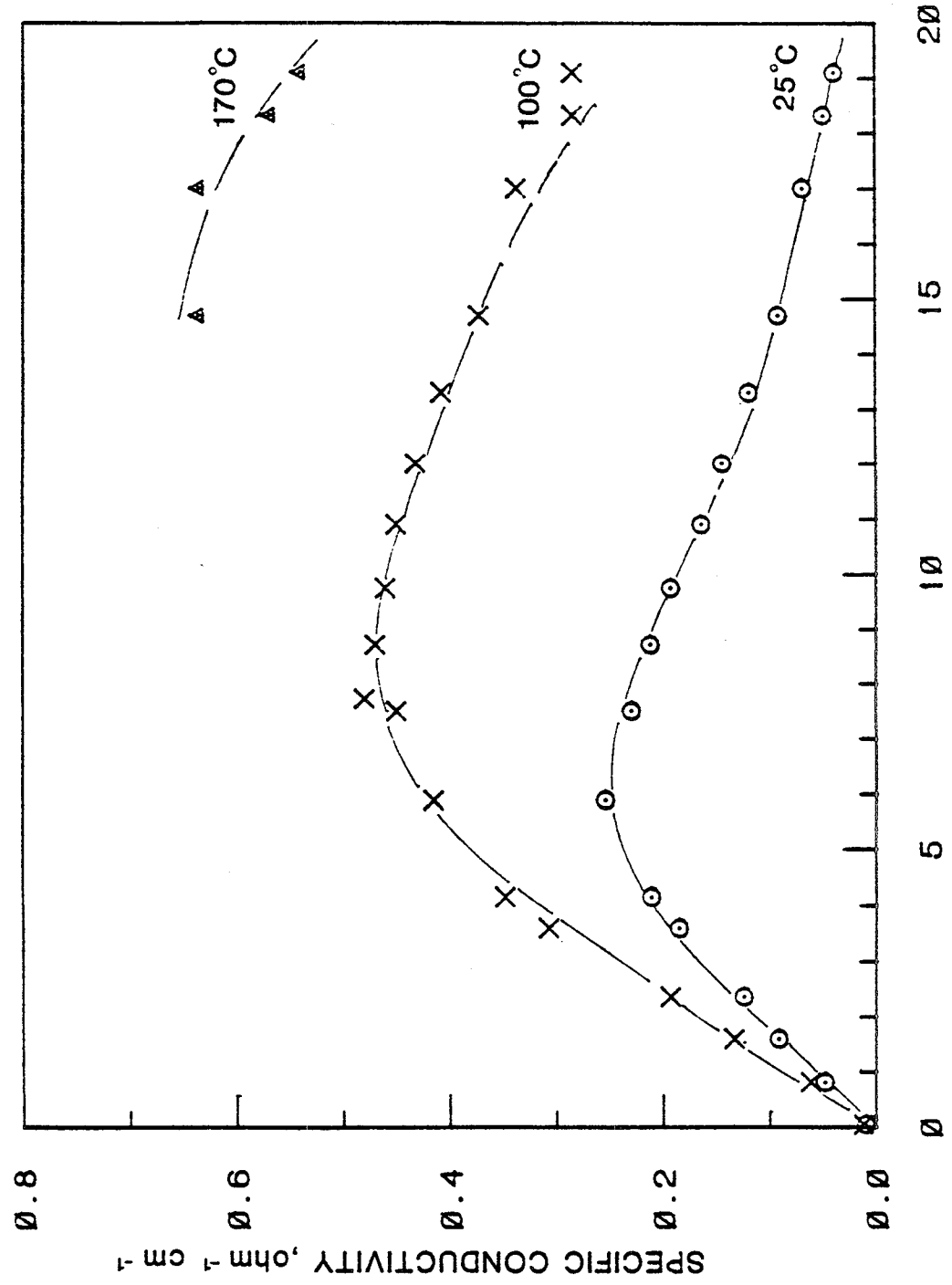

Figure 17 Effect of concentrations on conductivity at 25°, 100°, 170°C

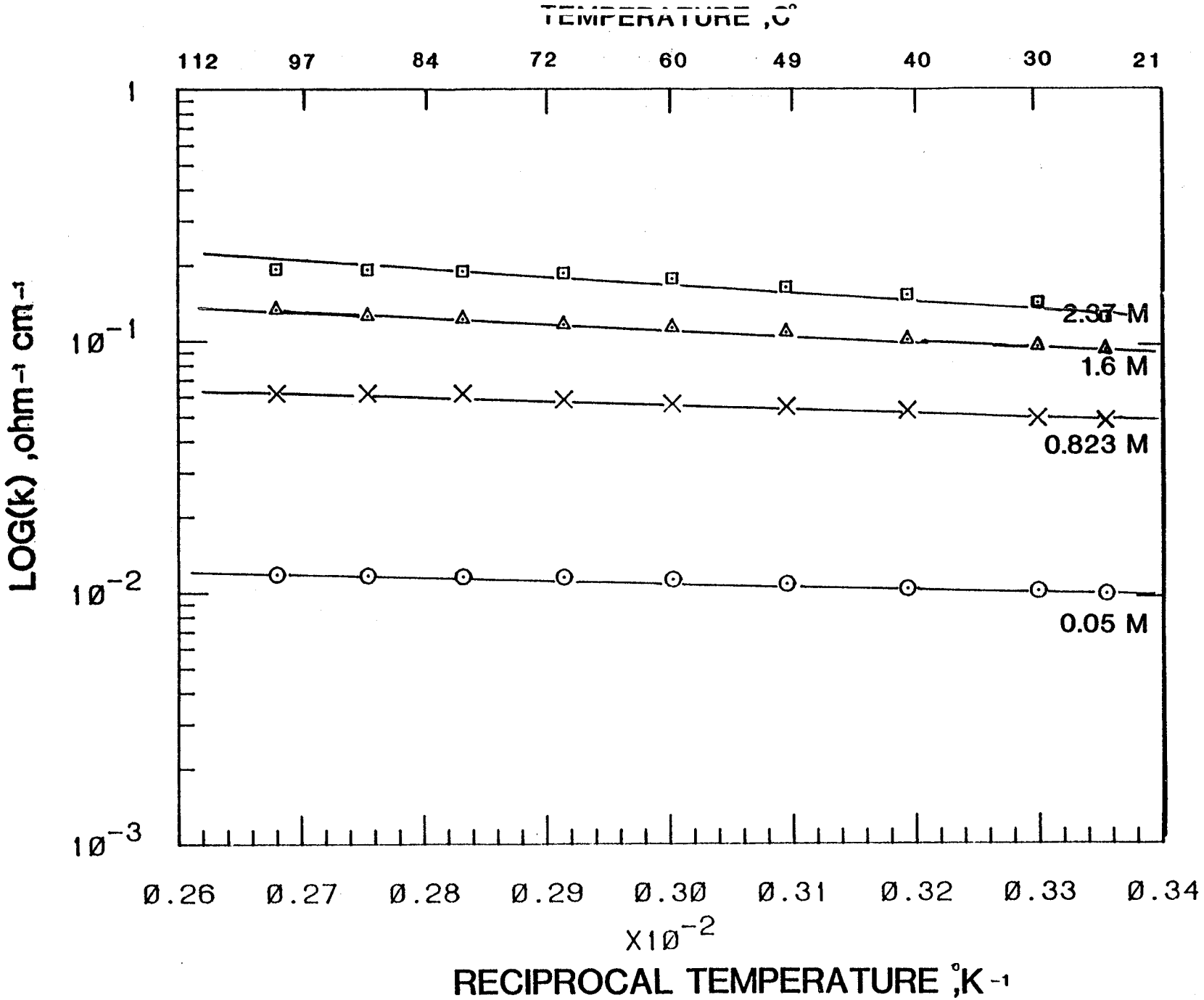

Figure 18 Plot of specific conductivity versus reciprocal temperatures at dilute concentrations

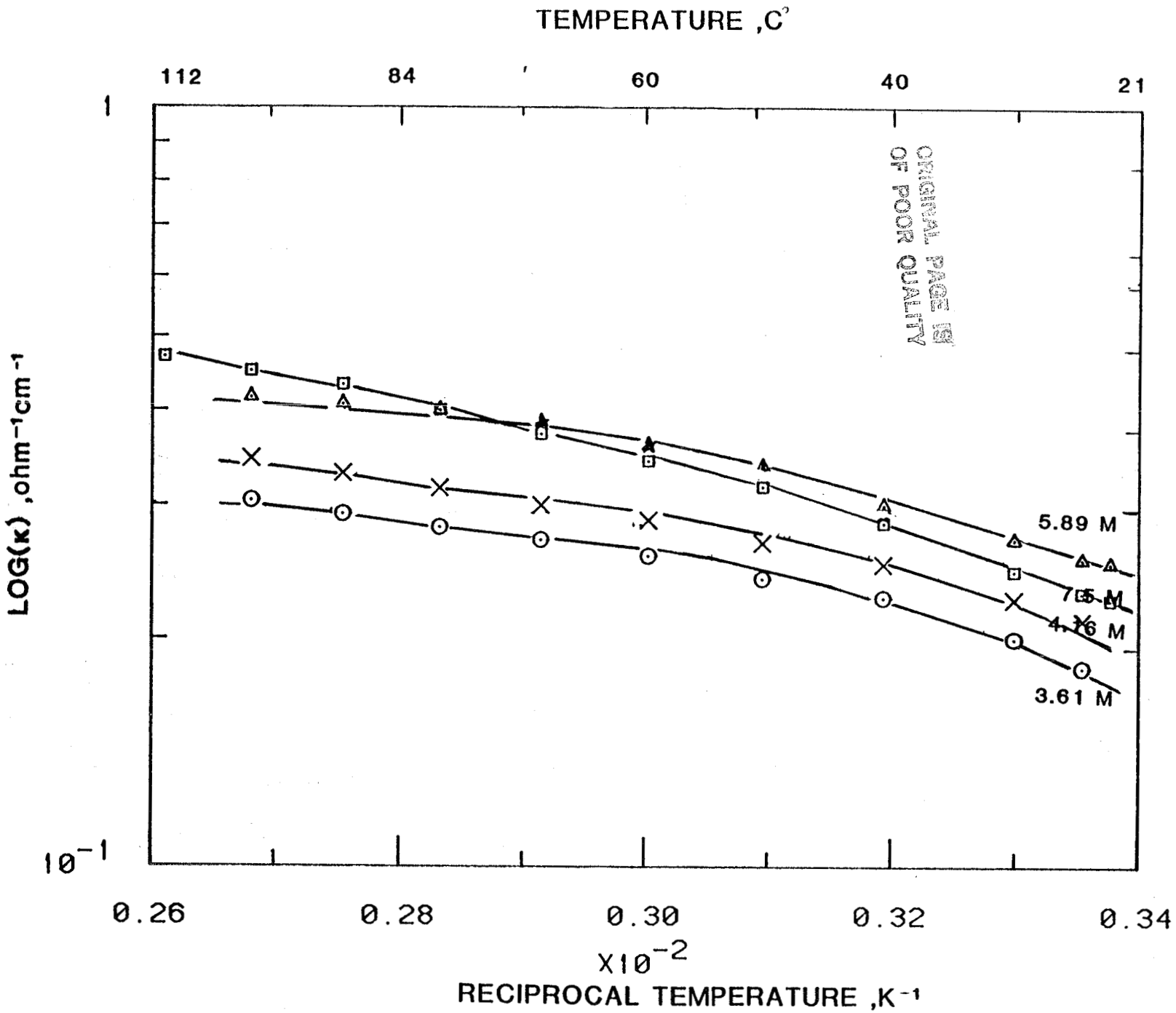

Figure 19 Plot of specific conductivity versus reciprocal temperatures at 3.6 to 6 M H_3PO_4

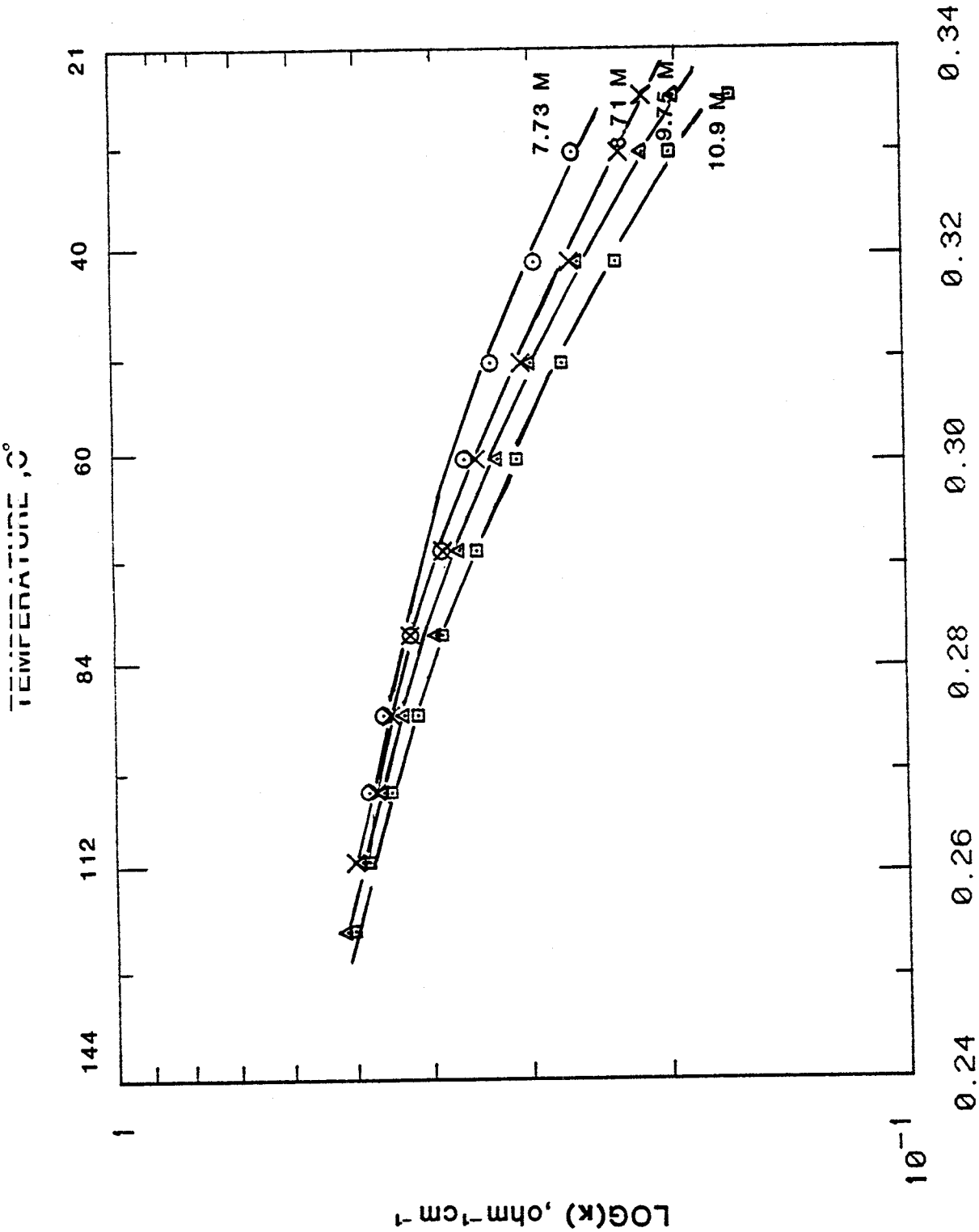

Figure 20 Plot of specific conducting versus reciprocal temperatures at 7.73 to 10.9 M H_3PO_4

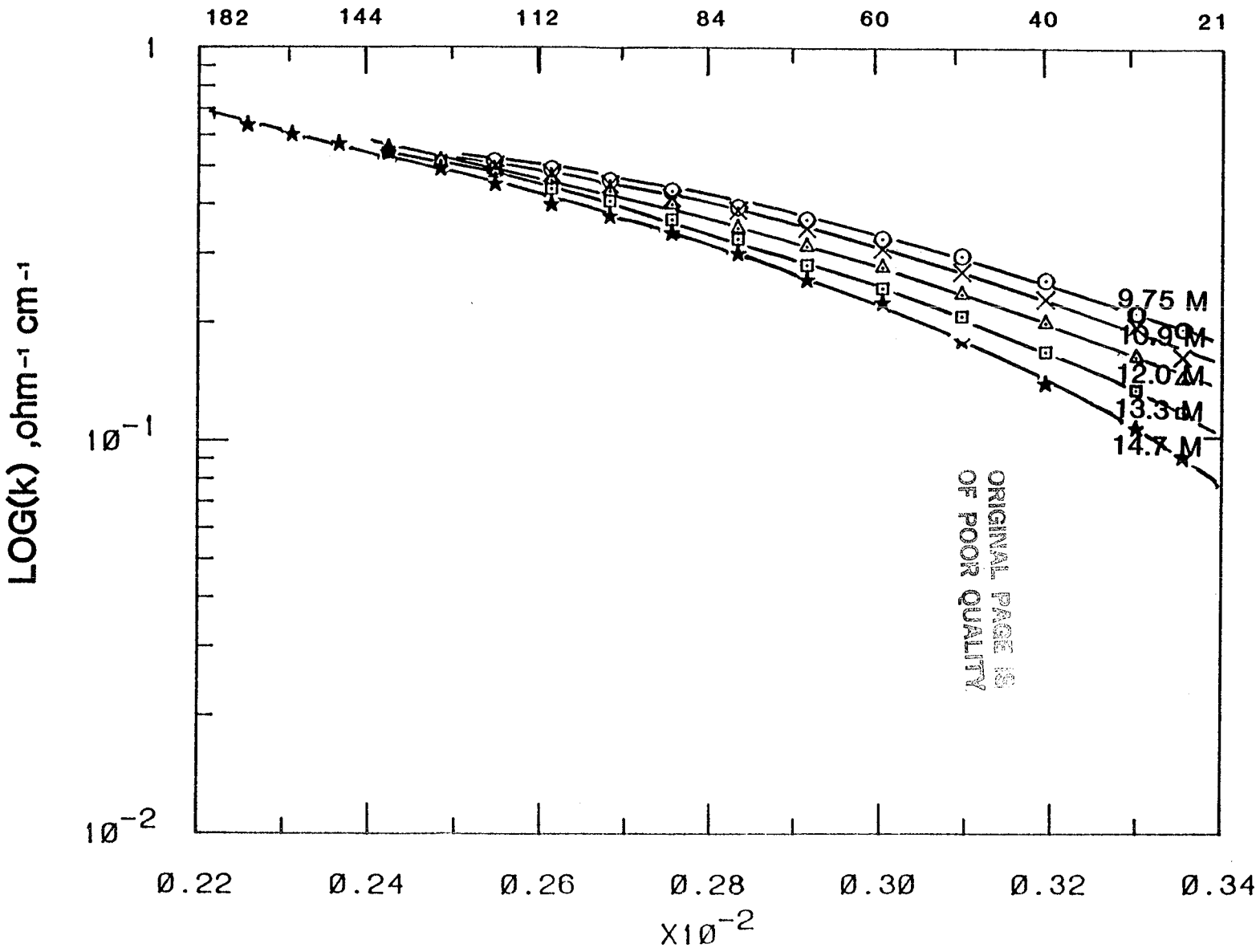

Figure 21 Plot of specific conductivity versus reciprocal temperature at 9.75 to 14.7 M H_3POP_4

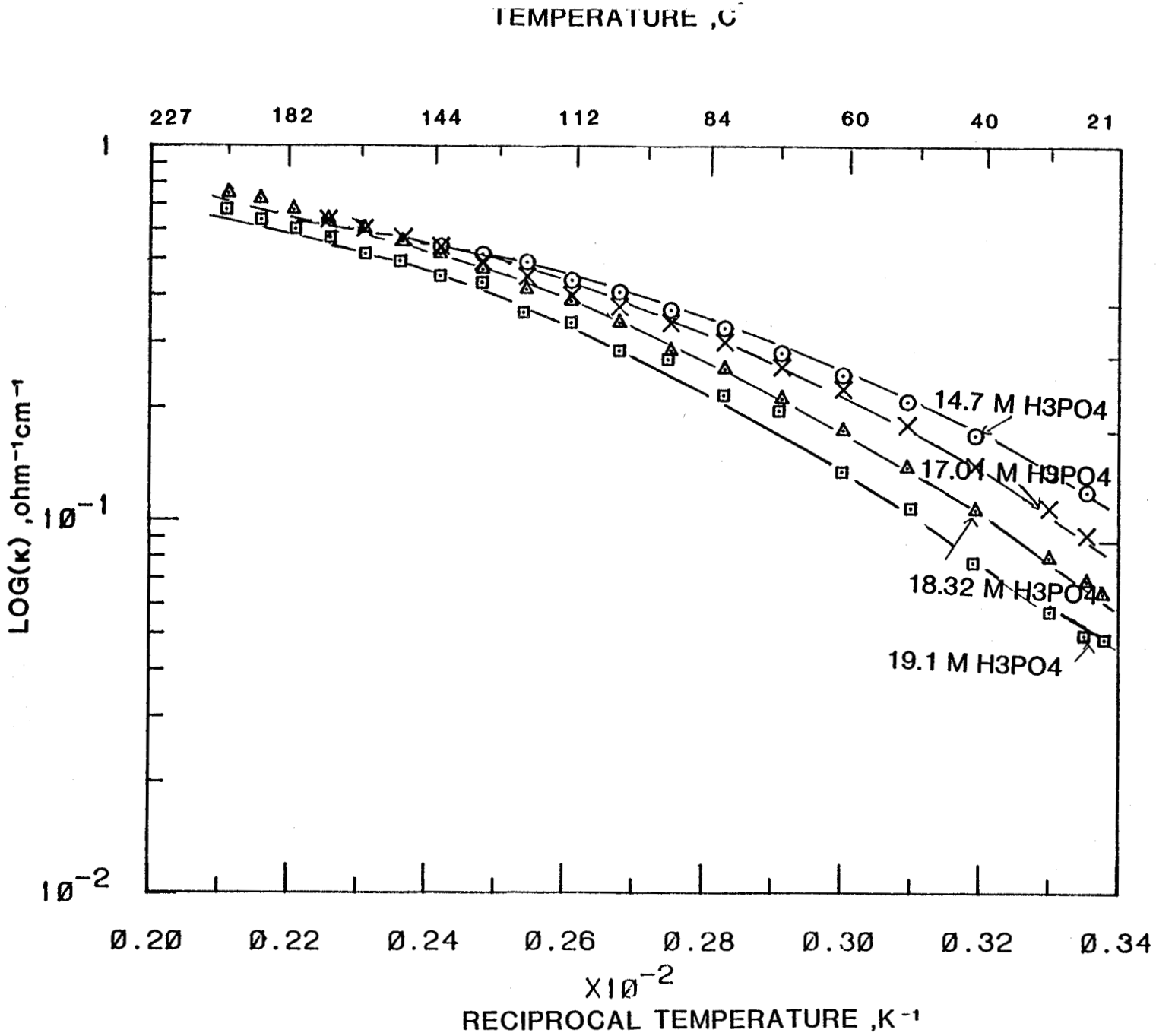

Figure 22 Plot of specific conductivity versus reciprocal temperature at concentrates H_3PO_4

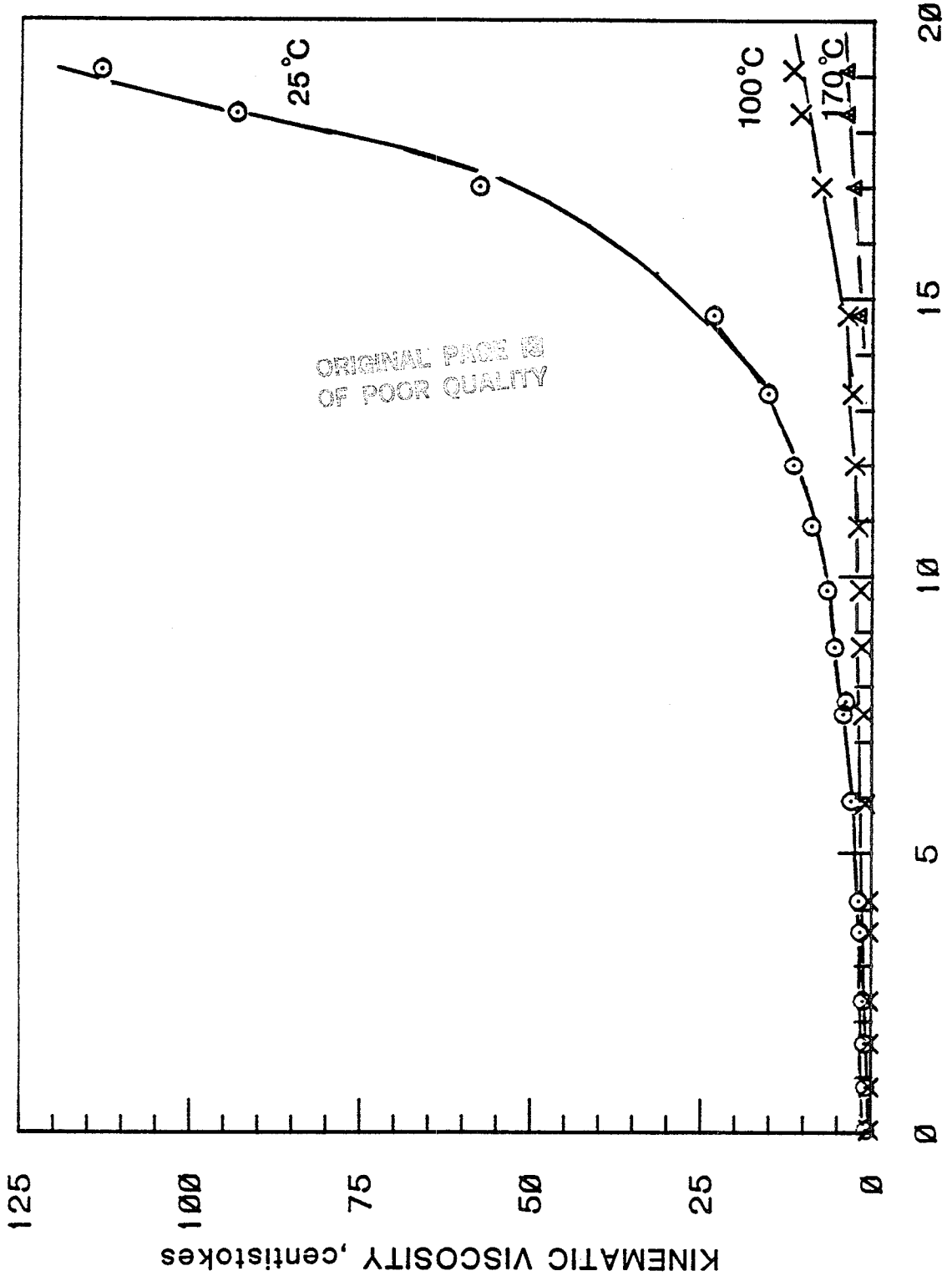

Figure 23 Effect of concentrations on kinematic viscosity at different temperatures

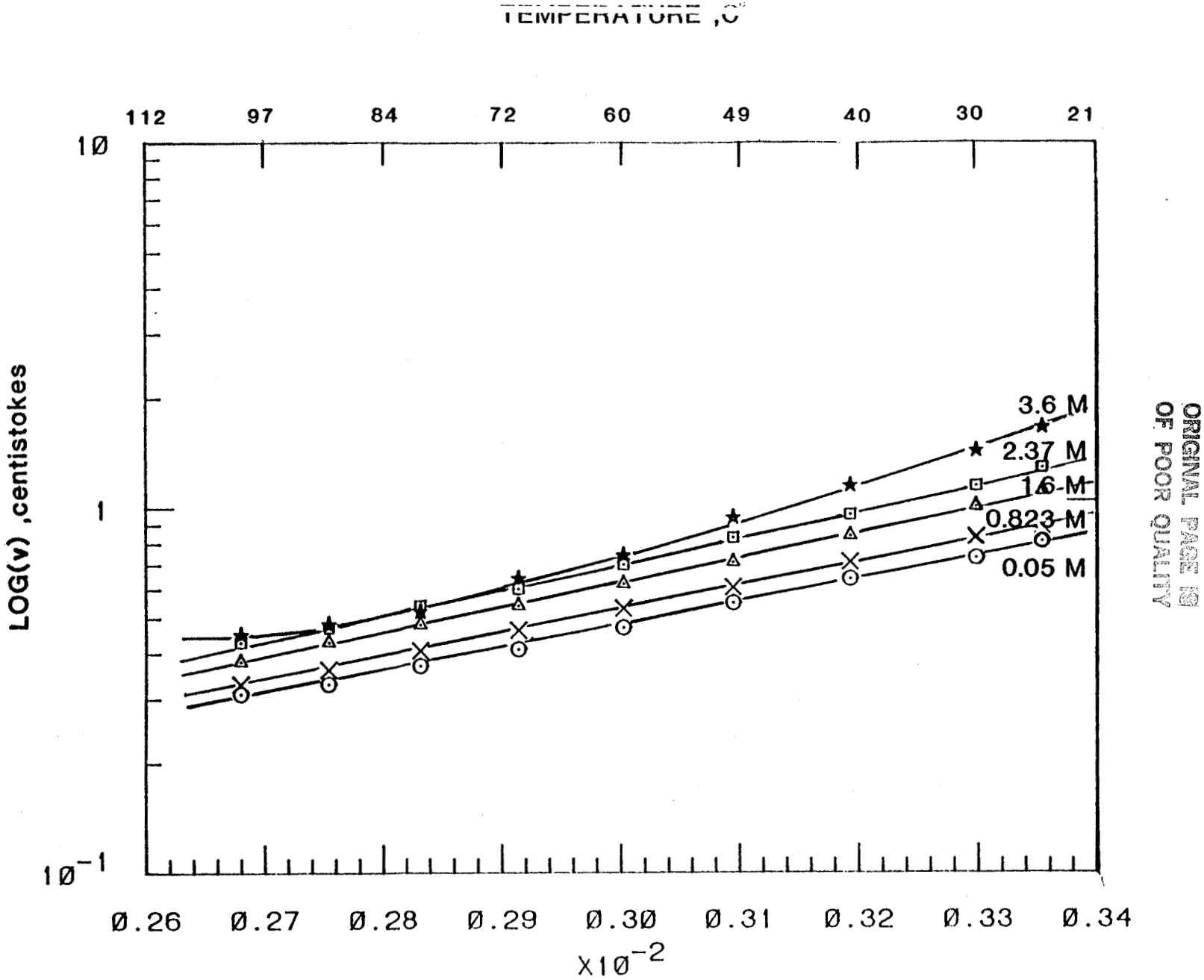

Figure 24 Plot of kinematic viscosity versus reciprocal temperature at dilute concentrations

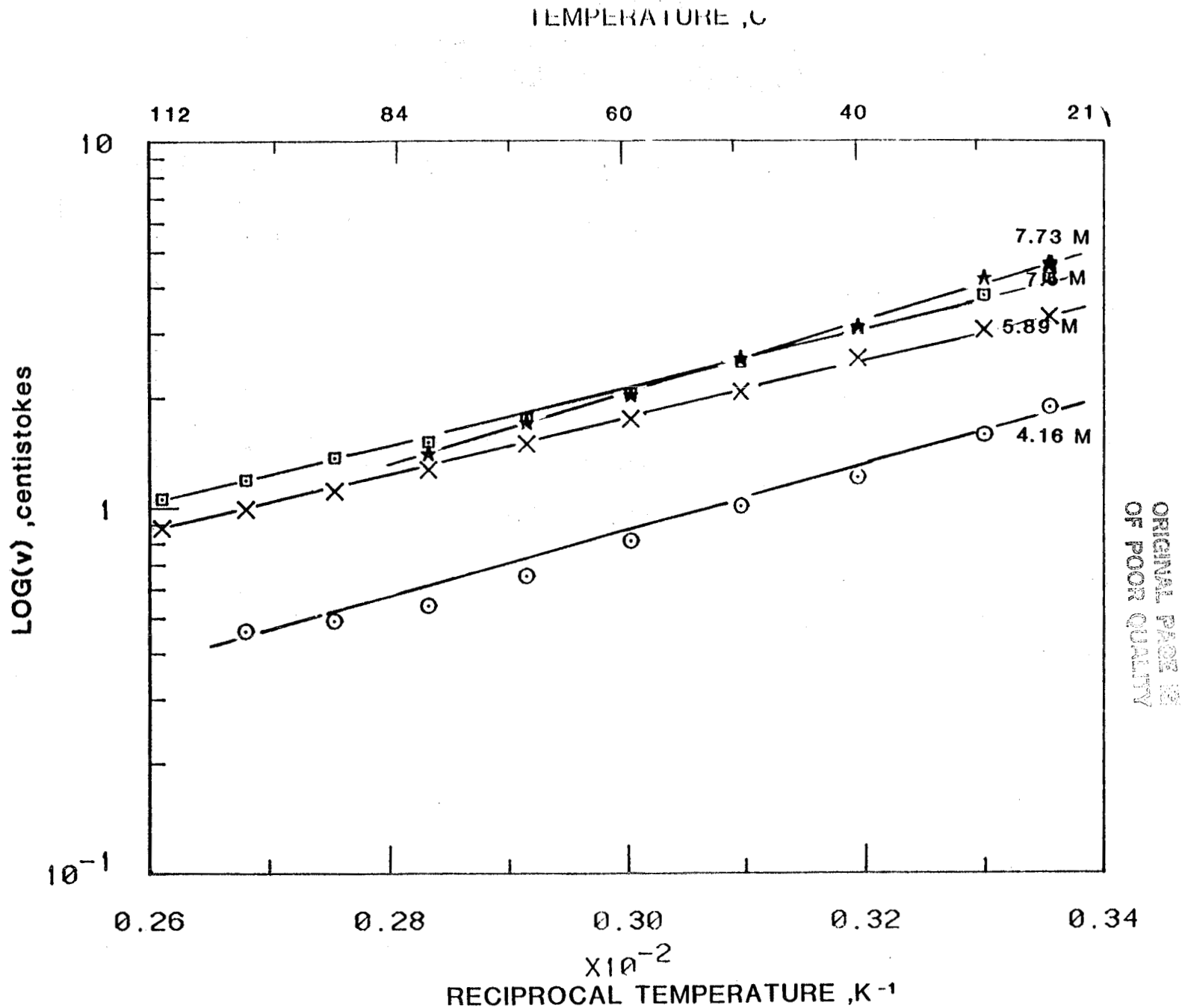

Figure 25 Plot of kinematic viscosity versus reciprocal temperatures at conc. range 4.16 to 7.73 M

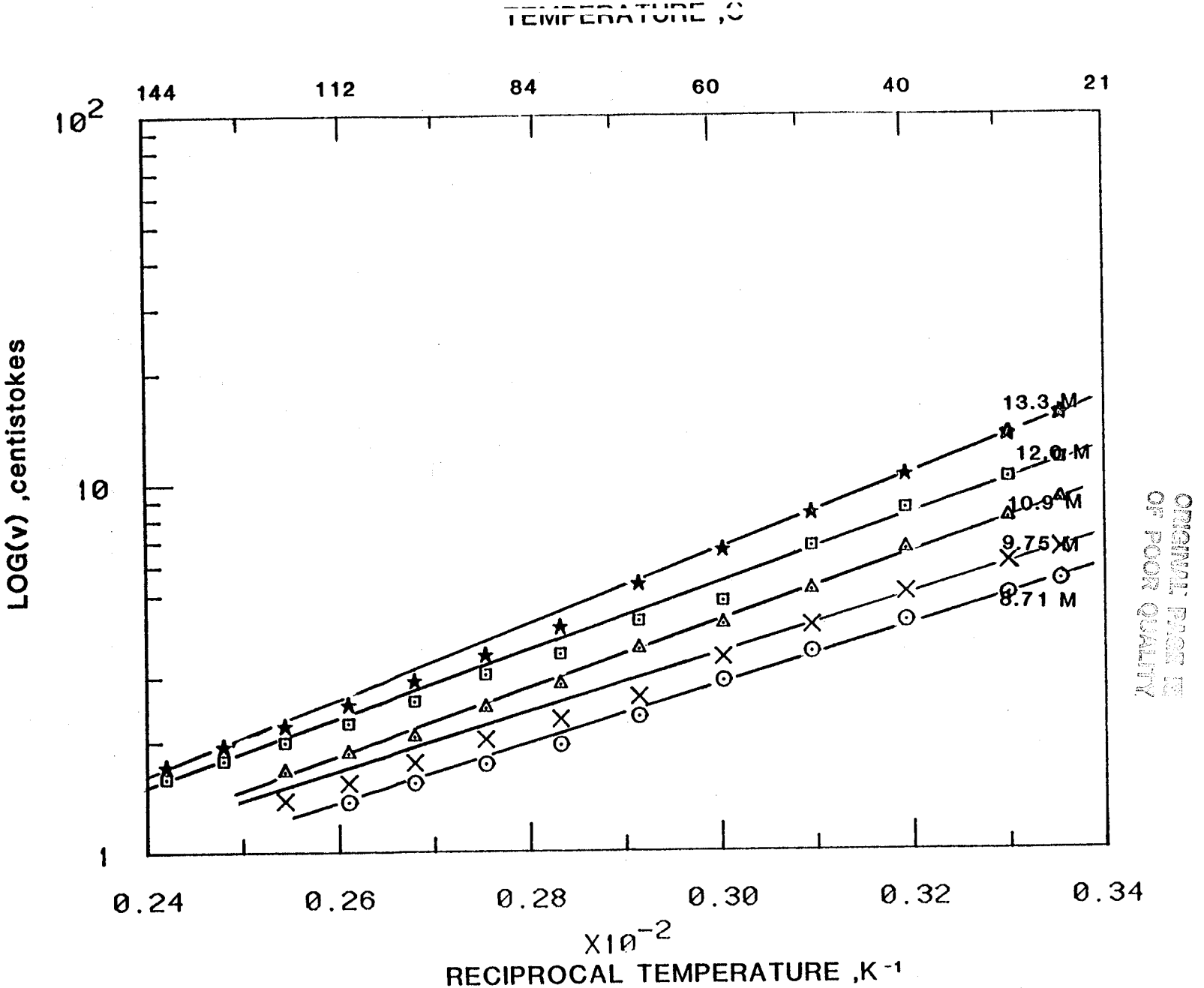

Figure 26 Plot of kinematic viscosity versus reciprocal temperatures at 8.71 to 13.3 M H_3PO_4

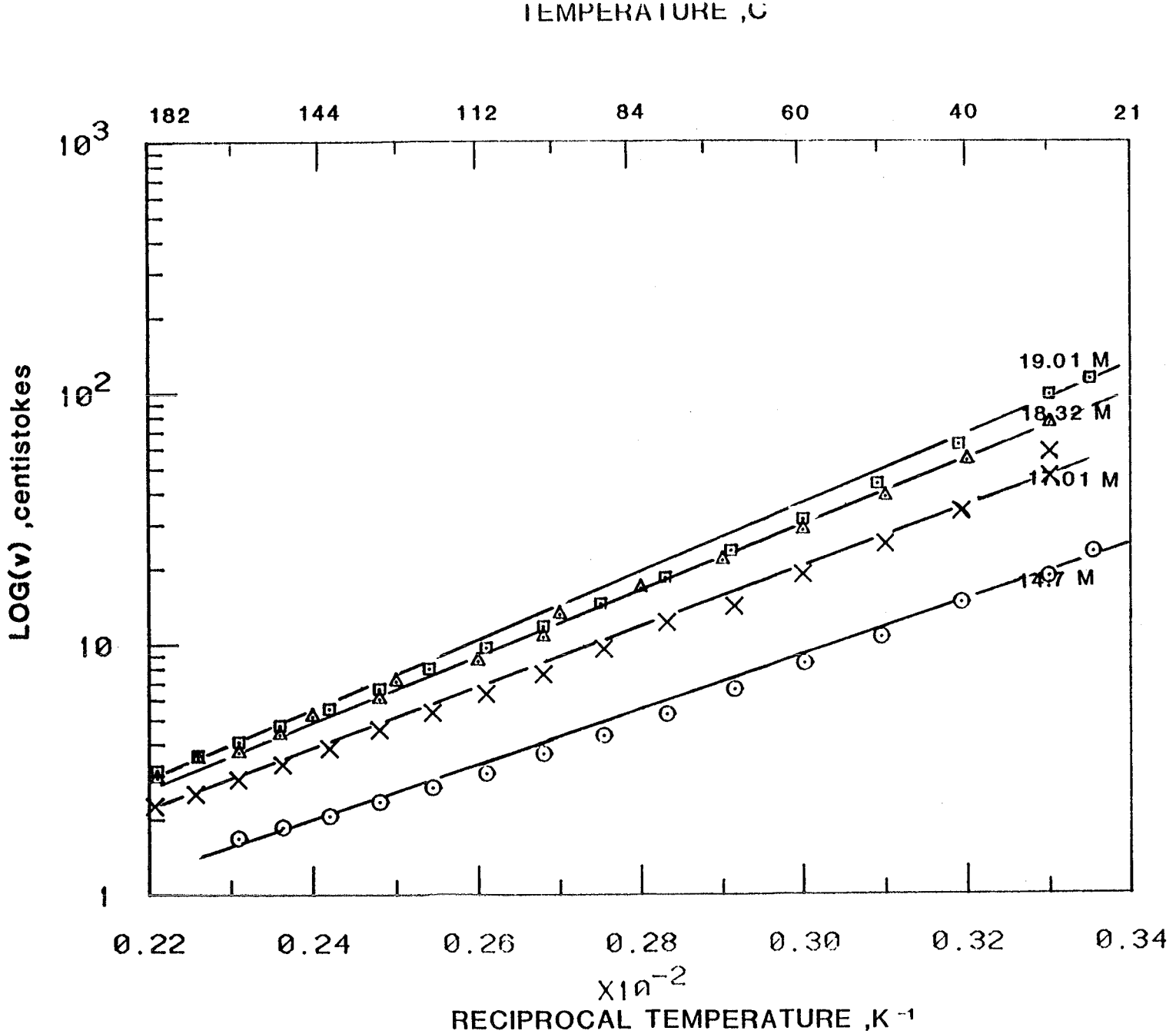

Figure 27 Plot of kinematic viscosity versus reciprocal temperature at concentrates H_3PO_4

3.4 CONCLUSIONS

(1) The electric conductivity of aqueous phosphoric acid solution has been measured over a range of concentrations from 0 to 100%, and temperatures from 25 to 200°C. Attempts were made to correlate the experimental data with the Arrhenius type expression; and the partial success was obtained for the data up to 2.37 M phosphoric acid.

(2) The kinematic viscosity of phosphoric acid as functions of concentraion and temperature was measured for the concentration range of 0–100% and the temperature range of 25–180°C. The data were described by the Arrhenius law.

IV REFERENCES

1. S. Srinivasan, ''Fuel Cell for Electric Utility and Transportation Applications'' Proceedings of the Fifth Australia Electrochemical Conference, Aug. 18-20 (1980).

2. J. O'M. Bockris and S. Srinivasan, ''Fuel Cells: Their Electrochemistry'', McGraw-Hill, N.Y., (1969).

3. S. Sarangapani, P. Bindra, and E. Yeager, ''Physical and Chemical Properties of Phosphoric Acid'', Case Western Reserve University, Cleveland, Ohio. Report to be published on Brookhaven National Laboratory Subcontract.

4. J.W. Harrison and K.M. Parker, ''Molton Carbonate Fuel Cell Design Requirements'', National Fuel Cell Seminar, Norfol, Virginia, June 23-25, (1981).

5. A.O. Isenberg in ''Proceedings of the Symposium on Electrode Materials and Processes for Energy Conversion and Storage'', J.D.E. McIntyre, S. Srinivasan, and F.G. Will, Editors, The Electrochemical Society, Princeton, N.J., 77-6 (1977).

6. K-L. Hsueh, ''Electrode Kinetics of Oxygen Reduction at Platinum in Fuel Cell Electrolytes'', Ph.D. Dissertation, Department of Chemical Engineering, Clarkson College of Technology, Potsdam, N.Y., 13676 (1983).

7. S. Srinivasan, J. McBreen and W.E. O'Grady, ''Survey of Status of Electrode Performance in Phosphoric Acid Fuel Cells'', Final Report. Brookhaven National Laboratory, Upton, N.Y., (1980).

8. W.E. O'Grady, S. Srinivasan and R.F. Dudley, Editors, ''Proceedings of the Workshop on the Electrocatalysis of Fuel Cell Reactions'', vol. 70-2, Electrochem. Soc., Princeton, N.J., (1979).

9. K-L. Hsueh, D-T. Chin, and S. Srinivasan, ''Electrode Kinetics of Oxygen Reduction: A Theoretical and Experimental Analysis of the Rotating Ring-Disk Electrode Method'', J. Electroanal. Chem., 153 (1983) 79.

10. K-L. Hsueh, E.R. Gonzalez, S. Srinivasan, and D-T. Chin, ''Effects of Phosphoric Acid Concentration on Oxygen Reduction Kinetics of Platinum'', J. Electrochem. Soc., accepted for publication.

11. K-L. Hsueh, H.H. Chang, D-T. Chin, and S. Srinivasan, ''Electrode Kinetics of Oxygen Reduction on Platinum in Trifluoromethanesulfonic Adic'', in the ''Proc. Sym. Chem. at Phys. Electrocatalysis,'' the Electro Chem. Soc., in press.

12. A.J. Appleby, ''Oxygen Reduction on Oxide-free Platinum in 85% Orthophosphoric Acid: Temperature and Impurity Dependence'', J. Electrochem. Soc., 117 (1970) 328.

13. A.J. Appleby and B.S. Baker, ''Oxygen Reduction on Platinum in Trifluormethane Sulfonic Acid'', J. Electrochem. Soc., 125 (1978), 404.

14. F. van der Brink, E. Barendrecht and W. Visscher, ''Hydrogen Peroxide as an Intermediate in Electrocatalytic Reduction of Oxygen, A New Method for the Determination of Rate Constant'', J. Electrochem. Soc., 127 (1980) 2003.

15. A. Damjanovic, M.A. Genshow and J. O'M. Bockris, ''Distinction Between Intermediates Produced in Main and Side Electrodic Reactions'', J. Chem. Phys., 45 (1966) 4057.

16. H.S. Wroblowa, Y.C. Pan, and G. Razumney, ''Electroreduction of Oxygen, A New Mechanistic Criterion'', J. Electroanal. Chem., 69 (1976) 195.

17. A.J. Appleby and M. Savy, ''Kinetics of Oxygen Reduction Reactions Involving Catalytic Decomposition of Hydrogen Peroxide'', J. Electroanal. Chem., 92 (1978) 15.

18. R.W. Zurilla, R.K. Sen, and E. Yeager, ''The Kinetics of the Oxygen Reduction Reaction on Gold in Alkaline Solution'', J. Electrochem. Soc., 125 (1978) 1123.

19. V.S. Bagotskii, M.R Tarasevich and V.Yu. Filinovskii, ''Calculation of the Kinetic Parameters of Conjugated Reactions of Oxygen and Hydrogen Peroxide'', Elektrokhimiya, 5 (1969), 1218.

20. E.R. Gonzalez, K-L. Hsueh, and S. Srinivasan, ''The Structure of the Double Layer at the Mercury-Phosphoric Acid Interface from Studies of Adsorption of Thiourea and Its Implications on Oxygen Reduction Kinetics'', J. Electrochem. Soc., 130 (1983).

21. J.C. Huang, R.K. Sen, and E. Yeager, ''Oxygen Reduction on Platinum in 85% Orthophosphoric Acid'', J. Electrochem. Soc., 126 (1979) 786.

22. A.J. Appleby, ''Oxygen Reduction on Active Platinum in 85% Orthophosphoric Acid'', J. Electrochem. Soc., 117 (1970) 641.

23. E.J. Taylor, ''Fundamental Investigations of Fuel Cells for Transportation Applications'', Ph.D. Dissertation, Department of Materials Science, University of Virginia, Virginia (1981).

24. D-T. Chin, ''Technique of Rotating Electrodes for Chemical Analysis'', Bull. Singapore National Inst. of Chem., 9, 35 (1981).

25. A. Damjanovic and V. Brusic, ''Electrode Kinetics of Oxygen Reduction on Oxide-Free Platinum Electrodes'', Electrochim. Acta, 12 (1967) 615.

26. Monsanto Technical Bulletin IC/DP 239.

27. Helmer, Combs and Lafforge, unpublished data of the Monsanto Co., St. Louis, MO.

28. Kakulin, G.P., Fedorchenko, I.A., ''Electrical Conductivity of Concentrated Phosphoric acids at 25-90^{o}C'', Russ. J. Inorg. Chem. 7, 1282 (1962).

29. Fedorchenko, J.A., Kakulin, H.P. and Kondratchenko, Z.V., ''Electrical Conductivity of Concentrated Phosphoric Acids at 100 - 200°C'', Russian J. Inorg. Chem. 10, 1061 (1965).

30 McDonald, D.I. and Boyack, J.R., ''Density, Electrical Conductivity, and Vapor Pressure of Concentrated Phosphoric Acid'', J. Chem. Eng. data 14, 380 (1969).

31. Wydeven, T., ''Electrical Conductivity, of Concentrated Phosphoric Acid from 25 to 60°C'', J. Chem. Eng. data 11, 174 (1966).

32. Greenwood and Thompson, ''The Mechanism of Electrical Conduction in Fused Phosphoric and Trideuterophosphoric Acids'', J. Chem. Soc. 1959 3485, (1959).

33. Greenwood and Thompson, ''Anomalous Conduction in Phosphoric Acid Hemi-hydrate, $2H_3PO_4.H_2O$'', J. Chem. Soc. 1959 3864 (1959).

34. Akiyama, A., Suzuki, T. and Saji, T., ''Electric Conduction and Density of Condensed Phosphoric Acids and their mixtures with Sulfuric Acid'', Bull. Chem. Solc. Japan 45, 146 (1972).

35. Maksimova, I.M., and Yushkevich, V.P., ''Electric Conductivity of Aqueous Solutions of Formic, Acetic, Oxalic, Sulfuric, and Phosphoric Acids at High Temperatures'', Soviet Electrochemistry, 2, 532 (1966).

36. Sarangpamri, S., Bindra, P., Yeager, E., ''Physical and Chemical Properties of Phosphoric Acid'', Report Prepares for the Department of Engergy, unpublished.

37. Gileadi, E., ''Electrochemistry in non-polar media'', A series of two lectures presented at Los Alamos National Laboratory, July 1982.

38. Munson, R.A., ''Self-Dissocaitive Equilibria in Molten Phosphoric Acid'', J. Phys. Chem. 68, 3374, (1964).

39. SaJi, T., Kogyo Kagaku Zaschi 67, 229 (1964).

40. SaJi, T., Kogyo Kagalu Zaschi 68, 609 (1965).

41. Cate, W.E., Deming, M.E., J. Chem. Eng data 15, 290 (1970).

42. Dahlgren, S.E., ''Phorphoric Acid'', Part I, (ed) Slack A.V., Marcel-Dekker, N.Y., Ch. 2, p. 91.

43. Kondratchenko, Z.U., Fedorchenko, I.G., Kovalov, I.Ho, ''Density, Viscosity of Concentrated Phosphoric Acids at 25-90°C'', Russ. J. Inorg. Chem. 4 985 (1959).

44. Kondratchenko, Z.V., Fedorchenko, I.G., Kovalov, I.A., ''Mathematical Calculation of the Density and Viscostiy of Concentrated Phosphoric Acid Solutions'', Russ. J. Applied Chem., 40 1882, (1968).

45. Gubbins, K.E., Walker, Ie., R.D., ''The Solubility and Diffusivity of Oxygen in Electrolytic Solutions'', J. Electrochem. Soc. 112, 469 (1965).

46. Yatskovskii, A.M., Fedotov, N.A., ''Solubility and Diffusion of Oxygen in Solutions of Potassium Hydroxide and Phosphoric Acid'', Russ. J. Phys. Chem. 43, 991 (1969).

47. Klinedinst, K., Bett, J.A.S., McDonald, J. Stonehart, P., ''Oxygen Solubility and Diffusivity in Hot Concentreated H_3PO_4'', J. Electroanal. Chem. 57, 281 (1974).

V NOTATION

Symbol	Description	Unit
a	cross-section area	cm^2
D_1	diffusivity of oxygen	cm^2/S
D_2	diffusivity of hydrogen peroxide	cm^2/S
E	electrode potential	V vs. RHE
Ez	potential of zero charge	V vs. RHE
F	Faraday's constant	C/mol.
I	Cell Current	A
I_d	Disk Current	A
I_{dl}	mass transfer limiting current at disk electrode	A
I_k	kinetic current at disk electrode	A
I_o	exchanging current	A
I_r	ring current	A
J	flux of ions	
K	overall rate constant	cm/S
k	cell constant of a conductivity cell	
ki	rate constant of step i	cm/S
L	specific conductance	mho/cm
l	length of the conductivity medium	cm

Symbol	Description	Unit
m	reaction order of oxygen	
N	collection efficiency	
R	gas constant	J/mol. ^{o}K
R	resistance	ohm
T	temperature	^{o}K
Z_1	$0.62\ D_1^{2/3}\ ^{-1/6}$	$cm/S^{0.5}$
Z_2	$0.62\ D_2^{2/3}\ ^{1/6}$	$cm/S^{0.5}$

GREEK SYMBOLS

α	transfer coefficient	
εeff	energy conversion efficiency	%
χ	specific conductivity	mho/cm
υ	kinematic viscosity	dm^2/S in Ch.2 (centistoke in Ch. 3)
ω	rotating speed of electrode	S^{-1}

VI PUBLICATIONS AND PRESENTATIONS

A. Publication*

1. K-L. Hsueh, D-T. Chin, and S. Srinivasan, ''Electrode Kinetics of Oxygen Reduction: A Theoretical and Experimental Analysis of the Rotating Ring-Disk Electrode Method'', J. Electroanal. Chem., 153 (1983) 79.

2. K-L. Hsueh, E.R. Gonzalez, S. Srinivasan, and D-T. Chin, ''Effects of Phosphoric Acid Concentration on Oxygen Reduction Kinetics at Platinum'', J. Electrochem. Soc., accepted for publication.

3. K-L. Hsueh, H.H. Chang, D-T. Chin, and S. Srinivasan, ''Electrode Kinetics of Oxygen Reduction on Platinum in Trifluoromethanesulfonic Acid'', in the ''Proceedings of the Symposium on the Chemistry and Physics of Electrocatalysis,'' edited by J.D.E. McIntrye, E.B. Zeager and M.J. Weaver, the Electrochemical Society, Inc., Pennington, New Jersey (in press).

B. Presentation

1. K-L. Hsueh, D-T. Chin, and S. Srinivasan, ''Modification of Rotating Ring-Disk Electrode Kinetics to Obtain Rate Constants of Intermediate Steps in Oxygen Reduction'', Electrochemical Society 160th meeting, Denver, Colorado, October 11-16, (1981).

2. K-L. Hsueh, E.R. Gonzalez, and D-T. Chin, ''Effect of the Double Layer Structure on the Oxygen Reduction Kinetics at the Platinum-Phosphoric Acid Interface'', Electrochemical Society 161st meeting, Montreal, Quebec, Canada, May 9-14, (1982).

3. K-L. Hsueh, S. Srinivasan, E.R. Gonzalez, and D-T. Chin, ''Electrolyte Effects on Oxygen Reduction Kinetics on Platinum: A Rotating Ring-Disk Electrode Analysis'', Electrochemical Society, 162nd meeting, Detroit, Michigan, October 17-21, (1982).

4. H.H. Chang, K-L. Hsueh, D-T. Chin, and S. Srinivasan, ''Transport Properties of Phosphoric Acid Fuel Cell Electrolytes'', Electrochemical Society 163rd meeting, San Francisco, California, May 8-13, (1983).

5. K-L. Hsueh, H.H. Chang, D-T. Chin, and S. Srinivasan, ''Electrokinetics of Oxygen Reduction on Platinum in Trifluoromethanesulfonic Acid'', Electrochemical Society 163rd meeting, San Francisco, California, May 8-13, (1983).

---

* A copy of each publication together with an abstract of K-L. Hsueh's dissertation are attached in the Appendix.

6. H.H. Chang, K-L. Hsueh, D-T. Chin, and S. Srinivasan, ''Phosphoric Acid Fuel Cell: Measurement of Transport Properties'', Spring Symposium of the Ontario-Quebec Section of Electrochemical Society, Sherbrooke, Quebec, Canada, April 29, (1983).

7. K-L. Hsueh, H.H. Chang, D-T. Chin, and S. Srinivasan, ''Phosphoric Acid Fuel Cells: Study of Oxygen Reduction Kinetics on Platinum in Trifluoromethanesulfonic and Phosphoric Acid Electrolytes'', Spring Symposium of the Ontario-Quebec Section of Electrochemical Society, Sherbrooke, Quebec, Canada, April 29, (1983).

J. Electroanal. Chem., 153 (1983) 79–95
Elsevier Sequoia S.A., Lausanne – Printed in The Netherlands

ELECTRODE KINETICS OF OXYGEN REDUCTION

A THEORETICAL AND EXPERIMENTAL ANALYSIS OF THE ROTATING RING-DISC ELECTRODE METHOD

K.-L. HSUEH and D.-T. CHIN

Department of Chemical Engineering, Clarkson College of Technology, Potsdam, NY 13676 (U.S.A.)

S. SRINIVASAN

Electronics Division, E-11, MSD429, Los Alamos National Laboratory, Los Alamos, NM 87545 (U.S.A.)

(Received 15th November 1982; in revised form 26th January 1983)

ABSTRACT

The previous theoretical treatments of the rotating ring-disc electrode method to distinguish between the mechanisms of electroreduction of O_2 to H_2O with and without the formation of H_2O_2 as an intermediate, were examined. A new expression was derived for $I_{dl}/(I_{dl} - I_d)$ as a function of $\omega^{-1/2}$ (where I_{dl} is the disc limiting current, I_d is the disc current and ω is the rotational speed of electrode) for five possible reaction models. This, along with the corresponding expressions for I_d/I_r vs. $\omega^{-1/2}$ (I_r is the ring current), enables the calculations of the individual rate constants for the intermediate steps of O_2 reduction. The experimental data of I_d and I_r were obtained for O_2 reduction on platinum in 0.55 *M* H_2SO_4 at 25°C. By use of these experimental results in the present theoretical treatment, it is shown that: (1) the most applicable model over the entire potential region was the one suggested by Damjanovic, Genshaw and Bockris; (2) the models involving the adsorption/desorption of H_2O_2 were applicable only over a narrow region of potential; and (3) the models involving the chemical decomposition of H_2O_2 were inconsistent with the dependence of $I_{dl}/(I_{dl} - I_d)$ vs. $\omega^{-1/2}$.

INTRODUCTION

The rotating ring-disc electrode (RRDE) technique has been extensively used for the investigation of the mechanism of the O_2 reduction reaction in which H_2O_2 is formed as an intermediate [1–5,9]. In this method, the reduction of O_2 takes place on a central disc electrode and the generated H_2O_2 is detected at a concentric ring electrode with a larger radius. Damjanovic et al. [2] proposed a criterion to distinguish two possible reaction mechanisms of O_2 reduction from the plot of the ratio of the disc (I_d) to the ring (I_r) currents vs. the reciprocal of the square root of the electrode rotating speed (ω). The first mechanism is a direct reduction path which reduces O_2 to H_2O through a four-electron transfer step. The second mechanism is a series reaction path where O_2 is first reduced to H_2O_2 followed by the

0022-0728/83/$03.00

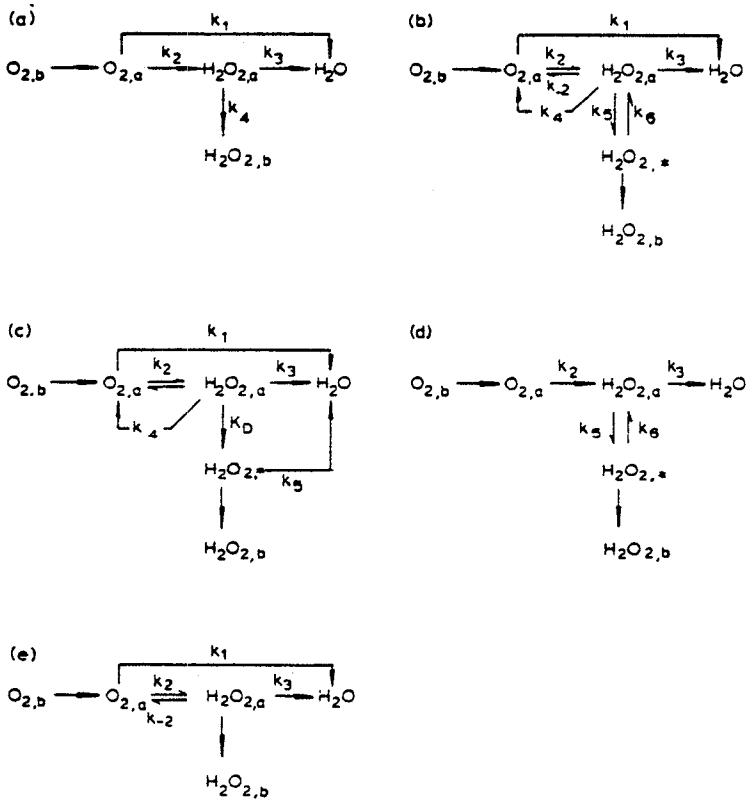

Fig. 1. Models for the electroreduction of O_2 proposed by (a) Damjanovic et al. [2], (b) Wroblowa et al. [3], (c) Appleby and Savy [4], (d) Zurilla et al. [5], and (e) Bagotskii et al. [10].

reduction of H_2O_2 to H_2O. These two reaction paths are presented in Fig. 1a. Wroblowa et al. [3] considered the adsorption–desorption step of H_2O_2 at the disc electrode (Fig. 1b) and developed a method to determine the mechanism of O_2 reduction from the plots of I_d/I_r vs. $\omega^{-1/2}$ and of the intercept vs. slope of the former plot at different potentials. The theory was extended by Appleby and Savy [4] to porous electrodes to include the catalytical decomposition of H_2O_2 to O_2 and H_2O (Fig. 1c). Zurilla et al. [5] proposed a reaction model for O_2 reduction on Au in alkaline solution where only the series reaction path was considered (Fig. 1d). For a given set of experimental data, the use of different models leads to different conclusions as was first pointed out by Zurilla et al. [5]. For example, if the intercept of the plot of I_d/I_r vs. $\omega^{-1/2}$ is greater than the reciprocal of collection efficiency of the RRDE ($1/N$), then according to Zurilla's model the conclusion will be that O_2 reduction is only via the series reaction path. However, if one uses the model by Damjanovic et al. [2], the same result would suggest that O_2 is reduced to H_2O via

both the series reaction path and the direct reduction path.

A quantitative understanding of the kinetics of O_2 reduction is as important as the qualitative determination of the mechanism of O_2 reduction. Several papers were devoted to the evaluation of the rate constants of the intermediate steps for the O_2 reduction reaction. On the basis of the equations derived by Damjanovic et al. [2,6,7], the rate constant k_3 and the ratio of k_1 to k_2 (see Fig. 1a for the definition of symbols) can be obtained from the intercepts and slopes of a plot of I_d/I_r vs. $\omega^{-1/2}$. Bagotskii et al. [8–14] derived two sets to equations: one for an electrolyte saturated with O_2 and the other for an electrolyte containing only H_2O_2. From the set of equations, a procedure was developed to calculated the rate constants k_1, k_2, k_{-2}, k_3 and k_4 (Fig. 1e). Huang et al. [15] used the same method as Wroblowa et al. [3] to calculate k_1/k_2 and k_6 (Fig. 1b) for oxygen reduction on Pt in 85% phosphoric acid. Appleby and Savy [4] derived two equations for NI_d/I_r as a function of $\omega^{-1/2}$. One equation was concerned with the reduction of O_2 with H_2O_2 as a reaction intermediate and the other equation was concerned with the reduction of H_2O_2. The rate constants were obtained from the intercept and the slope of the plot of NI_d/I_r vs.

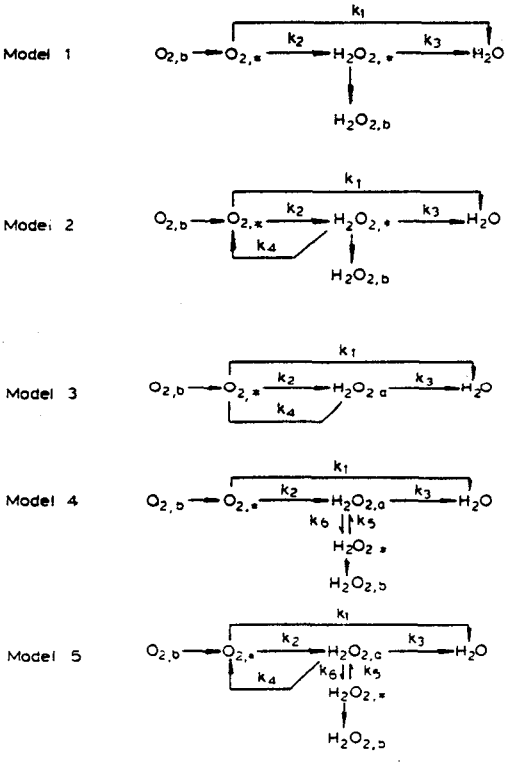

Fig. 2. Reaction schemes for the electroreduction of O_2 considered in the present work.

$\omega^{-1/2}$ at different potentials. Based on a reaction model proposed by Bagotskii et al. (Fig. 1e), Van den Brink et al. [16] calculated the value of k_4 by measuring the ring current in a solution containing only H_2O_2, while the disc was kept at the open-circuit potential.

The purpose of this work is to modify previous theoretical treatments of Damjanovic et al., Bagotskii et al. and Wroblowa et al., in order to calculate most of the rate constants for the intermediate steps of the models in Fig. 2. The rotating ring-disc electrode experimental data obtained for O_2 reduction in Pt in 0.55 M H_2SO_4 are used to illustrate the calculations of rate constants according to the present theoretical treatments. An analysis of the applicability of the various models is also made in this paper. A knowledge of the rate constants is essential in elucidating the role of electrocatalysts, electrolytes and anion adsorption on oxygen reduction kinetics and should lead to a rational basis for the selection of electrodes and electrolytes for oxygen reduction in fuel cells and metal–air batteries.

MODIFICATION OF THEORETICAL TREATMENTS FOR THE CALCULATION OF RATE CONSTANTS

The main aim of the present theoretical work is to derive mathematical expressions which would permit the calculations of the rate constants of the intermediate steps for the O_2 reduction reaction from the rotating ring-disc electrode experimental data. For this purpose, each of the reaction models depicted in Fig. 2 will be used. It is assumed that oxygen reduction is taking place in the Tafel regime for both direct and series reduction paths such that the values of k_{-1}, k_{-2} and k_{-3} are small and can be neglected in the analysis. In this section, the mathematical expressions are derived in detail for $I_{dl}/(I_{dl} - I_d)$ and I_d/I_r as a function of ω for the model suggested by Damjanovic et al. (Model 1, Fig. 2). For the sake of brevity of this article, only the final expressions for $I_{dl}/(I_{dl} - I_d)$ and I_d/I_r are presented for the other four models (see the Appendix).

Consideration of material balances for $O_{2,s}$ and $H_2O_{2,s}$ species in the model proposed by Damjanovic et al. (Model 1, Fig. 2) yields the following equations:

$$Z_1\omega^{1/2}(c_{1b} - c_{1,s}) - (k_1 + k_2)c_{1,s} = 0 \text{(for } O_{2,s}\text{)} \tag{1}$$

$$k_2c_{1,s} - (k_3 + Z_2\omega^{1/2})c_{2,s} = 0 \text{(for } H_2O_{2,s}\text{)} \tag{2}$$

where

$$Z_1 = 0.62D_1^{2/3}\nu^{-1/6} \tag{3}$$

$$Z_2 = 0.62D_2^{2/3}\nu^{-1/6} \tag{4}$$

The disc (I_d) and ring currents (I_r) are given by:

$$I_d = 2S_D F[(2k_1 + k_2)c_{1,s} - k_3c_{2,s}] \tag{5}$$

$$I_r = 2S_D FNZ_2c_{2,s}\omega^{1/2} \tag{6}$$

From eqns. (1), (2), (5) and (6), the relation between the concentration of $O_{2,s}$ and

that of $O_{2,b}$ can be expressed by:

$$c_{1s} = c_{1b}\left[1 - \frac{I_r/N + I_d}{I_{rl}/N + I_{dl}}\right] \tag{7}$$

It has been observed [6,7] that the ring current is much smaller than the disc current for O_2 reduction ($I_r \ll I_d$ and $I_{rl} \ll I_{dl}$). Therefore, eqn. (7) can be simplified to:

$$c_{1s} = c_{1b}[1 - I_d/I_{dl}] \tag{7a}$$

Rearranging eqns. (2), (5) and (6), yields:

$$\frac{I_d}{I_r} = \frac{1}{N}\left[1 + 2\frac{k_1}{k_2}\right] + \left[\frac{2(k_1/k_2 + 1)}{NZ_2}k_3\right]\omega^{-1/2} \tag{8}$$

which is the same equation derived by Damjanovic et al. [2]. Combining eqns. (1), (5) and (7a), gives:

$$\frac{I_{dl}}{I_{dl} - I_d} = 1 + \frac{k_1 + k_2}{Z_1}\omega^{-1/2} \tag{9}$$

This simple equation, which in combination with eqn. (8) is most valuable for calculating k_1 and k_2 independently, has not been derived in any of the previous theoretical treatments. The rate constants k_1, k_2 and k_3 are calculated from the intercepts and slopes of the plot of I_d/I_r vs. $\omega^{-1/2}$ and from the slopes of the plot of $I_{dl}/(I_{dl} - I_d)$ vs. $\omega^{-1/2}$ at different disc potentials. These rate constants are given by the expressions:

$$k_1 = S_2 Z_1 (I_1 N - 1)/(I_1 N + 1) \tag{10}$$

$$k_2 = 2Z_1 S_2/(I_1 N + 1) \tag{11}$$

$$k_3 = Z_2 N S_1/(I_1 N + 1) \tag{12}$$

By utilizing a similar procedure, the rate constants for the other four models (Models 2–5, Fig. 2) can also be calculated. The details are summarized in the Appendix.

EXPERIMENTAL

A glass cell with one compartment for the test and auxiliary electrodes and another for the reference electrode was used in the electrode kinetics experiment. A platinum ring-disc electrode (Pine Instrument) with a collection efficiency of 0.176 served as the working electrode. It was mechanically polished with 25 μm and 5μm polishing powder and then with 1 μm and 0.25 μm diamond paste before the experiment. Potentials were measured against a dynamic hydrogen electrode (DHE) and the readings were converted to a reversible hydrogen electrode (RHE) scale. A large platinum gauze was used as the counter electrode. The potentials of the disc and the ring electrodes were controlled by a potentiostat (Pine Instrument RDE 3) and the rotational speed of the electrode was controlled by an analytical rotator

(Pine Instrument ASR 2). The currents at the disc and ring electrodes were recorded on a dual pen X–Y–Y′ recorder (Soltec 6431).

The cell, the electrodes and the other glassware were cleaned with chromic acid (0.1 mol $K_2Cr_2O_7$ dissolved into 1 l H_2SO_4) followed by soaking in a 1 : 1 H_2SO_4/HNO_3 solution for 8 h and then in double distilled water for another 8 h. The 0.55 *M* H_2SO_4 solution was prepared by diluting concentrated H_2SO_4 (ultra pure, Alfa, Ventron Div.) with double distilled water. The purity of the solutions was ascertained by the cyclic voltammetry. The cyclic voltammograms at a scanning rate of 50 mV/s between 0.05 and 1.45 V vs. DHE, were recorded after the solution had been deaerated N_2 gas.

Before starting the RRDE experiments, O_2 (99.999% pure) was bubbled through the electrolyte for 1 h. During the RRDE experiments, the potential of the disc electrode was scanned from 1.0 to 0.3 V vs. DHE at a scan rate of 5 mV/s, while the potential of the ring electrode was maintained at 1.1 V vs. DHE (this is a limiting current potential for the oxidation of H_2O_2 to O_2). Experiments were carried out for a range of rotational speed from 400 to 4900 rpm at 25°C. Both N_2 and O_2 gas were purified by passing the gases through three columns of molecular sieves (Alumina–Silicate basis, Union Carbide, Linde Div.). The first column of molecular sieve was heated to 200–300°C and the other two columns were at room temperature.

RESULTS AND DISCUSSION

Mass transfer corrected Tafel behavior

From the RRDE experimental data, a plot of $1/i_d$ vs. $\omega^{-1/2}$ (Fig. 3) was made over the potential region from 0.7 to 0.4 V vs. RHE. In order to obtain i_d' from I_d, the surface area of the disc electrode was calculated from the total charge of H-adsorption in the cyclic voltammogram of Pt in 0.55 *M* H_2SO_4. The average solubility–diffusivity factor, $D_1^{2/3}c_{1b}$ as calculated from the slopes of the plot of $1/i_d$ vs. $\omega^{-1/2}$ (for the potential range from 0.6 to 0.4 V vs. RHE) is 6.4×10^{-10} $(cm^2/s)^{2/3}$ (mol/cm^3). From this value, the limiting current densities (i_{d1}) at different rotating speeds of electrode were calculated.

The mass transfer corrected Tafel equation is given by:

$$E = \frac{RT}{2.3\alpha nF}\log i_0 - \frac{RT}{2.3\alpha nF}\log\left[\frac{i_{d1}i_d}{i_{d1} - i_d}\right] \tag{13}$$

Fig. 4 shows a mass transfer corrected Tafel plot (E vs. $\log i_{d1}i_d/[i_{d1} - i_d]$) for O_2 reduction on Pt in 0.55 *M* H_2SO_4 (pH = 0). Within an accuracy of ±5%, this Tafel behavior is independent of ω which covers the range of rotational speeds from 400 to 4900 rpm. The apparent limiting current density which is also independent of ω is in all probability caused by a chemical reaction control prior to the first electron transfer step. The indication is that the adsorption of O_2 is probably the rate determining step in the potential region more negative than 0.5 V vs. RHE; further

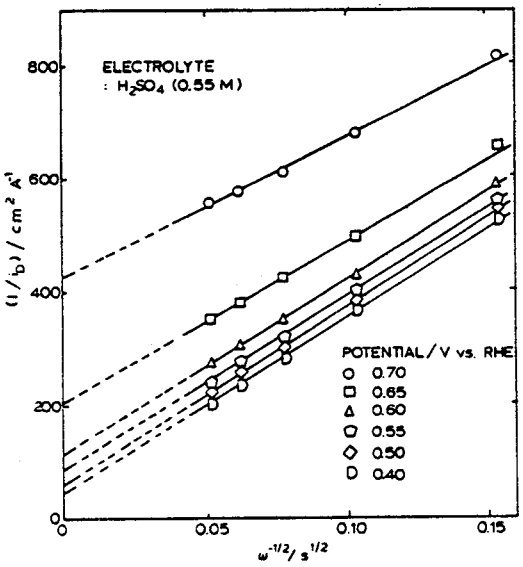

Fig. 3. $1/i_d$ vs. $\omega^{-1/2}$ at various disc potentials.

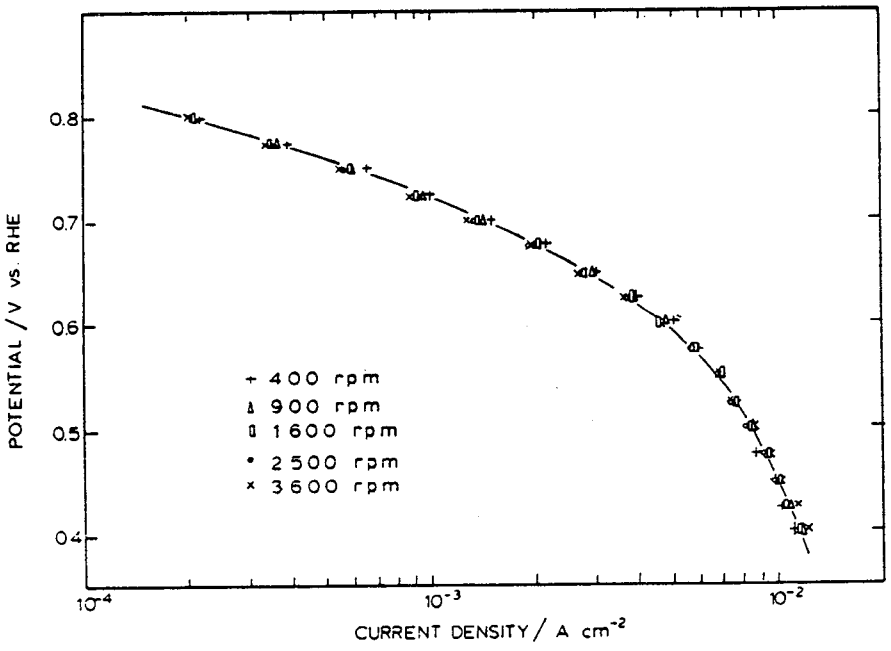

Fig. 4. Mass transfer corrected Tafel plot for O_2 reduction on Pt in 0.55 M H_2SO_4 at 25°C. The scale in the horizontal axis is for the mass transfer corrected current density, $i_{d1}i_d/(i_{d1} - i_d)$.

study within this potential region should give more insight into the oxygen adsorption phenomenon.

Evaluation of the rate constants

The two critical expressions for the calculation of the rate constants are: (1) $I_{dl}/(I_{dl} - I_d)$ as a function of $\omega^{-1/2}$; and (2) I_d/I_r as a function of $\omega^{-1/2}$ (except for Model 3 where it is assumed that there is no ring current). Figure 5 shows that the plot of $I_{dl}/(I_{dl} - I_d)$ vs. $\omega^{-1/2}$ at different electrode potentials exhibits a linear behavior with an intercept equal to 1. This linear relation between $I_{dl}/(I_{dl} - I_d)$ and $\omega^{-1/2}$ indicates that k_4 is relatively small. For the models involving k_4, this plot will not be linear (see Models 2, 3 and 5 in the Appendix).

The plots of I_d/I_r vs. $\omega^{-1/2}$ at various electrode potentials are given in Fig. 6 (from 0.75 to 0.55 V vs. RHE) and in Fig. 7 (from 0.55 to 0.35 V vs. RHE). From the plots of I_d/I_r vs. $\omega^{-1/2}$, it can be concluded that the reaction mechanism undergoes a change as the electrode potential is shifted toward the negative direction. This becomes obvious if one examines the potential dependence of the intercepts and of the slopes of the straight lines of I_d/I_r vs. $\omega^{-1/2}$ as shown in Fig. 8. The slope decreases as the potential becomes more negative in the potential region I ($0.8 \geqslant E \geqslant 0.7$ V vs. RHE). In the potential region II ($0.7 \geqslant E \geqslant 0.5$ V vs. RHE), the slope remains constant and the intercept decreases with decreasing potentials. In region III ($0.5 \geqslant E$, V vs. RHE), the slope increases and the intercept decreases as the potential decreases.

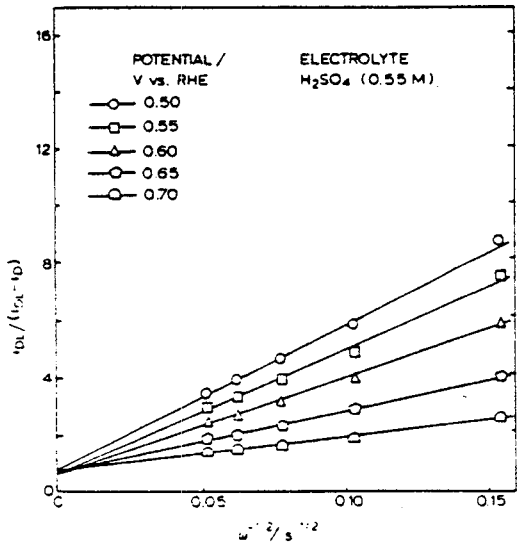

Fig. 5. $I_{dl}/(I_{dl} - I_d)$ as a function of $\omega^{-1/2}$ at various disc potentials.

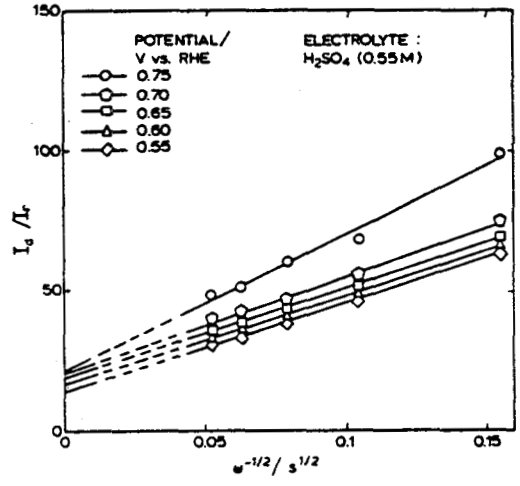

Fig. 6. I_d/I_r vs. $\omega^{-1/2}$ in the potential region 0.75–0.55 V vs. RHE.

Using Model 1, it is possible to calculate the rate constants over the entire potential range (from 0.8 to 0.4 V vs. RHE); the rate constants as a function of electrode potential are presented in Fig. 9. The potential dependence of k_1 is nearly the same as the mass transfer corrected Tafel behavior. The ratio of k_1 to k_2 is about 5–12 and is potential dependent. Since k_1 is larger than k_2, O_2 is mainly reduced to H_2O via the direct four-electron transfer reaction path and only trace amounts of O_2

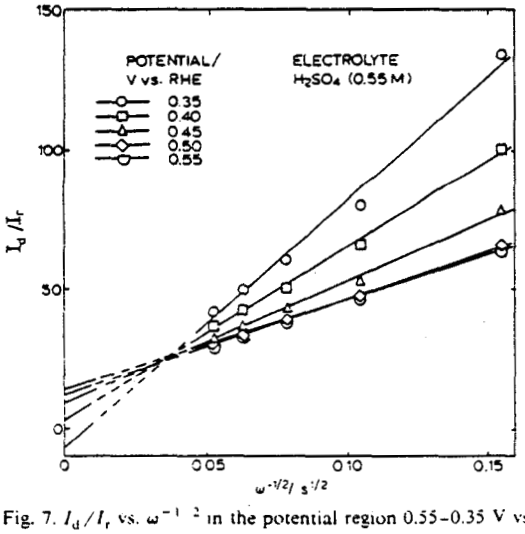

Fig. 7. I_d/I_r vs. $\omega^{-1/2}$ in the potential region 0.55–0.35 V vs. RHE.

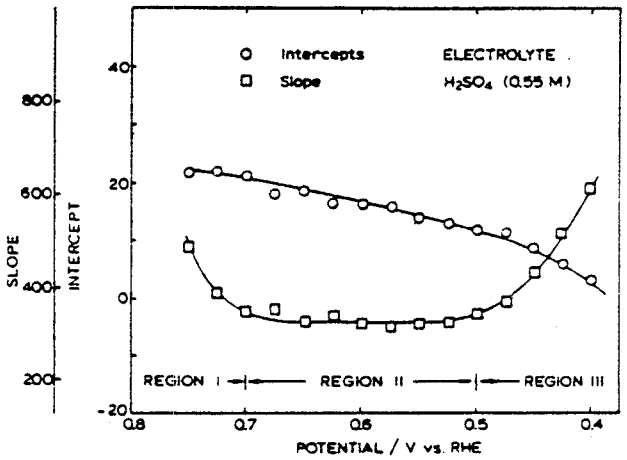

Fig. 8. Potential dependence of the intercepts and the slopes obtained from the plot of I_d/I_r vs. $\omega^{-1/2}$.

are reduced to H_2O via the series reaction path which involves H_2O_2 as an intermediate. The rate constant k_3 is greater than k_2. This indicates that H_2O_2 is reduced to H_2O at a relatively rapid rate. Therefore, only a little amount of H_2O_2 diffuses into the bulk electrolyte as evidenced by the small ring currents. The faradaic efficiency for O_2 reduction is about 97%.

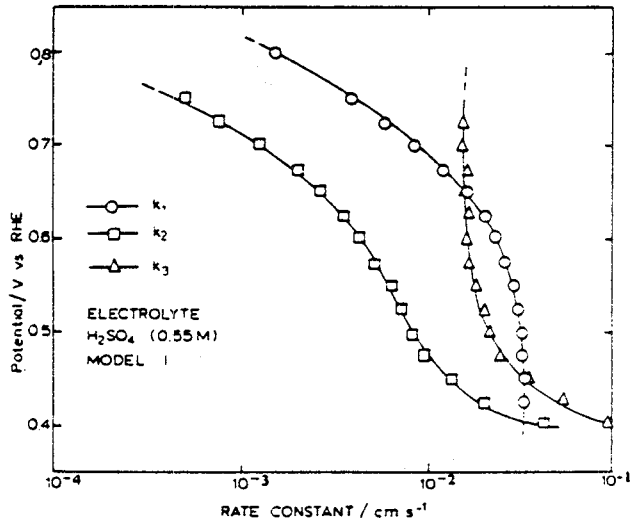

Fig. 9. Rate constants of intermediate steps for O_2 reduction on Pt in 0.55 M H_2SO_4. These constants were calculated based on Model 1.

Inapplicability of some of the proposed models

The linear behavior of $I_{dl}/(I_{dl} - I_d)$ vs. $\omega^{-1/2}$ for Pt in H_2SO_4, suggests that k_4 is negligibly small. An attempt has been made to evaluate the values of k_4 from the present experimental data according to Model 2 for which the expression of $I_{dl}/(I_{dl} - I_d)$ vs. $\omega^{-1/2}$ is not linear (see the Appendix). The accumulated errors in the non-linear curve fitting procedure were quite large, and because of the small values of k_4 some calculations even resulted in a negative value for k_4.

Since a ring current was observed for the O_2 reduction on Pt in 0.55 M H_2SO_4, Model 3 can be excluded. The sum of the rate constant $(k_1 + k_2)$ calculated using this model is higher than the value based on Model 1.

In order to calculate the rate constants k_1, k_2, k_6 and k_3/k_5 according to Model 4, it is necessary to have a linear relationship between the intercepts and the slopes (obtained from the plot of I_d/I_r vs. $\omega^{-1/2}$ at different potentials). In a previous work [17] such plots have been found to be linear only over a limited range of potential. A plot of intercept vs. slope from the present experimental data is given in Fig. 10. The non-linear behavior of the data points indicate that the assumption of k_1/k_2 being independent of potential is not correct as evidenced by the results shown in Fig. 9.

The same problems were also encountered with Model 5. Only over a narrow

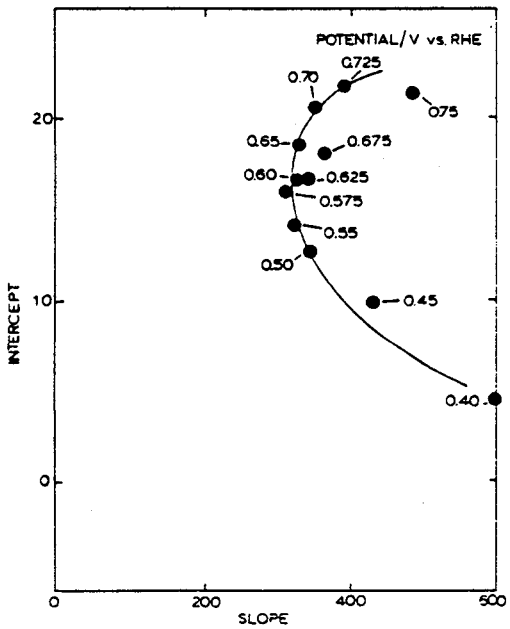

Fig. 10. Intercepts vs. slopes obtained from the plot of I_d/I_r vs. $\omega^{-1/2}$ (Figs. 6 and 7).

potential region was it possible to obtain acceptable values of rate constants. The calculations sometimes even led to negative values of rate constants. It should be noted that Model 5 is the most complete reaction scheme for O_2 reduction. The fact that it did not fit the present data is probably caused by too many unknowns (nine) and insufficient number of independent equations (five) as shown in Appendix (E). Additional experiments, such as oxidation or reduction of H_2O_2 in the electrolyte without the presence of O_2 will be needed to evaluate all the rate constants in the model.

CONCLUSIONS

A theoretical and experimental study has been carried out for the O_2 reduction reaction on a platinum rotating ring–disc electrode in 0.55 *M* H_2SO_4. The analytical procedures for the calculation of the intermediate reaction rate constants were developed for various reaction models. It was found that a simple reaction model as proposed by Damjanovic et al. is consistent with the present experimental data. The results indicate that O_2 (97%) reduces to H_2O via a direct four-electron transfer reaction. At potentials more negative than 0.5 V vs. RHE, a chemical reaction step or an adsorption process prior to the charge transfer reaction becomes the rate controlling step.

ACKNOWLEDGMENTS

This work was carried out under the auspicies of the U.S. Department of Energy. Helpful discussions with Dr. S. Feldberg of Brookhaven National Laboratory and Professor E. R. Gonzalez of the Instituto de Fisica e Quimica de Sao Carlos, USP are gratefully acknowledged. The experimental work and part of the theoretical work reported in this paper were carried out by K.-L. Hsueh at Los Alamos during the period May 1981–August 1982. The contribution of K.-L. Hsueh is in partial fulfillment of the requirements for his Ph.D. degree in Chemical Engineering from Clarkson College of Technology, Potsdam, NY.

NOTATIONS

Symbol	*Description*	*Unit*
c_{1b}	concentration of oxygen in the bulk solution	mol/cm^3
c_{1s}	concentration of oxygen near the electrode	mol/cm^3
c_{2s}	concentration of H_2O_2 near the electrode	mol/cm^3
D_1	diffusivity of oxygen	cm^2/s
D_2	diffusivity of H_2O_2	cm^2/s
E	electrode potential	V vs. RHE
F	Faraday's constant	C/mol
I_d	disc current	A
I_r	ring current	A

I_1	intercept of the plot of I_d/I_r vs. $\omega^{-1/2}$	
i_d	disc current density	A/cm^2
i_r	ring current density	A/cm^2
i_{dl}	disc limiting current density	A/cm^2
i_{rl}	ring current density at disc limiting current condition	A/cm^2
k_i	rate constants of step i	cm/s
N	collection efficiency	
n	charge number of electron transfer per mole of O_2	
R	gas constant	J/mol · K
S_D	surface area of disc electrode	cm^2
S_1	slope of the plot of I_d/I_r vs. $\omega^{-1/2}$	s$^{-1/2}$
S_2	slope of the plot of $I_{dl}/(I_{dl}-I_d)$ vs. $\omega^{-1/2}$	s$^{-1/2}$
T	temperature	K
α	transfer coefficient	
ν	kinematic viscosity	cm^2/s
ω	rotational speed of electrode	s^{-1}

APPENDIX

(A) Model 1 (reaction scheme proposed by Damjanovic et al. [2])

Reaction scheme

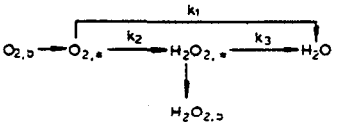

Assumptions

(1) No catalytical decomposition of H_2O_2.
(2) The adsorption and desorption reactions of H_2O_2 are fast and in equilibrium.
(3) Rate constant for electrochemical oxidation of H_2O_2 is negligible.

Material balance

For $O_{2,s}$: $Z_1\omega^{1/2}(c_{1b}-c_{1s})-(k_1+k_2)c_{1s}=0$
For H_2O_2: $k_2c_{1s}-(k_3+Z_2\omega^{1/2})c_{2s}=0$

Expressions for current

Disc current: $I_d = 2S_DF[(2k_1+k_2)c_{1s}+k_3c_{2s}]$
Ring current: $I_r = 2S_DFNZ_2\omega^{1/2}c_{2s}$

Expression for the calculation of rate constants

$$I_d/I_r = \frac{1+2k_1/k_2}{N}+\frac{2(1+k_1/k_2)}{NZ_2}k_3\omega^{-1/2}$$

$$\frac{I_{dl}}{I_{dl}-I_d} = 1+\frac{k_1+k_2}{Z_1}\omega^{-1/2}$$

Expressions for rate constants

$$k_1 = S_2Z_1\frac{I_1N-1}{I_1N+1}$$

$$k_2 = \frac{2Z_1S_2}{I_1N+1}$$

$$k_3 = \frac{Z_2 N S_1}{I_1 N + 1}$$

where I_1 and S_1 are the intercept and slope of the plot of I_d/I_r vs. $\omega^{-1/2}$, respectively. S_2 is the slope of the plot of $I_{d1}/(I_{d1} - I_d)$ vs. $\omega^{-1/2}$.

(B) Model 2 (reaction scheme proposed by Bagotskii et al. [9])

Reaction scheme

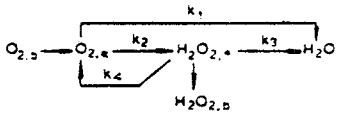

Assumptions

(1) The adsorption and desorption reactions of H_2O_2 are fast and in equilibrium.
(2) Rate constant for electrochemical oxidation of H_2O_2 is negligible.

Material balance

For $O_{2,s}$: $Z_1\omega^{1/2}(c_{1b} - c_{1s}) + k_4 c_{2s} - (k_1 + k_2)c_{1s} = 0$
For $H_2O_{2,s}$: $k_2 c_{1s} - (k_3 + k_4 + Z_2\omega^{1/2})c_{2s} = 0$

Expressions for current

Disc current: $I_d = 2S_D F[(2k_1 + k_2)c_{1s} + k_3 c_{2s}]$
Ring current: $I_r = 2S_D F N Z_2 \omega^{1/2} c_{2s}$

Expressions for the calculation of rate constants

$$\frac{I_d}{I_r} = \frac{1}{N}\left(1 + 2\frac{k_1}{k_2}\right) + \frac{(k_3 + k_4)(1 + 2k_1/k_2) + k_3}{NZ_2}\omega^{-1/2}$$

$$\frac{I_{d1}}{I_{d1} - I_d} = \frac{\left(1 + \dfrac{k_1 + k_2}{Z_1}\omega^{-1/2}\right)}{\left(1 + \dfrac{I_r k_4}{2S_D F N Z_1 Z_2 c_{1b}}\right)}$$

Expressions for rate constants

$k_1 = A_2(I_2 N - 1)/(I_2 N + 1)$
$k_2 = 2A_2/(I_2 N + 1)$
$k_3 = (S_3 N Z_2 - I_2 N A_3)/(I_2 N + 1)$
$k_4 = A_3$

where I_2 and S_3 are the intercept and slope of the plot of I_d/I_r vs. $\omega^{-1/2}$. A_2 and A_3 are obtained by least square fitting of the equation:

$$\frac{I_{d1}}{I_{d1} - I_d} = 1 + (k_1 + k_2)\frac{\omega^{-1/2}}{Z_1} - k_4 \frac{I_r I_{d1}}{2S_D F N Z_1 Z_2 c_{1b}(I_{d1} - I_d)\omega}$$

where $A_2 = k_1 + k_2$ and $A_3 = k_4$

(C) Model 3 (reaction scheme for oxygen reduction in which no ring current can be detected)

Reaction scheme

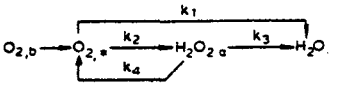

Assumptions

(1) No H_2O_2 diffuses into the bulk.
(2) Rate constant for electrochemical oxidation of H_2O_2 is negligible.

Material balance

For $O_{2,\bullet}$: $Z_1\omega^{1/2}(c_{1b} - c_{1\bullet}) + k_4 c_{2\bullet} - (k_1 + k_2)c_{1\bullet} = 0$

For $H_2O_{2,\bullet}$: $k_2 c_{1\bullet} - (k_3 + k_4)c_{2\bullet} = 0$

Expressions for current

Disc current: $I_d = 2S_D F[(2k_1 + k_2)c_{1\bullet} + k_3 c_{2\bullet}]$

Expressions for the calculation of rate constants

$$\frac{I_{dl} I_d}{2S_D F c_{1b}(I_{dl} - I_d)} = 2k_1 + k_2 + \frac{k_2 k_3}{k_3 + k_4}$$

$$\frac{I_{dl}}{I_{dl} - I_d} = 1 + \frac{1}{Z_1}(k_1 + k_2 - \frac{k_4 k_2}{k_3 + k_4})\omega^{-1/2}$$

Expressions for rate constant

$$k_1 + k_2 = \frac{I_d I_{dl}}{2S_D F c_{1b}(I_{dl} - I_d)} - Z_1 S_4$$

where S_4 is the slope of $I_{dl}/(I_{dl} - I_d)$ vs. $\omega^{-1/2}$

(D) Model 4 (reaction scheme proposed by Wroblowa et al. [3] with k_4 neglected)

Reaction scheme

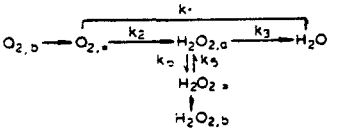

Assumptions

(1) No catalytical decomposition of H_2O_2.
(2) Rate constant for electrochemical oxidation of H_2O_2 is negligible.
(3) k_1 and k_2 have the same potential dependence.

Material balance

For $O_{2,\bullet}$: $Z_1\omega^{1/2}(c_{1b} - c_{1\bullet}) - (k_1 + k_2)c_{1\bullet} = 0$

For $H_2O_{2,\bullet}$: $k_2 c_{1\bullet} + k_6 c_{2\bullet} - (k_3 + k_5)c_{2a} = 0$

For $H_2O_{2,a}$: $k_5 c_{2a} - (k_6 + Z_2\omega^{1/2})c_{2\bullet} = 0$

Expressions for current

Disc current: $I_d = 2S_D F[(sk_1 + k_2)c_{1\bullet} + k_3 c_{2a}]$

Ring current: $I_r = 2S_D F N Z_2 c_{2\bullet}\omega^{1/2}$

Expressions for the calculation of rate constants

$$\frac{I_{dl}}{I_{dl} - I_d} = 1 + \frac{k_1 + k_2}{Z_1}\omega^{-1/2}$$

$$\frac{I_d}{I_r} = \frac{1}{N}\left[1 + 2\frac{k_1}{k_2} + \left(\frac{2k_1 k_3}{k_2 k_5} + 2\frac{k_3}{k_5}\right)\right]$$

Expressions for rate constants

$k_1 = S_2 Z_1 (I_4 - 1)/(I_4 + 1)$
$k_2 = 2S_2 Z_1/(I_4 + 1)$
$k_6 = Z_2/S_6$
$k_3/k_5 = S_5 S_6/(I_4 + 1)$
where S_2 is the slope of the plot of $I_{d1}/(I_{d1} - I_d)$ vs. $\omega^{-1/2}$, I_3 and S_5 are the intercept and slope of the plot of I_d/I_r vs. $\omega^{-1/2}$, respectively. I_4 and S_6 are the intercept and slope of the plot of NI_3 vs. NS_5, respectively.

(E) Model 5 (reaction scheme proposed by Wroblowa et al. [3])

Reaction scheme

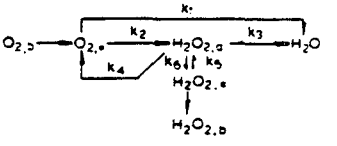

Assumption

(1) Rate constant for electrochemical oxidation of H_2O_2 is negligible.

Material balance

For $O_{2,s}$: $Z_1\omega^{1/2}(c_{1b} - c_{1s}) + k_4 c_{2a} - (k_1 + k_2)c_{1s} = 0$
For $H_2O_{2,a}$: $k_2 c_{1s} + k_6 c_{2s} - (k_3 + k_4 + k_5)c_{2a} = 0$
For $H_2O_{2,s}$: $k_5 c_{2a} - (k_6 + Z_1\omega^{1/2})c_{2s} = 0$

Expressions for current

Disc current: $I_d = 2S_D F[(2k_1 + k_2)c_{1s} + k_3 c_{2s}]$
Ring current: $I_r = 2S_D FNZ_2\omega^{1/2}c_{2s}$

Expressions for the calculation of rate constants

$$\frac{I_{d1}}{I_{d1} - I_d} = \frac{(k_1 + k_2 - Z_1\omega^{1/2})}{\dfrac{\left(\dfrac{k_4 k_6}{k_5} + \dfrac{k_4}{k_5} Z_2\omega^{1/2}\right) I_r}{2S_D FNZ_2\omega^{1/2}c_{1b}} - Z_1\omega^{1/2}}$$

$$\frac{I_d}{I_r} = \frac{1}{N}1 + 2\frac{k_1}{k_2} + [2\frac{k_1(k_3 + k_4)}{k_2 k_5} + \frac{2k_3 + k_4}{k_5}]$$
$$+ \frac{1}{N}2\frac{k_1(k_3 + k_4)}{k_2 k_5} + \frac{2k_3 + k_4}{k_5}\frac{k_6}{Z_2}\omega^{-1/2}$$

Expressions of rate constants

$$k_1 = \frac{A_3[I_5 N - 1 - (Z_2 A_2 S_7/A_1)]}{I_5 N + 1 - (Z_2 A_2 S_7 N/A_1)}$$

$$k_2 = \frac{2A_3}{I_5 N + 1 - (Z_2 A_2 S_7 N/A_1)}$$

$k_6 = A_1/A_2$

$$\frac{k_3}{k_5} = \frac{(Z_2 A_2 S_7 N/A_1) - [NI_5 - (Z_2 A_2 S_7 N/A_1)]A_2}{2[I_5 N + 1 - (Z_2 A_2 S_7 N/A_1)]}$$

$k_4/k_5 = A_2$

where I_5 and S_7 are the intercept and slope of the plot of I_d/I_r vs. $\omega^{-1/2}$. A_1, A_2 and A_3 are obtained from the least

square fitting of equation:

$$A_1 + A_2 Z_2 \omega^{1/2} = \left[A_3 + Z_1 \omega^{1/2} \left(\frac{I_d}{I_d - I_{dl}} \right) \right] \frac{I_{dl} - I_d}{I_{dl} I_r}$$

$$2 S_D F N Z_2 \omega^{1/2} c_{1b}$$

where

$$A_1 = k_4 k_6 / k_5$$
$$A_2 = k_4 / k_5$$
$$A_3 = k_1 + k_2$$

REFERENCES

1 L. Muller and L.N. Nekrasov, Electrochim. Acta, 9 (1964) 1015.
2 A. Damjanovic, M.A. Genshaw and J.O.'M. Bockris, J. Chem. Phys., 45 (1966) 4057.
3 H.S. Wroblowa, Y.C. Pan and G. Razumney, J. Electroanal. Chem., 69 (1976) 195.
4 A.J. Appleby and M. Savy, J. Electroanal. Chem., 92 (1978) 15.
5 R.W. Zurilla, R.K. Sen and E. Yeager, J. Electrochem. Soc., 125 (1978) 1123.
6 A. Damjanovic, M.A. Genshaw and J.O'M. Bockris, J. Electrochem. Soc., 114 (1967) 446.
7 A. Damjanovic, M.A. Genshaw and J.O'M. Bockris, J. Electrochem. Soc., 114 (1967) 1107.
8 M.R. Tarasevich, Elektrokhimiya, 4 (1968) 210.
9 V.S. Bagotskii, V.Yu. Filinovskii and N.A. Shumilova, Elektrokhimiya, 4 (1968) 1247.
10 V.S. Bagotskii, M.R. Tarasevich and V.Yu. Filinovskii, Elektrokhimiya, 5 (1969) 1218.
11 M.R. Tarasevich, R.Kh. Burshtein and K.A. Radyushkina, Elektrokhimiya, 5 (1969) 372.
12 M.R. Tarasevich and K.A. Radyushkina, Elektrokhimiya, 6 (1970) 376.
13 K.A. Radyushkina, M.R. Tarasevich and R.Kh. Burshtein, Elektrokhimiya, 6 (1970) 1352.
14 M.R. Tarasevich, K.A. Radyushkina, V.Yu. Filinovskii and R.Kh. Burshtein, Elektrokhimiya, 6 (1970) 1522.
15 J.C. Huang, R.K. Sen and E. Yeager, J. Electrochem. Soc., 126 (1979) 786.
16 F. van den Brink, E. Barendrecht and W. Visscher, J. Electrochem. Soc., 127 (1980) 2003.
17 W.E. O'Grady, E.J. Taylor and S. Srinivasan, J. Electroanal. Chem., 132 (1982) 137.

Effects of Phosphoric Acid Concentration on Oxygen Reduction Kinetics at Platinum*

K-L. Hsueh,* E. R. Gonzalez,** and S. Srinivasan**,[1]

Los Alamos National Laboratory, Los Alamos, New Mexico 87545

D-T. Chin**

Department of Chemical Engineering, Clarkson College of Technology, Potsdam, New York 13676

ABSTRACT

The oxygen reduction reaction was investigated at platinum electrodes in phosphoric acid in the concentration range 0.7M (6.6%) to 17.5M (95%) at 25°C using the rotating ring-disk electrode technique. As a complement, cyclic voltammograms on platinum and potentials of zero charge of mercury were obtained as a function of phosphoric acid concentration. The mechanism of the oxygen electrode reaction is discussed in terms of the direct four-electron transfer reduction to water and the formation of hydrogen peroxide as an intermediate in a parallel two-electron transfer reaction. The rate constants of the intermediate reaction steps were calculated from the ring-disk data for various potentials and electrolyte concentrations. The characteristics of the reaction were found to be markedly dependent on the concentration of phosphoric acid. These results are interpreted in terms of changes in oxygen solubility, proton activity, and double layer characteristics when passing over from a water to a phosphoric acid solvent structure.

Concentrated phosphoric acid is presently used as the electrolyte in advanced fuel cells. The factor limiting the efficiency of this fuel cell system is the overpotential for oxygen reduction reaction in the concentrated acid medium. In fact, this reaction is approximately two orders of magnitude slower in concentrated H_3PO_4 than in aqueous solutions of strong acids, such as trifluoromethanesulfonic acid (1, 2).

Previous studies on the reduction of oxygen on platinum in concentrated H_3PO_4 focused on examining the Tafel behavior over a wide temperature range (3-5). The conclusions can be summarized as follows. (*i*) Three Tafel regions can be observed. Above 0.8V (*vs.* RHE), a 60 mV Tafel slope is obtained. This slope changes to 120 mV in the region of potentials between 0.8 and 0.6V. Below 0.5V, very high Tafel slopes (over 200 mV) are observed. The mechanism of the reaction in the third region is not completely understood. (*ii*) Tafel slopes in the intermediate range (120 mV) are independent of temperature, contrary to predictions from electrode kinetic theory. Appleby (5) suggested that this phenomenon could be associated with a change in the double layer structure with temperature. But the question is far from settled. Yeager *et al.* (6) suggested that this phenomenon is due to a compensating effect of the entropic and enthalpic terms in the rate expression. (*iii*) Rotating ring-disk investigations (7, 8) have shown that the reduction of oxygen in concentrated phosphoric acid follows two parallel paths: a direct four-electron reduction to water and a couple of two-electron transfer reduction reactions to water with hydrogen peroxide as the intermediate. (*iv*) The rate of the reaction is first order with respect to the oxygen partial pressure (4). (*v*) The reaction order with respect to proton activity is 3/2 in the low current density region (60 mV Tafel slope) and 1 in the high current density region (120 mV Tafel slope).

The structure and properties of concentrated H_3PO_4 are not well understood, but these certainly are expected to play a role in the slow reduction of oxygen at platinum. Recently, the authors examined the structure of the mercury/concentrated H_3PO_4 interface (9) and concluded that the double layer in concentrated H_3PO_4 is thicker than in aqueous media. Thus, it seems reasonable to assume that a transition with respect to both the interfacial and bulk properties will occur when passing over from a water to a phosphoric acid solvent structure. For this reason, the present study was undertaken to elucidate the effect of the struc-

* Electrochemical Society Student Member.
** Electrochemical Society Active Member.
[1] Leave of absence from LANL; at Institute for Hydrogen Systems, Mississauga, Ontario L5N 1P1, Canada.
Key words: gas, electrode, metals, electrolyte.

*Report copied from Electrochemical Science and Technology, J. Electrochemical Soc., April 1984.

ture of H_3PO_4 solutions, ranging in concentration from 7 to 95%, on the kinetics of oxygen reduction at platinum electrodes.

Experimental

The equipment, preparation of the electrode, and the experimental procedure for the rotating ring-disk experiment have already been described (10). The same setup was used for the cyclic voltammetric experiments. Phosphoric acid (85%, electronic grade, J. T. Baker) was treated with 10% hydrogen peroxide (90%, stabilizer free, FMC) and heated to 50°-70°C for 1h. The solution was concentrated to 85% by evaporation at 160°C in Teflon vessels. This solution was diluted with double-distilled water that was previously treated with alkaline permanganate. Further evaporation of the 85% stock solution was done to obtain the 95% concentration. Before use, solutions were pre-electrolyzed for 24h with platinum electrodes to eliminate electroactive impurities.

All potentials were measured against a dynamic hydrogen electrode (DHE). The values were converted to a reversible hydrogen electrode (RHE) scale by measuring, for each solution, the potential difference between the DHE and a floating-type fuel cell hydrogen electrode.

Results and Discussion

Cyclic voltammetry.—Figure 1 shows the cyclic voltammograms on Pt, obtained as a function of H_3PO_4 concentration. No difference was observed for a stationary or a rotating electrode, which is indicative of the absence of impurities in the electrolyte. According to this figure, it is apparent that for concentrations of H_3PO_4 up to about 4M there is no effect on the characteristics of the voltammogram. On the other hand, for higher concentrations, it is observed that the potential of oxide formation commencement progressively shifts to more positive values. Also, the total charges for oxide formation and reduction decrease for these increasing acid concentrations. These findings can be associated with a strong adsorption of phosphate species on the electrode that interferes with the oxide formation. However, the effect may be partly due to a decrease in the activity of water as the concentration of H_3PO_4 increases (11).

Mass-transfer-corrected Tafel behavior.—The mass-transfer-corrected Tafel behavior for oxygen reduction on platinum for different H_3PO_4 concentrations is shown in Fig. 2. The plots correspond to the equation

$$E = \frac{2.3RT}{\alpha_c F}\log i_o - \frac{2.3RT}{\alpha_c F}\log\frac{i_{dl}\, i_d}{i_{dl} - i_d} \qquad [1]$$

where α_c is the transfer coefficient, i_o the exchange current density, i_d the disk current density, and i_{dl} the limiting disk current density. The Tafel plots presented in Fig. 2 are independent of rotation speed. In the region from 0.6 to 0.8V, Tafel slopes are about 120 mV. This result is similar to that obtained by others (3-7, 11) in acid media. Thus, it seems reasonable to conclude that the overall reduction of oxygen is controlled by the first charge transfer step under Langmuir adsorption conditions. Below 0.5V, higher Tafel slopes (> 200 mV/decade) are observed and the current seems to reach a limiting value. Because these limiting currents are not due to mass transfer, a change in the reaction mechanism must be taking place. This change probably involves a chemical rate-determining step, which may be the dissociative adsorption of the oxygen molecule. This point was not investigated further because the potential region lies outside the range of interest for fuel cells.

Mechanistic aspects of electroreduction of oxygen.—Recently, theoretical aspects of the reduction of oxygen on rotating ring-disk platinum electrodes have been considered (10). In this work, it was concluded that the mechanism proposed by Damjanovic *et al.* (12) is the most appropriate. The reaction scheme is as follows

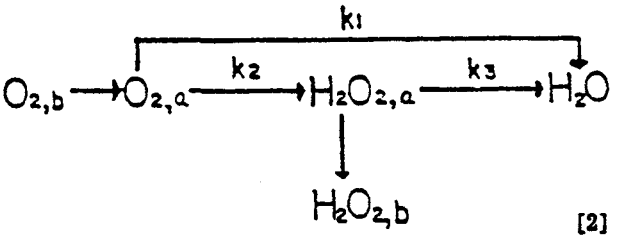

[2]

where a indicates an adsorbed state and b is the bulk of the solution. Two equations for calculating the reaction rate constants k_1, k_2, and k_3 are (10)

$$\frac{I_{dl}}{I_{dl} - I_d} = 1 + \frac{k_1 + k_2}{0.62\, D_{O_2}^{2/3}\, \nu^{-1/6}}\, \omega^{-1/2} \qquad [3]$$

$$\frac{I_d}{I_r} = \frac{1}{N}1 + 2\frac{k_1}{k_2} + \frac{2(k_1/k_2 + 1)k_3}{0.62\, N D_{H_2O_2}^{2/3}\, \nu^{-1/6}}\, \omega^{-1/2} \qquad [4]$$

where I_d and I_r are the disk and ring currents, respectively; I_{dl} is the limiting current on the disk electrode; N is the collection efficiency; ω is the rotational speed; ν is the kinematic viscosity of the electrolyte; and D_{O_2} and $D_{H_2O_2}$ are the diffusion coefficients of oxygen and hydrogen peroxide, respectively. Accordingly, plots of $I_{dl}/(I_{dl} - I_d)$ *vs.* $\omega^{-1/2}$ and I_d/I_r *vs.* $\omega^{-1/2}$ should yield two straight lines, and the rate constants can be calculated from the intercepts and the slopes of these straight lines. In this way, the values of k_1, k_2, and k_3, as functions of electrode potential for oxygen reduction on Pt, were evaluated from the ring-disk data for various phosphoric acid concentrations (Fig. 3-6).

In all cases, it was found that the ratio k_1/k_2 is greater than 10, which means that most of the oxygen reduces to water directly through the four-electron transfer reaction. Because $k_1 >> k_2$, the relationship between i and k_1 can be written approximately as

$$i \cong 4FA\, k_1 c_{O_2} = 4FA\, k_1' c_{O_2} a_{H^+} \exp\left(-\frac{\alpha_c F}{RT}E\right) \qquad [5]$$

Therefore, k_1 should have the same dependence on phosphoric acid concentration as i/c_{O_2} at any potential. This can be seen in Fig. 7 where k_1, i, and i/c_{O_2} for a potential of 0.7V are plotted as a function of H_3PO_4 concentration. Clearly, k_1 and i/c_{O_2} have the same concentration dependence.

From Fig. 3, 4, and 5, it is apparent that for H_3PO_4 concentrations up to 8M, k_2 has the same potential dependence as k_1. This means that the rate-determining step is probably the same for both reactions. At higher concentrations, k_2 is surprisingly independent of potential, which means that the rate of the reaction is chemically controlled (chemical step prior to electron transfer step). In this case, the rate of the reaction may be determined by the adsorption of the O_2 molecule, which must be oriented preferentially at the interface in order to lead to H_2O_2 formation. This can be inhibited by a predominance of phosphate species at the interface, which is supported by the fact that the constant value of k_2 shows a marked decrease with the increase in H_3PO_4 concentration.

The behavior of k_3 is similar to that of k_2 (*cf.* Fig. 5 and 6); k_3 increases with the overpotential in the low overpotential regime and is more or less independent of potential when E becomes more negative than 0.5V *vs.* RHE. Increased phosphoric acid concentration results in decreased k_3. It can be shown that the significant decrease in k_2 and k_3 with increasing H_3PO_4 concentration leads to an increase in the faradaic efficiency for the reduction of oxygen to water. This is

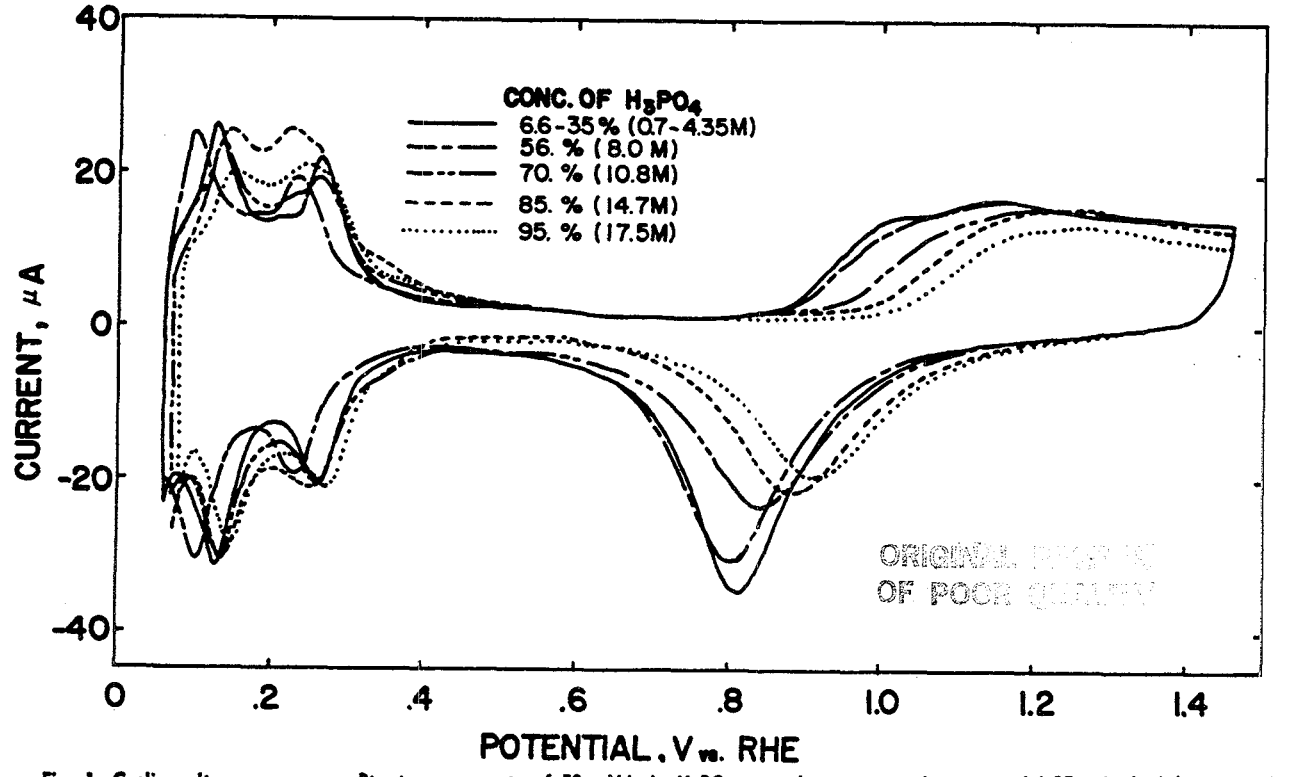

Fig. 1. Cyclic voltammograms on Pt at a scan rate of 50 mV/s in H_3PO_4 over the concentration range 6.6-95 w/o (weight percent) at 25°C.

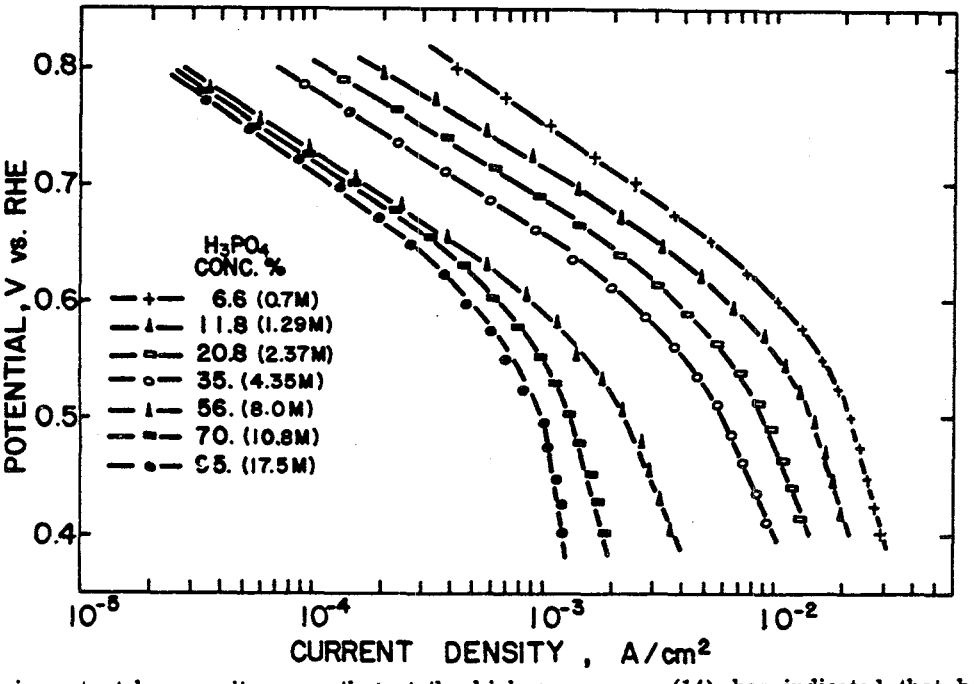

Fig. 2. Mass-transfer-corrected Tafel behavior for oxygen reduction on Pt in H_3PO_4 over the concentration range 6.6-95 w/o at 25°C. Tafel behavior is independent of electrode rotating speed in the 400-3600 rpm region.

important because it means that at the high concentrations used in fuel cells the amount of formation of H_2O_2 is negligible and the faradaic efficiency is close to unity.

Effect of anion adsorption on the rate of oxygen reduction.—The decrease in the oxygen reduction rate with increasing H_3PO_4 concentrations can be attributed to several factors. These include the oxygen solubility, proton activity, and changes in double layer structure. In the region of potential considered, the rate of oxygen reduction in acid media as shown by Eq. [3] is first order with respect to the oxygen concentration and the proton activity (4, 13). Experimental evidence (14) has indicated that both oxygen solubility and proton activity decrease with increasing H_3PO_4 concentration; one would, therefore, expect a lower oxygen reduction current in concentrated H_3PO_4 solutions.

However, the most significant factor in determining the rate of oxygen reduction may be due to the change in the double layer structure at the electrode/electrolyte interface with H_3PO_4 concentration. A recent study (9) has shown that the double layer thickness is greater at a mercury electrode/concentrated H_3PO_4 interface than at a mercury electrode/aqueous electrolyte interface. Thus, the distance for electron tunneling can be expected to be greater at the electrode/phosphoric

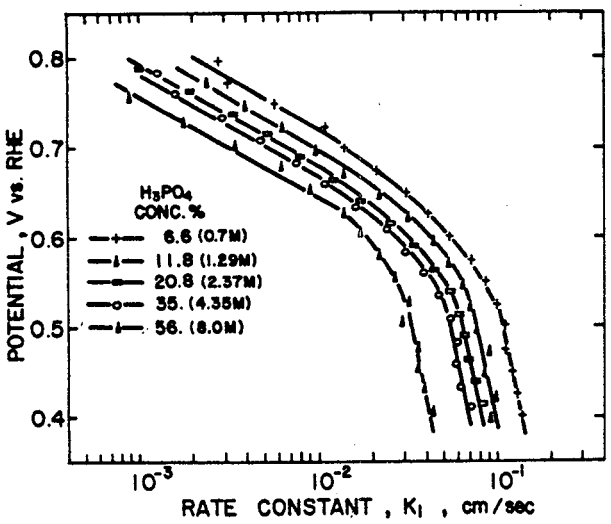

Fig. 3. Potential dependence of rate constant k_1 for oxygen reduction at Pt in H_3PO_4 in the concentration range 6.6-56 w/o at 25°C.

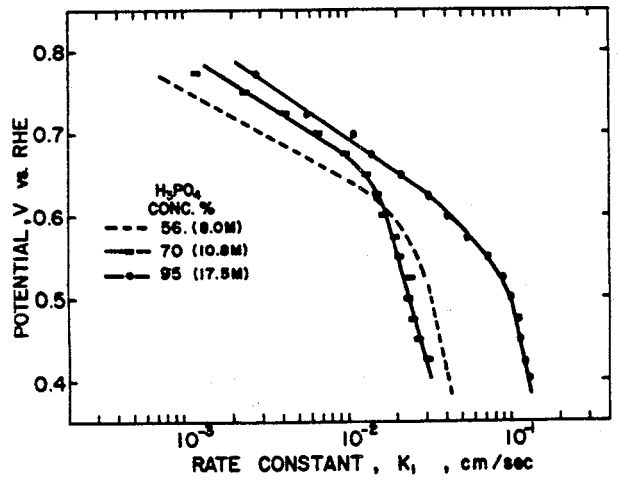

Fig 4. Potential dependence of rate constant k_1 for oxygen reduction at Pt in H_3PO_4 in the concentration range 56-95 w/o at 25°C.

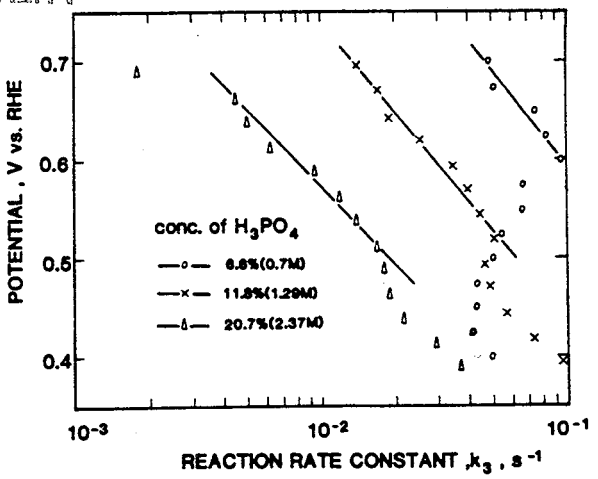

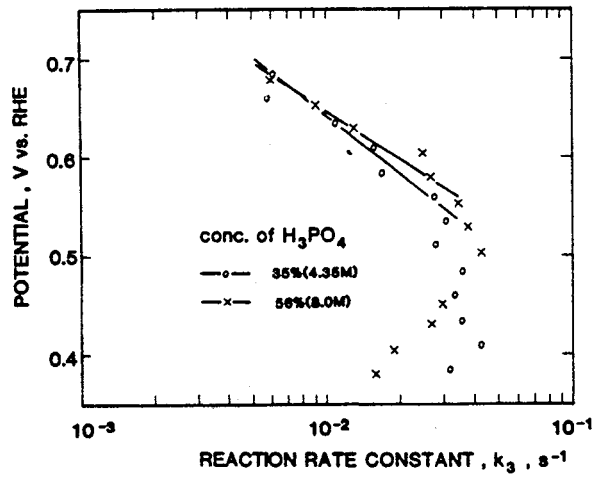

Fig. 6. Potential dependence of rate constant k_3 for oxygen reduction of Pt in H_3PO_4 in the concentration range 6.6-56 w/o at 25°C.

acid interface than at the electrode/aqueous electrolyte interface. At the same time, the presence of phosphate species on the electrode surface could interfere with the adsorption of reactants and/or intermediates. To

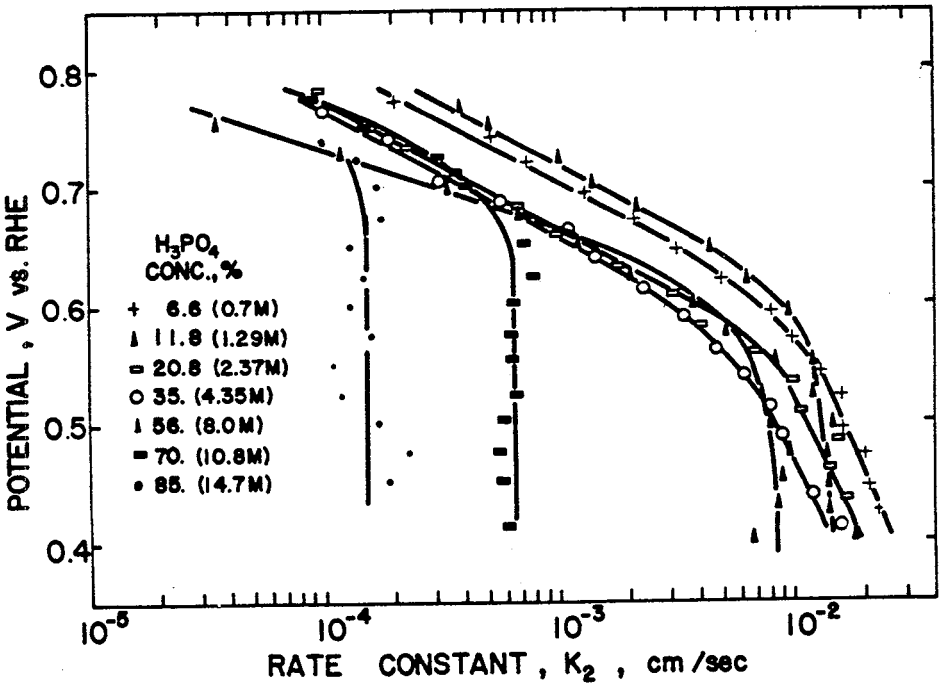

Fig. 5. Potential dependence of rate constant k_2 for oxygen reduction at Pt in H_3PO_4 in the concentration range 6.6-85 w/o at 25°C.

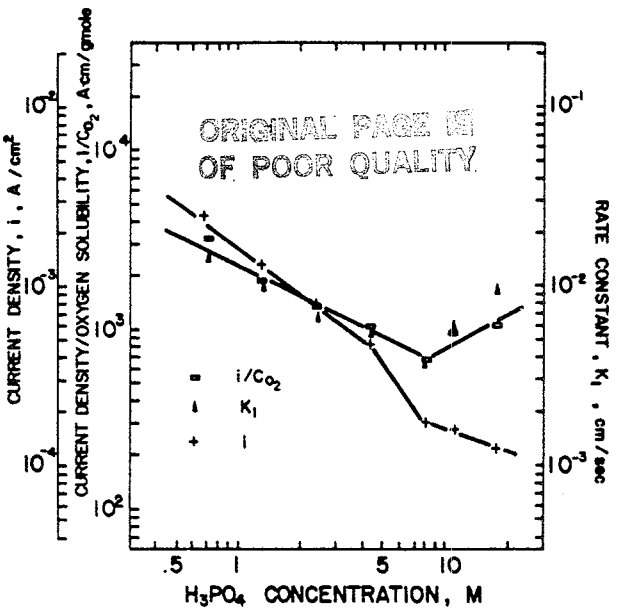

Fig. 7. Dependences of i, i/c_{O_2}, and k_1 for oxygen reduction at Pt on H_3PO_4 concentration at 25°C.

provide further evidence of strong anion adsorption, a separate experiment using a streaming electrode technique (15) was made to determine the effect of phosphoric acid concentration on the potential of zero charge on a mercury electrode. Figure 8 shows the plot of the potential of zero charge (E_z) as a function of H_3PO_4 concentration. A large change of E_z toward more negative values was observed as the concentration of H_3PO_4 increased, which is evidence for increasing adsorption of phosphate species at the interface. The change of E_z with H_3PO_4 concentration is linear, which means that the properties of the double layer undergo a gradual change. It can be expected that the extent of adsorption of the phosphate ion on platinum is at least as much as that on mercury. The presence of phosphate ions on the electrode surface blocks the active sites for the charge-transfer reaction and causes a decrease in the oxygen reduction current.

The plots of i/c_{O_2} *vs.* H_3PO_4 concentration (Fig. 7) indicate that the rate of the reaction has a minimum at a certain H_3PO_4 concentration. This behavior has sometimes been observed for electrode reactions in mixed solvents (16). The phenomenon can be attributed to differential solvation between the electrode and the reacting species. Thus, if the latter is preferentially solvated with water molecules while the electrode is covered by phosphate species, a lower rate of reaction should then be expected. On the other hand, if the electrode and the reactant share the same solvating species, as would be the case in dilute or very concentrated phosphoric acid electrolytes, then the activated complex may be nearer the electrode surface and higher rates should be expected.

Conclusions

The results of the cyclic voltammetric and rotating ring-disk electrode experiments make it possible to reach the following conclusions on the effects of phosphoric acid concentration on oxide formation and oxygen reduction kinetics at platinum.

1. At concentrations below 4M, phosphoric acid has hardly any effect on the cyclic voltammograms. Above 4M, there is a progressive shift of the potential for commencement of oxide formation in the positive direction. Strong anion adsorption is indicated.

2. In the potential range 0.8-0.6V, the slope of the mass-transfer-corrected Tafel plots is nearly equal to 120 mV/decade and is practically independent of concentration. Below 0.6V, the slope becomes quite high (≈ 200 mV/decade), and then the current densities tend to a limiting value, which decreases with increasing acid concentration.

3. The mechanism proposed by Damjanovic *et al.*, that is, the four-electron transfer reduction in which the first electron transfer step is rate determining, appears most appropriate at potentials above 0.6V. The limiting current densities are probably due to a rate-determining dissociative adsorption of oxygen.

4. The rate constants for the two (k_2)- and four (k_1)-electron transfer reduction reactions have the same potential dependence. The ratio k_1/k_2 is greater than

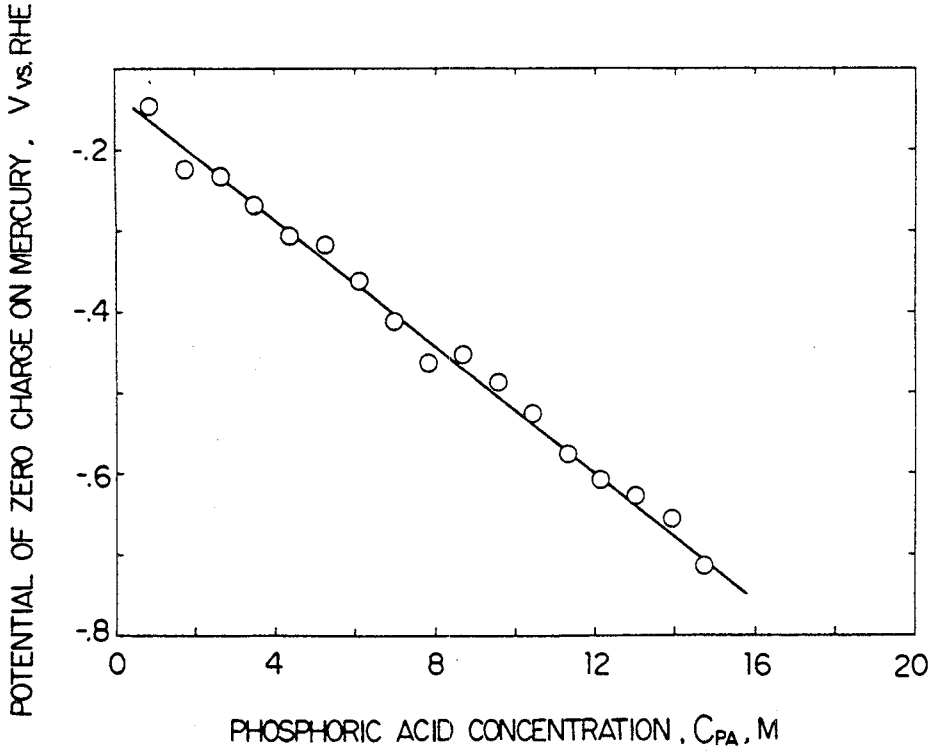

Fig. 8. Dependence of the potential of zero charge on mercury on H_3PO_4 concentration at 25°C.

10, which again supports the second conclusion. At concentrations above 8M, k_2 is independent of potential, probably because of the need for a preferential orientation of oxygen leading to the formation of H_2O_2.

5. The decrease in reaction rates at higher concentrations can be attributed to four causes: lower oxygen solubility, lower proton activity, increased specific adsorption of anions, and a thicker double layer. Complementary experiments that yielded the concentration dependence of the potential of zero charge on mercury support the view that specific adsorption of anions is quite strong.

6. Minima in the plots of i/c_{O_2} and of k_1 *vs.* concentration at a fixed potential illustrate the effects of differential solvation between electrode and reaction species on oxygen reduction kinetics. Similar phenomena have been observed for other reactions in mixed solvents.

Acknowledgments

This work was performed under the auspices of the U.S. Department of Energy. E. R. Gonzalez thanks CNPq, Brazil, for a travel grant to Los Alamos National Laboratory during the summers of 1982 and 1983. The contribution of K-L. Hsueh partially fulfilled requirements toward his Ph.D. degree from the Department of Chemical Engineering, Clarkson College of Technology, Potsdam, New York. The authors wish to thank Dr. E. O'Sullivan of Case Western Reserve University, Dr. S. Gottesfeld of Tel Aviv University, and Dr. S. W. Feldberg of Brookhaven National Laboratory for helpful discussions and suggestions.

Manuscript submitted July 26, 1982; revised manuscript received July 8, 1983. This was Paper 677 presented at the Montreal, Quebec, Canada, Meeting of the Society, May 9-14, 1982.

Los Alamos National Laboratory assisted in meeting the publication costs of this article.

REFERENCES

1. A. J. Appleby and B. S. Baker, *This Journal*, **125**, 404 (1978).
2. A. A. Adams, R. T. Foley, and H. J. Barger, Jr., *ibid.*, **124**, 1228 (1977).
3. A. J. Appleby, *ibid.*, **117**, 328 (1970).
4. A. J. Appleby, *ibid.*, **117**, 641 (1970).
5. A. J. Appleby, *ibid.*, **117**, 91 (1970).
6. S. J. Clouser, J. C. Huang, and E. Yeager, Abstract 348, p. 572, The Electrochemical Society Extended Abstracts, 82-1, Montreal, Que., Canada, May 9-14, 1982.
7. J. C. Huang, R. K. Sen, and E. Yeager, *This Journal*, **126**, 786 (1979).
8. W. E. O'Grady, E. J. Taylor, and S. Srinivasan, *J. Electroanal. Chem.*, **132**, 137 (1982).
9. E. R. Gonzalez, K-L. Hsueh, and S. Srinivasan, *This Journal*, **130**, 1 (1983).
10. K-L. Hsueh, D-T. Chin, and S. Srinivasan, *J. Electroanal. Chem.*, **153**, 79 (1983).
11. B. E. Conway and D. M. Novak, *This Journal*, **128**, 956 (1981).
12. A. Damjanovic, M. A. Genshaw, and J. O'M. Bockris, *J. Chem. Phys.*, **45**, 4057 (1966).
13. D. B. Sepa, M. V. Vojnovic, and A. Damjanovic, *Electrochim. Acta*, **26**, 781 (1981).
14. K-L. Hsueh, Ph.D. Dissertation, Clarkson College of Technology, Potsdam, New York (1983).
15. D. C. Grahame, R. P. Larsen, and M. A. Poth, *J. Am. Chem. Soc.*, **71**, 298 (1949).
16. T. Biegler, E. R. Gonzalez, and R. Parsons, *Coll. Czech. Chem. Comm.*, **36**, 414 (1971).

ELECTRODE KINETICS OF OXYGEN REDUCTION ON PLATINUM IN TRIFLUOROMETHANESULFONIC ACID

K-L. Hsueh, H. H. Chang, D-T. Chin
Department of Chemical Engineering
Clarkson College of Technology
Potsdam, New York 13676

and

S. Srinivasan
Electronics Division, MS D429
Los Alamos National Laboratory
Los Alamos, New Mexico 87545

ABSTRACT

The kinetics of oxygen reduction at Pt in trifluoromethanesulfonic acid (TFMSA) (0.05 - 6.0M) and in 1.0M TFMSA with addition of small concentrations of phosphoric acid (0.003 - 0.1M) was investigated using the rotating ring-disc electrode technique. In TFMSA, the oxygen reduction current on the oxide-covered Pt was found to be smaller than that on the oxide-free Pt surface. This result is consistent with the greater amount of hydrogen peroxide produced on the oxide-covered Pt. A reaction order of one-half with respect to the oxygen concentration for the oxygen reduction reaction was obtained from the ring-disc data. Addition of increasing amounts of phosphoric acid to TFMSA resulted in a progressive decrease in the oxygen reduction current and in an increase of the reaction order with respect to oxygen. On the basis of these experimental results the reaction mechanism proposed for the oxygen reduction on Pt in TFMSA is the fast dissociative adsorption of oxygen, followed by the first slow electron transfer step.

I. INTRODUCTION

Trifluoromethanesulfonic acid (CF_3SO_3H, TFMSA) and its homologues of higher molecular weight are considered alternatives to phosphoric acid as acid electrolytes for fuel cells. The reaction rate of oxygen reduction at Pt in TFMSA is about two orders of magnitude higher than that in phosphoric acid.[1] This fast reaction rate of oxygen reduction in TFMSA has been attributed to the high oxygen

solubility and weak adsorption of anions from TFMSA on the electrode.[2] Two Tafel regions for oxygen reduction at Pt in TFMSA were observed[2], i.e., 60 mV/decade at low overpotentials and 120 mV/ decade at high overpotentials. Although there have been some investigations of oxygen reduction on platinum in aqueous TFMSA and in TFMSA monohydrate on smooth and porous electrodes[1], its kinetics in this electrolyte is not yet fully understood.

The purpose of this study is to investigate the kinetics of oxygen reduction at smooth Pt in aqueous TFMSA (0.05-6M) and in a mixed acid containing 1.0M TFMSA and 0.003 - 0.1M phosphoric acid at room temperature. Rotating ring-disc electrode and cyclic voltammetric techniques were used. From the calculated reaction orders with respect to oxygen and mass transfer corrected Tafel plots, a reaction mechanism is proposed for the oxygen reduction on Pt in TFMSA.

II. EXPERIMENTAL

The electrochemical cell incorporated the platinum ring-disc electrodes (Pine Instrument DT 6 #1004), a large platinum gauze counter electrode and a dynamic hydrogen as the reference electrode (DHE). The potential of the ring and disc electrodes vs the DHE electrode was converted to the reversible hydrogen (RHE) scale by use of the measured potential of the DHE vs a floating type Pt fuel cell electrode which was saturated with hydrogen. The electrolytes used were 0.05 - 6M TFMSA, and 1.0M TFMSA containing small concentrations (0.003 - 0.1M) of phosphoric acid. Trifluoromethanesulfonic acid (3M Co.), was distilled twice under vacuum (B.P. < 40°C). The distillate was added to double distilled water to form TFMSA monohydrate which was then vacuum-distilled (B.P. < 80°C). The monohydrate was stored in the crystallized form. Before use, the monohydrate was diluted with double distilled water to the desired concentration and was preelectrolyzed for 24 hours. Phosphoric acid (J. T. Baker, electronic grade) was treated with 10% hydrogen peroxide (90% stabilizer free, FMS) and heated to 50 - 100°C for one hour to remove excess peroxide. Before use, the acid was anodically pre-electrolyzed for 24 hours using a platinum gauze electrode to eliminate electroactive impurities.

The ring-disc electrode was polished using 25-μ and 5-μ polishing powder, followed by 1-μ and 0.25-μ diamond paste (Buehler LTD). After polishing, the electrode was degreased with acetone, washed with distilled water, and then transferred into the cell. The potentials of the disc and ring electrodes were controlled by a potentiostat (Pine Instrument, RDE 3). The rotation speed of the electrode was controlled by a high speed rotator (Pine Instrument, ASR 2).

Before the electrode kinetic experiments, the solution was deaerated with purified nitrogen gas and a cyclic voltammogram on the platinum disc electrode was recorded at a scan rate of 50 mV/s.

Oxygen (1 atm) was then bubbled through the electrolyte for half an hour. During the rotating ring-disc electrode experiments, the potential of the ring electrode was maintained at 1.1 V vs DHE for the oxidation of hydrogen peroxide (which was formed at the disc electrode and diffused to the ring electrode) to oxygen at the limiting current density. The potential of disc electrode was scanned from 1.0 - 0.3 V vs DHE and in the reverse direction between these potentials at a scan rate 5 mV/s. The ring and disc currents were recorded on a dual pen X-Y-Y' recorder (Soltec 6431). All the experiments were carried out at a temperature of 25°C.

III. RESULTS AND DISCUSSION

Effects of the Surface Oxide at Pt on the Kinetics of Oxygen Reduction in TFMSA

The cyclic voltammograms on Pt in different TFMSA concentrations are presented in Fig. 1. There was a significant change in the position and shape of the peaks corresponding to the formation/reduction of oxide, and the adsorption/desorption of hydrogen as the TFMSA concentration was varied from 0.05 to 6.0M. The observed concentration dependence of the cyclic voltammograms indicates that either the water activity decreased or the adsorption of anions increased with increase of TFMSA concentration. The oxide on the Pt surface formed at a potential close to 1.0 V vs RHE was completely reduced at 0.3 V vs RHE. When the electrode potential was scanned from 1.0 to 0.3 V vs RHE in the rotating ring-disc electrode experiments, the electrode surface was first covered with a layer of oxide and then gradually reduced to bare Pt at the end of the scan. Conversely when the electrode potential was scanned from 0.3 to 1.0 V vs RHE, the electrode started with an oxide-free surface and then the oxide gradually formed at potentials above 0.8 V vs RHE.

The influence of the surface oxide on the kinetics of oxygen reduction at Pt in 0.05M TFMSA is shown in Fig. 2 (at ω = 900 rpm). The disc current (I_d) for oxygen reduction on the oxide-free surface (potential scanned from 0.3 to 1.0 V vs RHE) was higher at all potentials than that on the oxide-covered surface (potential scanned from 1.0 to 0.3 V vs RHE). The maximum amount of hydrogen peroxide detected on the ring electrode (I_r) for the oxide-covered disc electrode was 400% higher than that for the oxide-free disc electrode.

In the same potential region (0.3 - 1.0 V vs RHE), the amount of surface oxide on Pt in 6.0M TFMSA was less than that in 0.05M TFMSA (Fig. 1). Accordingly, the influence of direction of the scan of the electrode potential on the kinetics of oxygen reduction in 6.0M TFMSA should have been less than that in 0.05M TFMSA. This can be observed by comparing the ring currents as a function of disc potential in 0.05M TFMSA (Fig. 2) and in 6.0M TFMSA (Fig. 3). The difference in the maximum ring current between the forward (1.0 - 0.3 V vs RHE) and the backward (0.3 - 1.0 V vs RHE) scan in 6.0M TFMSA was 35%, whereas

the difference in 0.05M TFMSA was 400%. All the data reported in the next section were obtained with the scan of the disc electrode potential from 1.0 to 0.3 V vs RHE.

Reaction Order with Respect to Oxygen for the Oxygen Reduction Reaction at Pt in TFMSA

An attempt was made to determine the rate constants for oxygen reduction at Pt in TFMSA with a reaction scheme proposed in previous publications:[6-8]

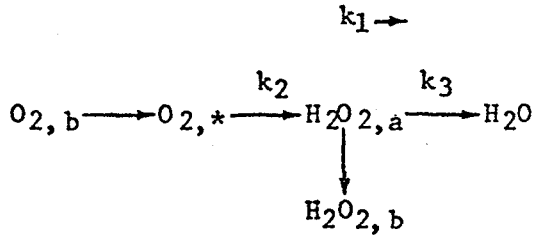

Mathematical expressions have been derived for the case when the intermediate steps are first order with respect to the surface concentration of oxygen and hydrogen peroxide. Two important equations, which are used for the calculation of rate constants, k_1, k_2, and k_3, are:

$$\frac{I_{d\ell}}{I_{d\ell} - I_d} = 1 + \frac{k_1 + k_2}{Z_1} \omega^{-1/2} \qquad (1)$$

and

$$\frac{I_d}{I_r} = \frac{1}{N}\left(1 + 2\frac{k_1}{k_2}\right) + \left[\frac{2(k_1/k_2+1)}{N Z_2} k_3\right] \omega^{-1/2} \qquad (2)$$

These equations have been used to calculate the rate constants for the oxygen reduction reaction in several aqueous electrolytes, including H_3PO_4, H_2SO_4, $HClO_4$, and KOH.[7] However in the present study, difficulties were encountered in using Eqs. (1) and (2) to interpret the rotating ring-disc data for oxygen reduction in TFMSA solutions. Negative intercepts were observed for both the $I_{d\ell}/(I_{d\ell}-I_d)$ vs $\omega^{-1/2}$ and I_d/I_r vs $\omega^{-1/2}$ plots in all TFMSA solutions (0.05-6.0M) as well as in 1.0M TFMSA solution with phosphoric acid additivies (0.003 - 0.1M).

The indications are that the above reaction scheme does not apply for oxygen reduction at Pt in TFMSA solutions and in the mixtures of TFMSA/H_3PO_4. One possible explanation is that the reaction order with respect to oxygen in the TFMSA medium is not unity. An equation which

can be utilized for the determination of reaction order with respect to oxygen, m, is:[9]

$$\frac{I_d}{I_k} = (1 - \frac{I_d}{I_{d\ell}})^m \quad . \tag{3}$$

According to this equation, a plot of log I_d vs log $(1 - I_d/I_{d\ell})$, Eq. (3) should be linear with a slope equal to m. The applicability of this equation was tested with the experimental data for oxygen reduction at Pt in 0.5 M sulfuric acid and is demonstrated in Fig. 4. The reaction order obtained from this plot is 1 ± 0.2 which is consistent with the previous observations.[3] The reaction orders with respect to oxygen in TFMSA and in mixtures of TFMSA/H_3PO_4 were calculated from similar plots using the present experimental results. A typical plot of log I_d vs log $(1 - I_d/I_{d\ell})$ in 0.05M TFMSA, presented in Fig. 5, reveals a fractional reaction order. The calculated reaction orders in TFMSA solutions and in mixtures of TFMSA/H_3PO_4 in the potential region from 0.6 - 0.4 V vs RHE are listed in Table 1. In the concentrations of TFMSA investigated, the reaction orders of oxygen were between 0.4 and 0.5. In the mixtures of 1.0 M TFMSA and 0.003 - 0.1M phosphoric acid, the reaction order of oxygen increased from one half as the concentration of phosphoric acid was increased. The reaction order is equal to one in pure phosphoric acid solution.

Mass Transfer Corrected Tafel Behavior

The fractional reaction order of oxygen, as derived, can be verified by use of the mass transfer corrected Tafel equation

$$E = \frac{2.3RT}{\alpha F} \log I_o - \frac{2.3RT}{\alpha F} \log I_d \left(\frac{I_{d\ell}}{I_{d\ell} - I_d}\right)^m \quad . \tag{4}$$

The plot of E vs log $I_d\,[I_{d\ell}/(I_{d\ell} - I_d)]^m$ should be independent of the rotating speed of electrode, ω, if m is chosen properly. This plot in 0.05M TFMSA is given in Fig. 6 for m = 1 and in Fig. 7 for m = 1/2. The plot for m = 1 was dependent on ω while that for m = 1/2 was independent of ω. This behavior was observed in all other TFMSA electrolytes and in mixtures of TFMSA and H_3PO_4. The reaction order of one half for oxygen in TFMSA is different from that in other acids, such as phosphoric acid and sulfuric acid. A possible explanation for a reaction order of one half is discussed in a later section.

Kinetics of Oxygen Reduction at Pt in TFMSA and in Mixtures of TFMSA/H_3PO_4

The plots of E vs log $I_d[I_{d\ell}/(I_{d\ell}-I_d]^{0.5}$ for oxygen reduction at Pt in TFMSA and in 1 M TFMSA containing three concentrations of phosphoric acid are shown in Figs. 8 and 9 respectively. At a given potential, the oxygen reduction current decreased as the concentration of TFMSA or of phosphoric acid was increased. The decreases in the oxygen reduction current in concentrated TFMSA might be due to a lower oxygen solubility and/or higher anion adsorption. It has been noticed in a previous study[10] that the adsorption of phosphate ion is stronger than that of TFMSA anion. In TFMSA containing phosphoric acid additives, the phosphate ion tends to adsorb on the electrode surface. The decrease in the oxygen reduction current with the addition of phosphoric acid was probably due to the electrochemical active sites being blocked by the adsorption of phosphate ions.

Possible Mechanism of Oxygen Reduction at Pt in TFMSA

The mechanism of oxygen reduction at Pt in aqueous acid and alkaline electrolytes has been proposed by Damjanovic and Brusic[11] and by Huang, Sen, and Yeager.[6] The first step in the reaction is the adsorption of oxygen on the electrode surface. According to the latter workers, bridged adsorption of oxygen leads to the four electron transfer reduction of oxygen while end-on adsorption favors the production of hydrogen peroxide.[6] The bridged adsorption of oxygen can occur via path 2 where the adsorbed molecular oxygen is dissociated into atomic oxygen. This atomic oxygen then takes part in the charge-transfer and protonation reaction to form water as the final product (path 3). Bridged adsorption of oxygen can also lead to water or hydrogen peroxide via path 4. End-on adsorption of oxygen is followed by charge-transfer and protonation (path 6), and hydrogen peroxide is the final product. By assuming that the first charge-transfer and protonation step is rate determining, the Tafel slope is 60 mV/decade under Temkin adsorption conditions and is 120 mV/decade for Langmuir adsorption conditions.[11,12] In the referenced publications, the dissociation step (path 2) was not considered and a reaction order of unity with respect to oxygen was assumed.

Based on the proposed mechanism[6,11], the reaction order of one-half with respect to oxygen can be explained by considering a fast dissociation step (path 2 in Fig. 10) and that step 3 is rate determining. It should also be assumed that the adsorption of oxygen is under Langmuir conditions (in the electrode potential region 0.6 to 0.4 V vs RHE). Since step 3 is rate determining, the reduction current I_d can be expressed as

$$I_d = \vec{k}_3[O_{ads}][\overset{+}{H}]\exp\frac{\beta EF}{RT} \quad . \tag{5}$$

Assuming that the steps before the rate determining step 4 are in equilibrium,

$$\vec{k}_2\theta = \overleftarrow{k}_2[O_{ads}]^2 \qquad \text{for step 2, and} \tag{6}$$

$$\vec{k}_1[O_2](1-\theta) = \overleftarrow{k}_1\theta \qquad \text{for step 1} \tag{7}$$

Under Langmuir adsorption conditions,

$$1 - \theta \simeq 1 \tag{8}$$

By use of equations (6) - (8) in eq. (5), I_d can be expressed by:.

$$I_d = k[H^+][O_2]^{1/2} \exp -\frac{-\alpha F}{RT}E \tag{9}$$

where

$$k = \vec{k}_3 (\vec{k}_1\vec{k}_2/\overleftarrow{k}_1\overleftarrow{k}_2)^{1/2} \tag{10}$$

According to Eq. (9), the oxygen reduction current, I_d, is first order with respect to $[H^+]$, and one-half order for $[O_2]$. The Tafel slope is 120 mV/decade (assuming $\beta = 1/2$) under Langmuir adsorption conditions.

IV. CONCLUSIONS

The surface chemistry of Pt electrode has been shown to be an important factor in the kinetics of oxygen reduction in TFMSA. A lower oxygen reduction current and a larger amount of hydrogen peroxide were observed for the oxide-covered Pt surface (when the electrode potential is scanned from 1.0 to 0.3 V vs RHE) as compared to the oxide-free surface (when the electrode potential is scanned from 0.3 to 1.0V vs RHE). The rotating ring-disc electrode analysis resulted in a reaction order of one-half with respect to the oxygen concentration. Addition of phosphoric acid to the TFMSA decreased the rate of oxygen reduction and increased the reaction order with respect to oxygen. On the basis of the present experimental results, a reaction mechanism involving the fast dissociative adsorption of oxygen followed by the first slow electron transfer step was proposed for oxygen reduction at platinum in TFMSA

ACKNOWLEDGMENTS

The experimental work presented in this paper was carried out at Los Alamos National Laboratory. The results were analyzed at Clarkson College. The authors wish to thank Professor Shimshon Gottesfeld of Tel Aviv University and Professor Ernesto R. Gonzalez of the University of Sao Paulo in Sao Carlos for helpful discussions. This work was supported by a grant to Clarkson College from NASA Lewis Research Center (U.S. Department of Energy Fossil Energy Program) and by a contract to Los Alamos National Laboratory from the U.S. Department of Energy.

REFERENCES

1. E. J. Taylor, Ph.D. Dissertation, Department of Materials Science, University of Virginia, Virginia (1981).

2. A. J. Appleby and B. S. Baker, J. Electrochem. Soc., 125, 404 (1978).

3. D. B. Sepa, M. V. Vojnovic, and A. Damjanovic, Electrochimica Acta, 26, 781 (1981).

4. A. A. Adam, R. T. Foley, and H. J. Barger, Jr., J. Electrochem. Soc., 124, 1228 (1977).

5. G. W. Walker and R. T. Foley, J. Electrochem. Soc., 128, 1502 (1981).

6. J. C.Huang, R. K. Sen, and E. Yeager, J. Electrochem. Soc., 126, 786 (1979).

7. K-L. Hsueh, Ph.D. Dissertation, Department of Chemical Engineering, Clarkson College of Technology, Potsdam, New York 13676 (1983).

8. K-L. Hsueh, D-T. Chin, and S. Srinivasan, J. Electroanal. Chem., in press.

9. D-T. Chin, Singapore National Inst. of Chem., in press.

10. E. R. Gonzalez and S. Srinivasan, Electrochimica Acta, 27, 1425 (1982).

11. A. Damjanovic and V. Brusic, Electrochimica Acta, 12, 615 (1967).

12. A. J. Appleby, J. Electrochem. Soc., 117, 328 (1970).

LIST OF SYMBOLS

D_1	diffusion coefficent of oxygen, cm^2/s
D_2	diffusion coefficient of hydrogen peroxide, cm^2/s
E	electrode potential, V vs RHE
F	Faraday constant, 96500 c/eqv
I_d	disc current, A
$I_{d\ell}$	mass transfer limited disc current, A
I_k	kinetic current, I_d at $\omega = \infty$, A
I_o	exchange current, A
I_r	ring current, A
k	overall rate constant, refer to Eq. (9), $A/[H^+][O_2]^{1/2}$
k_1	rate constant of the electrochemical reduction of oxygen to water, cm/s
k_2	rate constant of the electrochemical reduction of oxygen to hydrogen peroxide, cm/s
k_3	rate constant of the electrochemical reduction of hydrogen peroxide to water, cm/s
$\vec{k}_1$	rate constant of bridged adsorption of oxygen of step 1 in Fig. 10, 1/s $[O_2]$
$\overleftarrow{k}_1$	rate constant of bridged desorption of oxygen of step 1 in Fig. 10, 1/s
$\vec{k}_2$	rate constant of dissociation of molecular oxygen of step 2 in Fig. 10, 1/s
$\overleftarrow{k}_2$	rate constant of recombination of atomic oxygen of step 2 in Fig. 10, 1/s $[O]^2$
$\vec{k}_3$	forward rate constant of first charge transfer and protonation of step 3 in Fig. 10, $A/[O][H^+]$

m	reaction order with respect to oxygen
N	collection efficiency of the ring-disk electrode
n	number of electrons transferred for reduction of one g-mol of oxygen, eqv/g-mol
R	ideal gas constant
T	temperature, °K
Z_1	diffusivity-viscosity factor for oxygen, equal to 0.62 $D_1^{2/3} \nu^{1/6}$, cm $s^{-1/2}$
Z_2	diffusivity-viscosity factor for hydrogen peroxide, equal to 0.62 $D_2^{2/3} \nu^{-1/6}$, cm $s^{-1/2}$
α	charge transfer coefficient, dimensionless
β	symmetric factor, dimensionless
θ	fractional surface coverage, dimensionless
ν	kinematic viscosity of electrolyte, cm^2/s
ω	rotation speed of electrode, s^{-1}

The reaction order of oxygen in oxygen reduction at Pt in the potential region from 0.6 to 0.4 V vs. RHE

ELECTROLYTE	REACTION ORDER
0.05 M TFMSA	0.47±0.05
0.1 M TFMSA	0.40±0.05
1.0 M TFMSA	0.40±0.04
6.0 M TFMSA	0.5 ±0.2

1.0 M TFMSA	0.40 ± 0.04
1.0 M TFMSA + 0.003 M H_3PO_4	0.45 ± 0.03
1.0 M TFMSA + 0.1 M H_3PO_4	0.60 ± 0.05
0.7 M H_3PO_4	1.0 ± 0.1

C-2

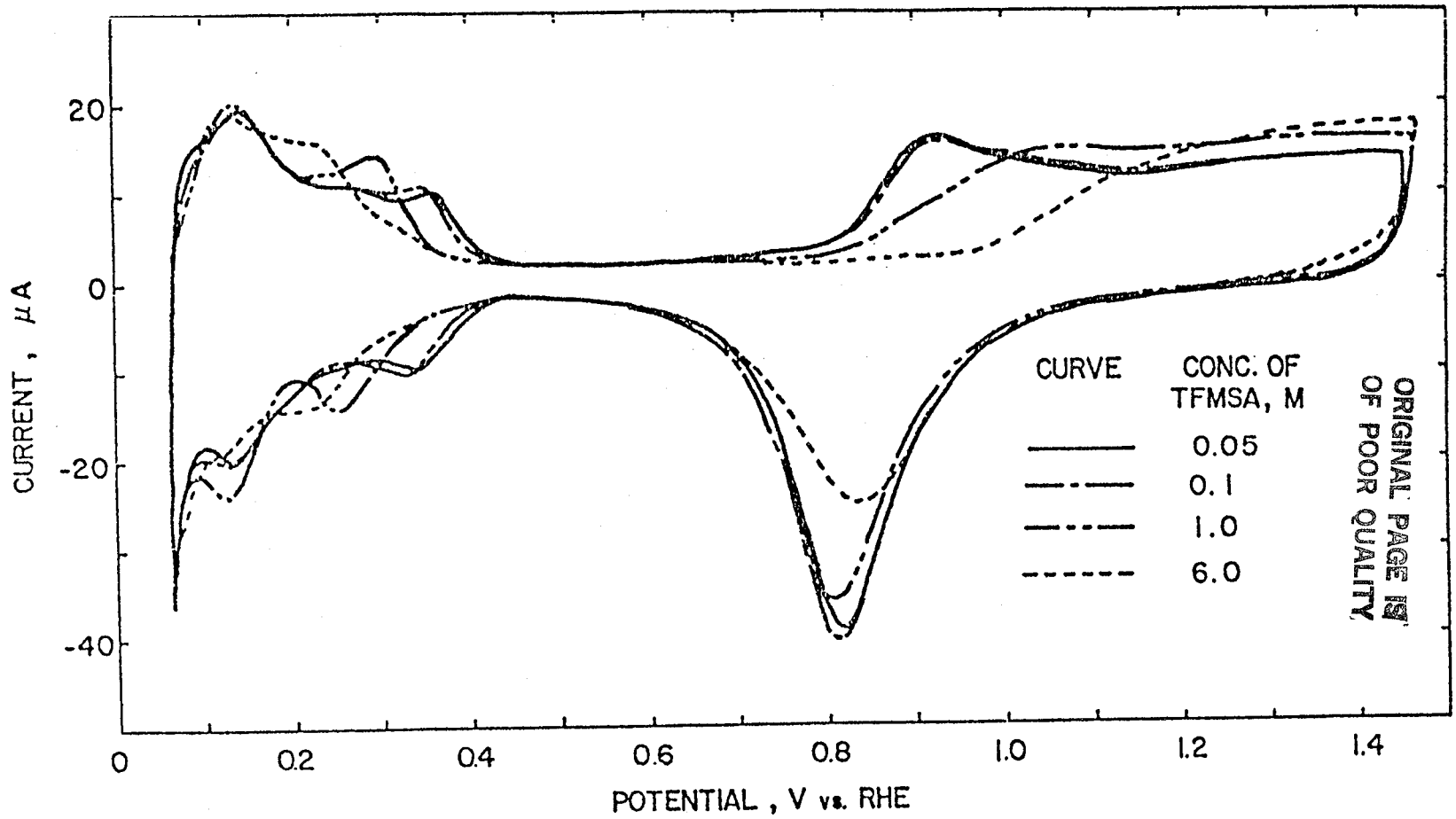

The cyclic voltammograms at Pt, scan rate 50 mV/s, in TFMSA over the concentration range 0.05 M to 6.0 M.

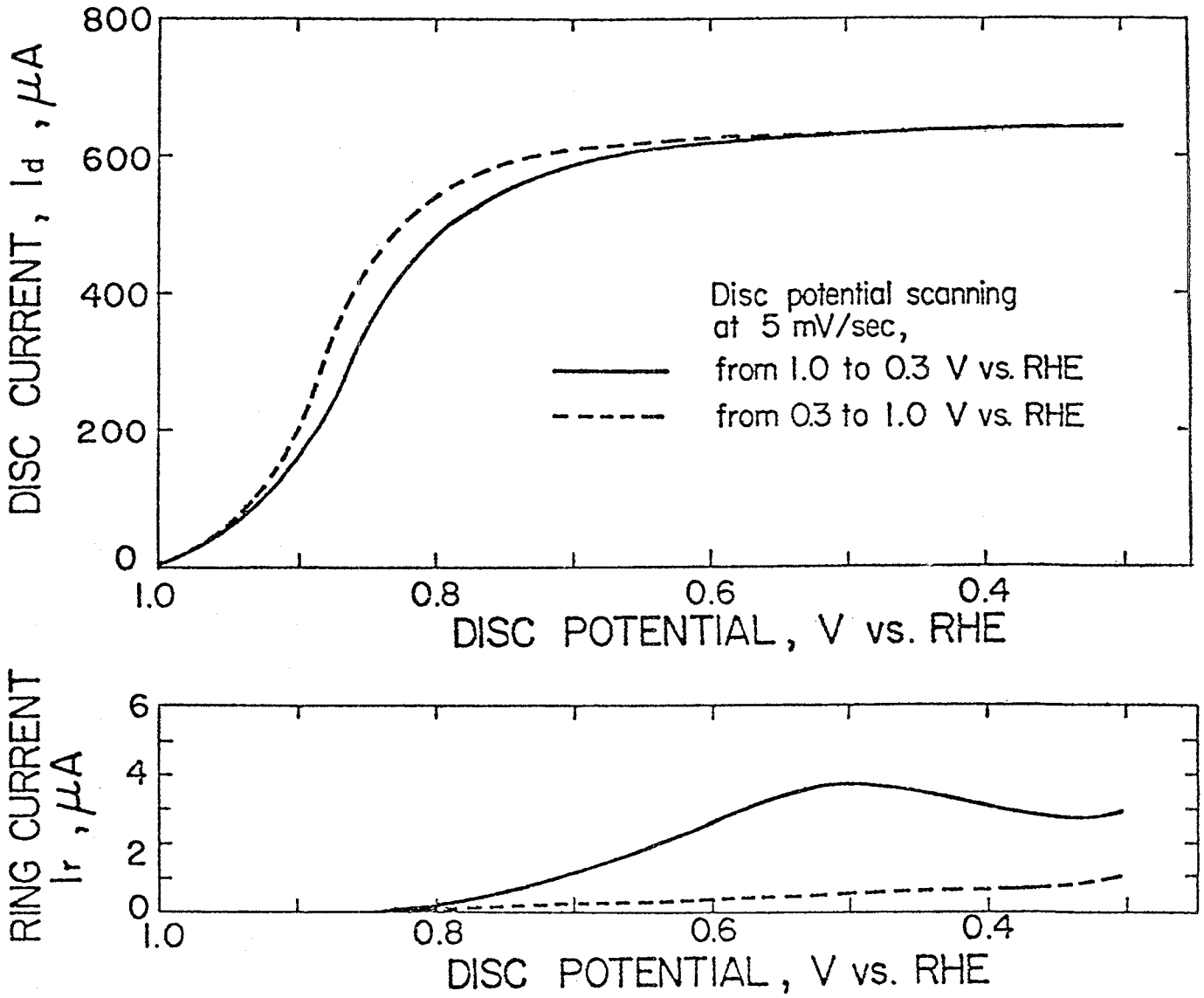

The rotating ring-disc electrode data at ω = 900 rpm for oxygen reduction at Pt in 0.05 M TFMSA.

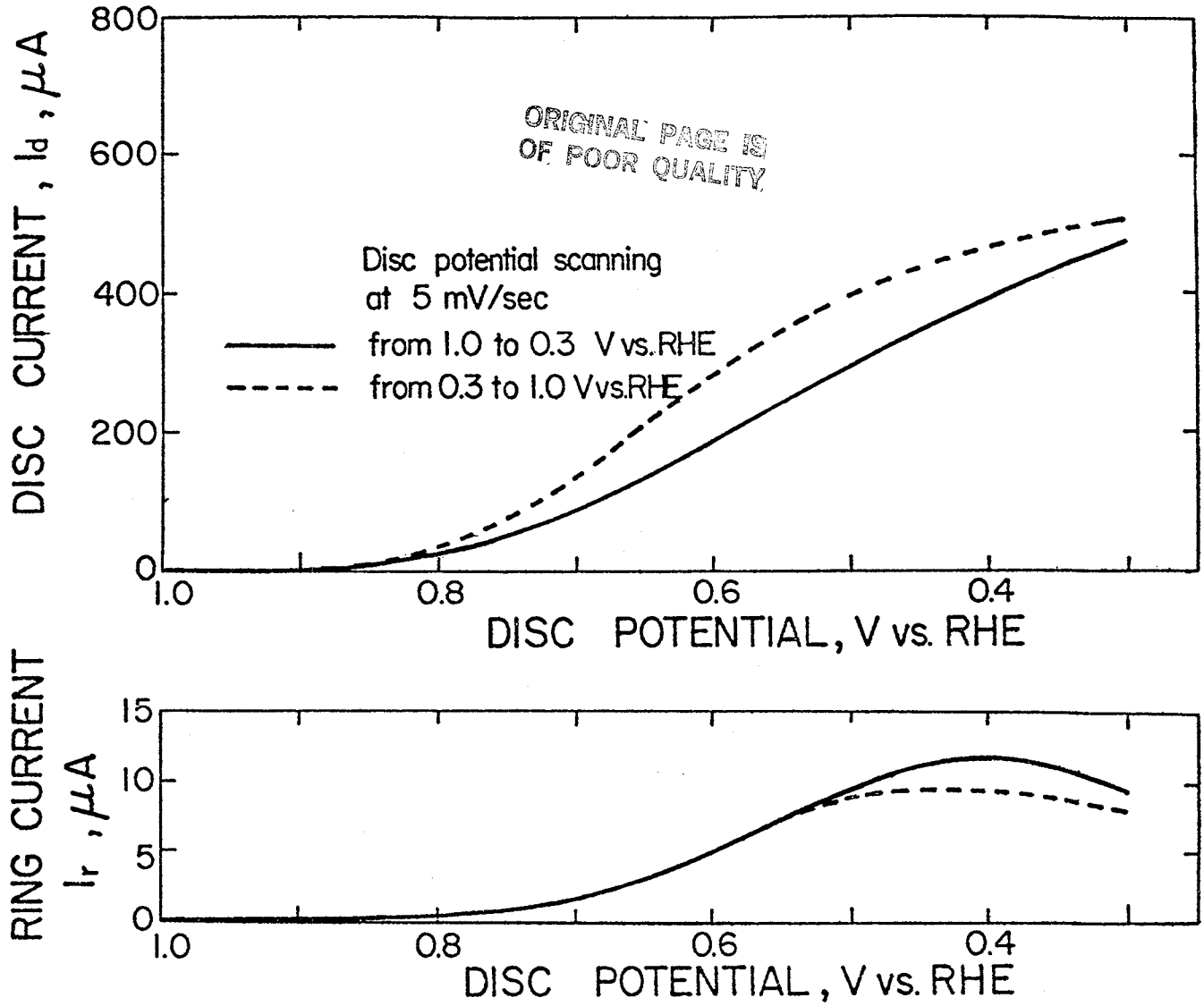

The rotating ring-disc electrode data at ω = 900 rpm for oxygen reduction at Pt in 6.0 M TFMSA.

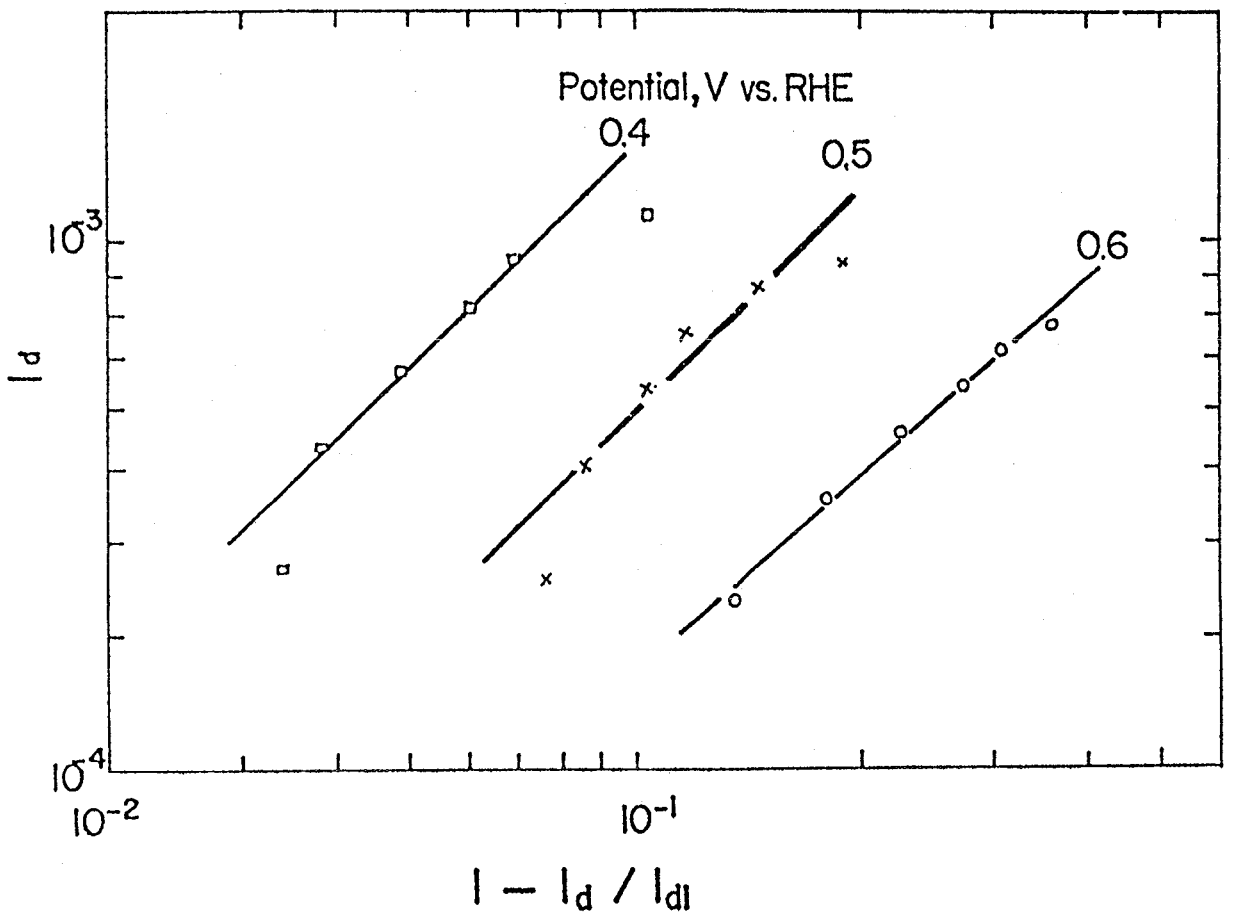

Plot of log I_d vs. log(1 - I_d/I_{dl}). Data were obtained from the rotating ring-disc electrode experiments for oxygen reduction at Pt in 0.55 M H_3SO_4.

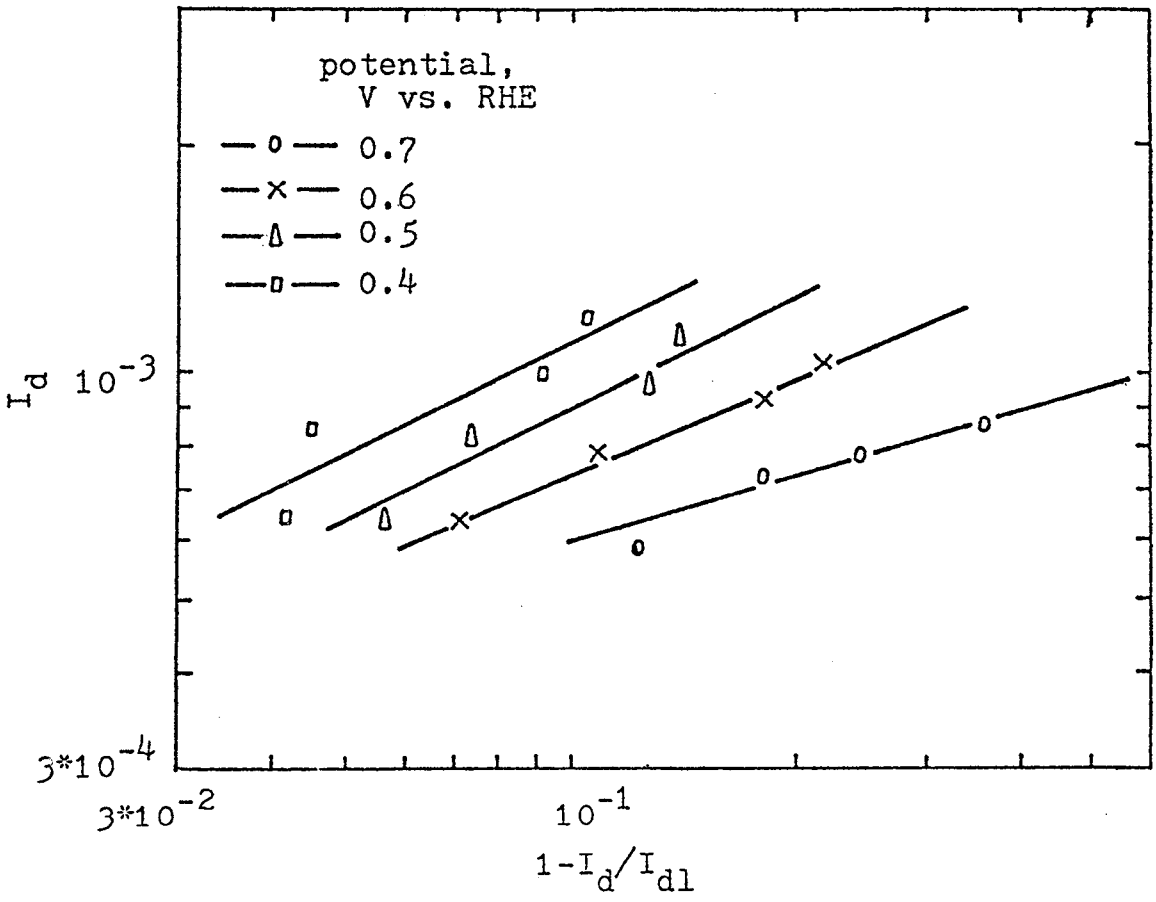

Plot of log I_d vs. log(1 - I_d/I_{dl}). Data were obtained from the rotating ring-disc electrode experiments for oxygen reduction at Pt in 0.05 M TFMSA.

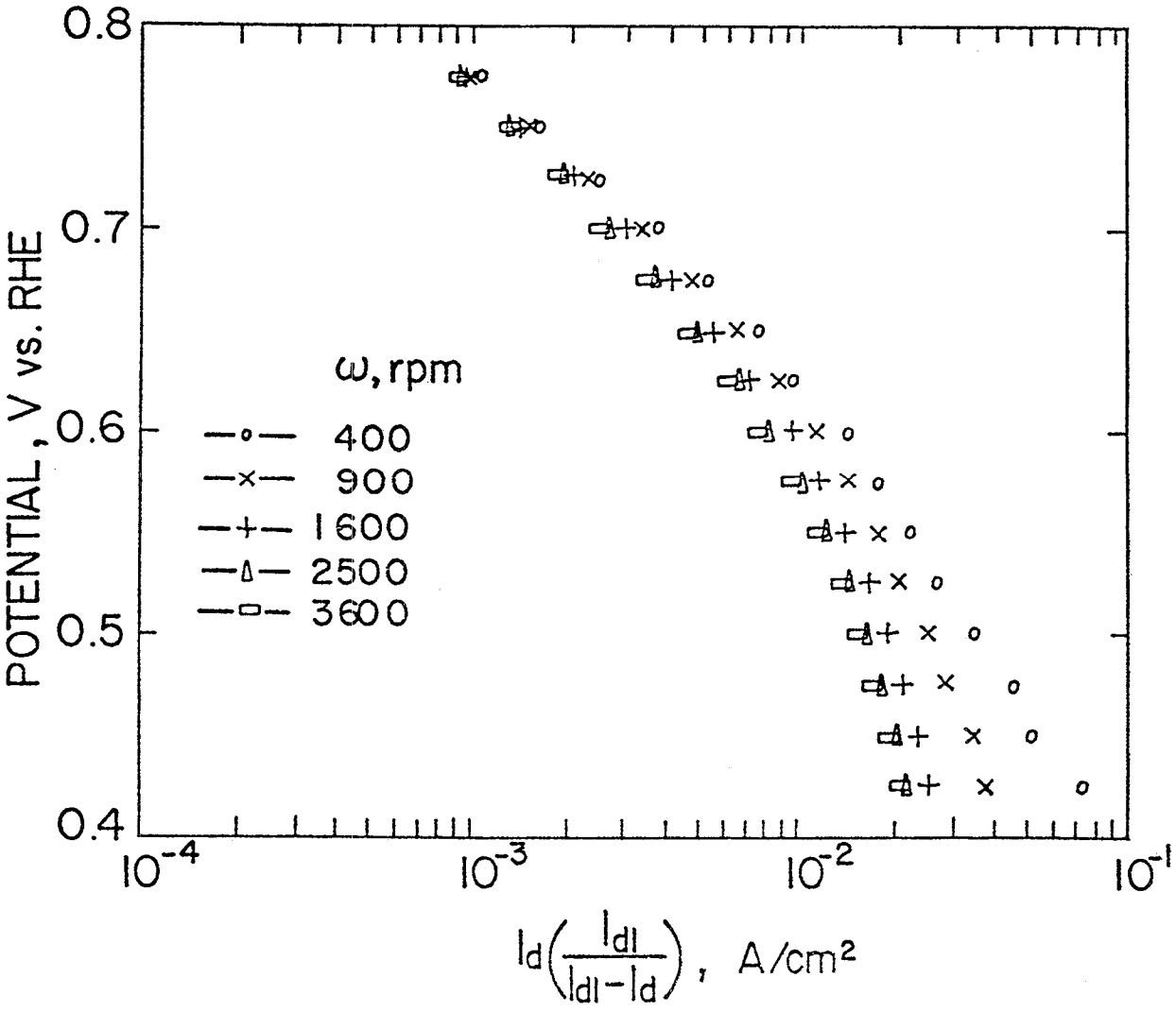

The plot of potential against log $I_d[I_{dl}/(I_{dl} - I_d)]$ for oxygen reduction at Pt in 0.05 M TFMSA for different ω . This plot assumes m = 1.

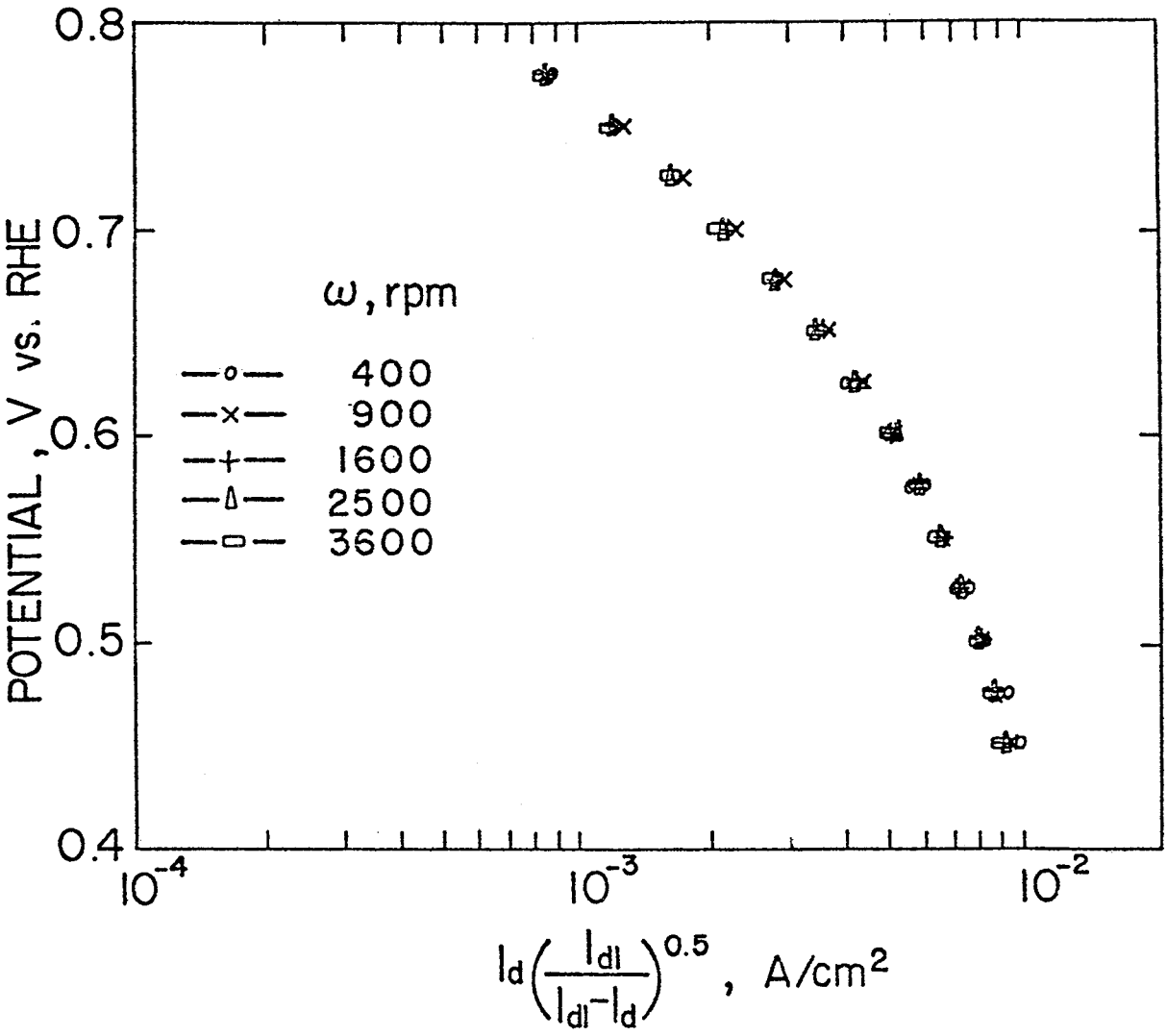

The plot of potential against log $I_d[I_{dl}/(I_{dl} - I_d)]^{1/2}$ for oxygen reduction at Pt in 0.05 M TFMSA for different ω . This plot assumes m = 1/2.

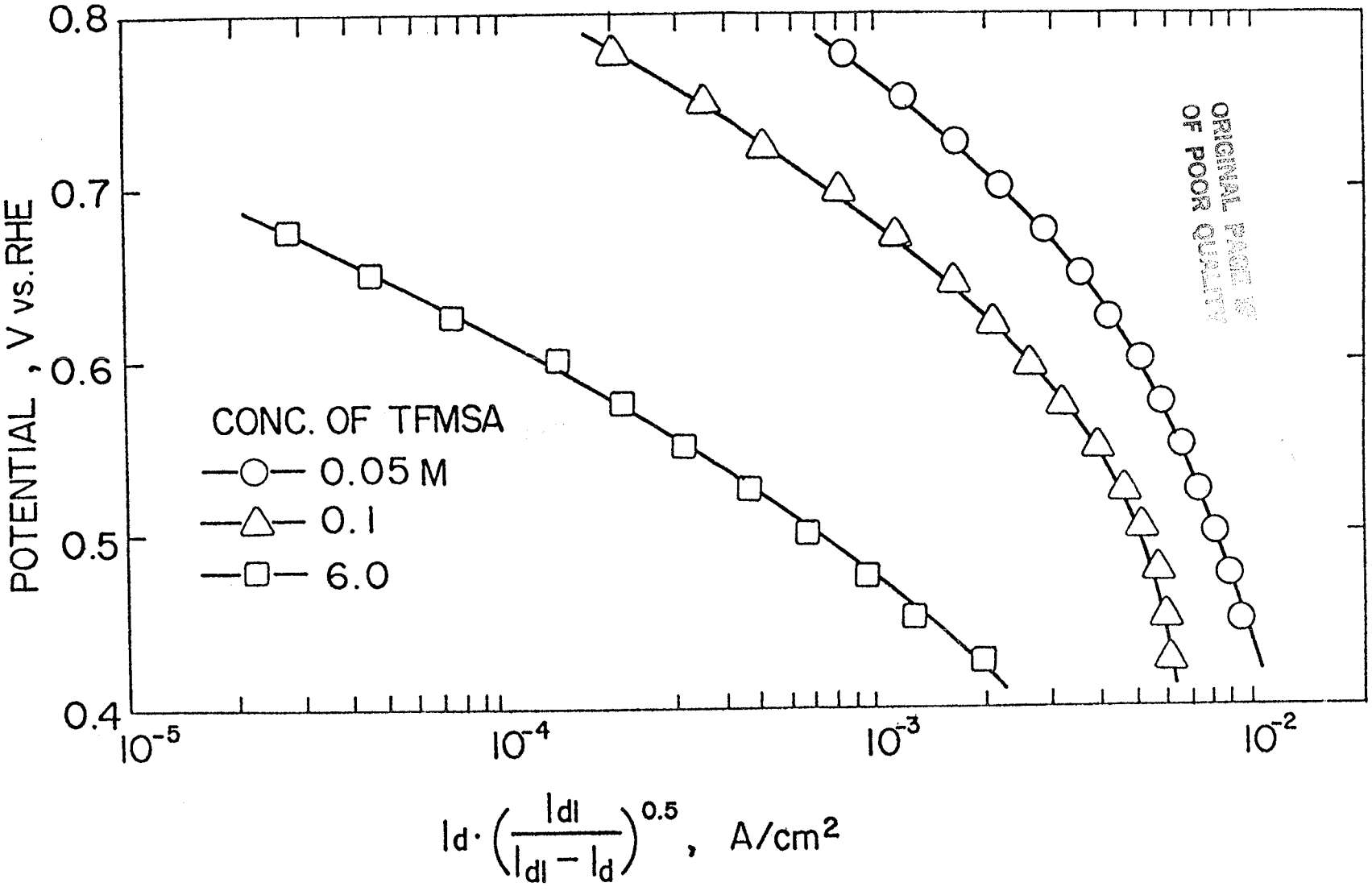

The plot of potential against log $I_d[I_{dl}/(I_{dl} - I_d)]^{1/2}$ for oxygen reduction at Pt in different concentrations of TFMSA. This plot is independent of ω over the range of (400-3600 rpm).

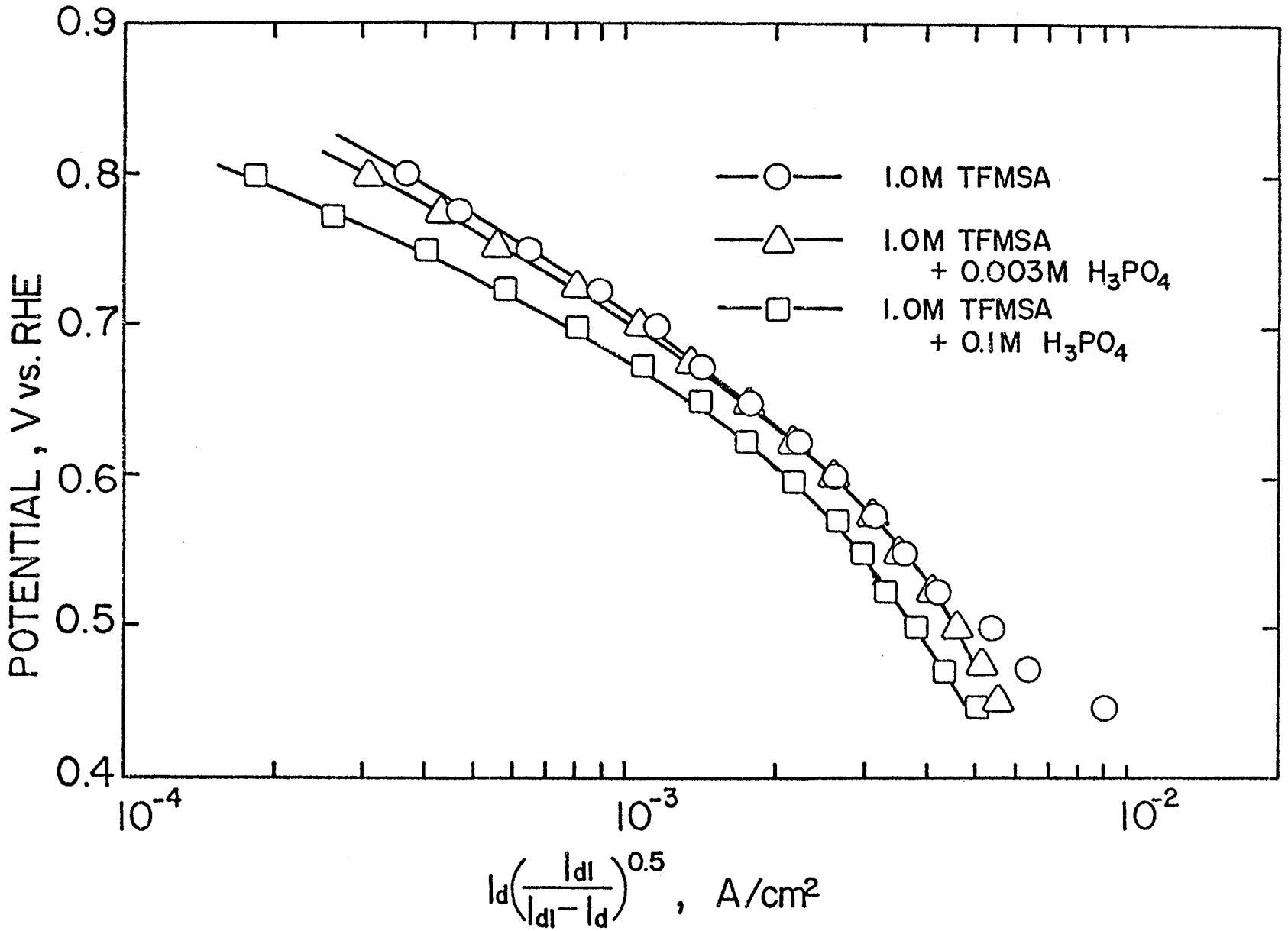

The plot of potential against log $I_d[I_{dl}/(I_{dl} - I_d)]^{1/2}$ for oxygen reduction at Pt in 1.0 M TFMSA with the additives of H_3PO_4. This plot is independent of ω over the range of (400-3600 rpm).

BRIDGE TYPE ADSOPTION :

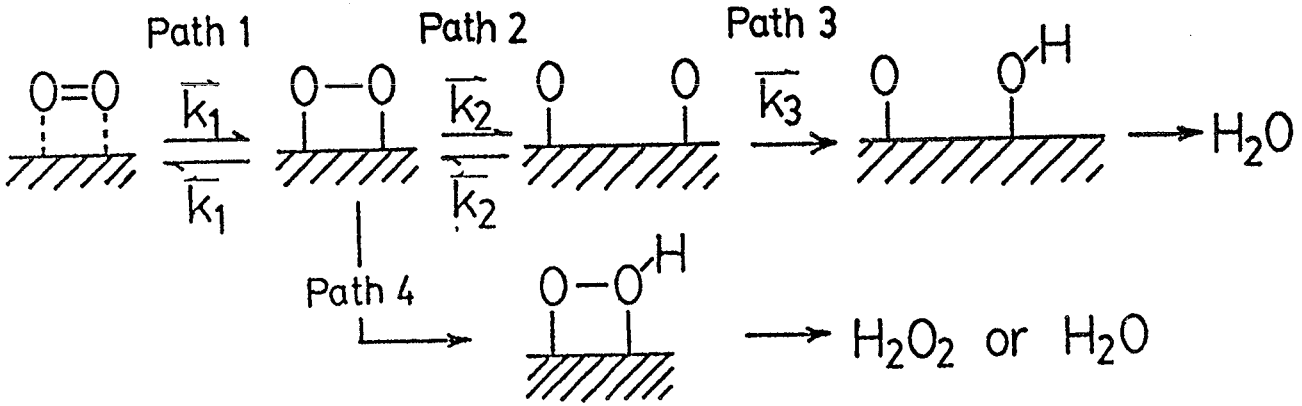

END-ON ADSORPTION :

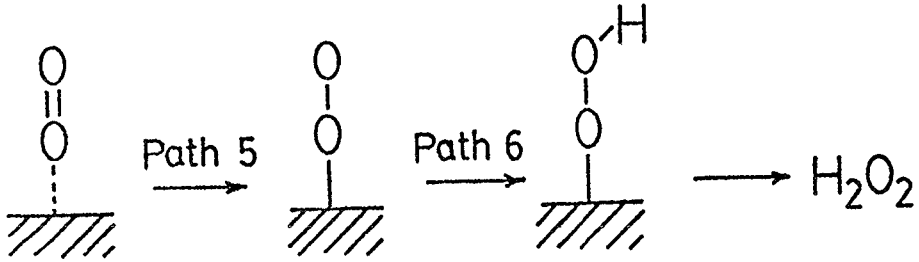

Electrode Kinetics of Oxygen Reduction at Platinum in Fuel Cell Electrolytes

Kan-Lin Hsueh
Clarkson College of Technology
Department of Chemical Engineering
Potsdam, New York 13676

ABSTRACT

Fuel cell power plants are being developed for power generation and on-site integrated energy systems and for transportation applications. For the first two applications, reformed fuels from natural gas, naphtha, or coal are being considered while for the third, methanol converted to hydrogen on board the vehicle is the most likely candidate fuel. With reformed fuels, it is only possible to use acids, molten carbonates, or solid oxides as the electrolytes for fuel cells and of these only the first it suitable for mobile power plants.

The phosphoric acid fuel cell system is in the most advanced state of development. Though the emphasis has been on stationary applications, it has potential for transportation applications as well. The oxygen overpotential of nearly 400 mV is the main cause of efficiency loss in this fuel cell system. The introductory chapter in this thesis briefly reviews the status of the fuel cell technology and an engineering analysis (heat, mass and energy balance of a 20-kw fuel cell power plant for electric vehicles, based on data from the United Technologies

---

[1]Abstract of work submitted in partial fulfillment of the requirements for the degree of Doctor of Philosophy, May 1982.

Corporation). This analysis, made by the author, showed that a 100 mV reduction in oxygen overpotential will have a significant effect in improving the efficiency and decreasing the weight, volume and cost of the power plant.

The main objectives of this thesis are to investigate the effects of the electrolyte on oxygen reduction kinetics at platinum with the hope of understanding why the electrocatalysis is worse in phosphoric acid than in some other acids and also to investigate model electrolytes (e.g., CF_3SO_3H, H_2SO_4, $HClO_4$, and KOH) which will make it possible to find new electrolytes for fuel cells.

Rotating ring-disc electrode techniques were mainly used for the electrode kinetic studies. Cyclic voltammetry was employed to characterize the surface of platinum electrodes in the above mentioned electrolytes over the region of potential of fuel cell reactions. Capacitance techniques were used to elucidate the double layer structure at the electrode-phosphoric acid interface and to determine the adsorption behavior of the trifluoromethane sulfonate anions.

The results of the theoretical and experimental studies may be summarized as follows:

(1) The theory of the rotating ring-disc electrode method was modified so as to calculate several of the rate constants for the intermediate steps in oxygen reduction. Application of the theory revealed that the reaction scheme

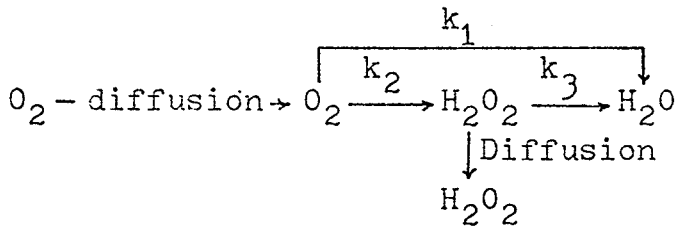

fits the experimental results better than other proposed reaction schemes which involve adsorption or desorption steps of hydrogen peroxide. The present theory involves the development of an equation for $I_{dl}/(I_{dl} - I_d)$ vs. $\omega^{-1/2}$ (where I_{dl} and I_d are the disc limiting and disc currents and ω is the rotational speed of the electrode) which combined with the previously derived expression for I_d/I_r (I_r is the ring current) vs. $\omega^{-1/2}$ makes it possible to calculate the rate constants (k_1, k_2 and k_3).

(2) The rate of oxygen reduction at platinum in the investigated electrolytes (acids at pH = 0 and alkali at pH = 14) follows the order $KOH \geqq H_2SO_4 \approx CF_3SO_3H > H_3PO_4 > HClO_4$. This order of activities is reflected in the effects of the electrolytes, in respect to specific adsorption of anions, on the platinum oxide formation reaction.

(3) The double layer is thicker at the mercury-phosphoric acid (95%) than at the mercury-aqueous electrolyte interface. There is strong adsorption of H_3PO_4 or phosphate species on mercury from concentrated phosphoric acid.

(4) The solvent structure change (from H_2O to H_3PO_4) appears to occur at about 56% H_3PO_4 (molar ratio of H_2O to H_3PO_4 is 4:1). The slow kinetics of oxygen reduction kinetics at platinum in concentrated phosphoric acid can be attributed to double layer effects (thicker double layer and strong adsorption of phosphoric acid or phosphate species), low oxygen solubility.

(5) The specific adsorption of trifluoromethane-sulfonate anions on mercury is relatively small and is lower at 40° than at 25°C. The low electrosorption of the CF_3SO_3H anions on electrodes and the opposite behavior of H_3PO_4 and $H_2PO_4^-$ anions partially account for the considerably better oxygen reduction kinetics at platinum in CF_3SO_3H than in H_3PO_4. The reaction order with respect to oxygen for this reaction is less than one for all the TFMSA concentration studied (0.05 to 6.0 M).

*U.S. GOVERNMENT PRINTING OFFICE: 1984/559-109/10415

1. Report No.	2. Government Accession No.	3. Recipient's Catalog No.
NASA CR-174753		

4. Title and Subtitle	5. Report Date
Electrocatalysis of Fuel Cell Reactions: Investigation of Alternate Electrolytes	January 1984
	6. Performing Organization Code

7. Author(s)	8. Performing Organization Report No.
Der-Tau Chin, K-L. Hsueh, and H. H. Chang	
	10. Work Unit No.

9. Performing Organization Name and Address	11. Contract or Grant No.
Clarkson College of Technology Potsdam, New York 13676	NAG 3-238
	13. Type of Report and Period Covered
12. Sponsoring Agency Name and Address	Contractor Report
U.S. Department of Energy Morgantown Energy Technology Center Morgantown, West Virginia 26505	14. Sponsoring Agency ~~Code~~ Report No.
	DOE/NASA/0238-1

15. Supplementary Notes

Final Report. Prepared under Interagency Agreement DE-AI21-80ET17088. Project Manager, Robert B. King, Energy Technology Division, NASA Lewis Research Center, Cleveland, Ohio 44135.

16. Abstract

This work is concerned with a study of oxygen reduction and transport properties of the electrolyte in the phosphoric acid fuel cell. The areas covered in the work were: (i) development of a theortical expression for the rotating ring-disk electrode technique; (ii) determination of the intermediate reaction rate constants for oxygen reduction on platinum in phosphoric acid electrolyte; (iii) determination of oxygen reduction mechanism in trifluoromethanesulfonic acid (TFMSA) which has been considered as an alternate electrolyte for the acid fuel cells; and (iv) the measurement of transport properties of the phosphoric acid electrolyte at high concentrations and temperatures.

17. Key Words (Suggested by Author(s))	18. Distribution Statement
Fuel cells; Phosphoric acid; Oxygen electrode reaction kinetics	Unclassified - unlimited STAR Category 44 DOE Category UC-97d

19. Security Classif. (of this report)	20. Security Classif. (of this page)	21. No. of pages	22. Price*
Unclassified	Unclassified	106	A06

*For sale by the National Technical Information Service, Springfield, Virginia 22161